ACCURATE IDENTIFICATION OF PAVEMENT MATERIALS SUSCEPTIBLE TO MOISTURE DAMAGE WITH ADVANCED TEST METHODS AND MACHINE LEARNING TECHNIQUES

By

Ram Kumar Veeraragavan

A Thesis

Submitted to the Faculty

of the

Worcester Polytechnic Institute

in partial fulfillment of the requirements for the

Degree of Doctor of Philosophy

in

Civil Engineering

May 2020

Approved

____

Dr. Aaron Sakulich

____

Dr. Rajib B. Mallick

____

Dr. Mingjiang Tao

____

Dr. Xiangnan kong

ACCURATE IDENTIFICATION OF PAVEMENT MATERIALS SUSCEPTIBLE TO MOISTURE DAMAGE WITH ADVANCED TEST METHODS AND MACHINE LEARNING TECHNIQUES

Abstract

Moisture induced damage in Hot Mix Asphalt (HMA) mixture is a prevalent problem all over the world. It is one of the leading causes of premature failures in asphalt pavements and a significant concern to the paving industry. It is, therefore, necessary to identify mixes that are susceptible to moisture damage during the mix design process. Extensive research has been carried out by several researchers over the years to develop a reliable and practical laboratory test procedure that can simulate field moisture damage conditions and that can make predictions that are likely to correlate to field performance. However, it is inferred from literature that no single laboratory test method can accurately predict the moisture induced damage performance HMA mixtures.

The objectives of the present study are to: Develop a framework that considers different test methods to predict the moisture induced damage of Hot Mix Asphalt (HMA); Develop a suitable machine learning method to achieve significantly high accuracy in predicting the moisture damage potential of Hot Mix Asphalt (HMA); and develop a tool (App) for use by practicing engineers to identify HMA mixes that are likely to be susceptible to moisture induced damage.

A total of 35 in-plant produced asphalt mixtures with known field performance were sampled, and compacted in the laboratory, and the compacted samples were subjected to mechanical tests before and after moisture conditioning with the Moisture Induced Stress Tester (MiST). In addition, the effluent from the MiST was checked for Dissolved Organic Carbon (DOC) content and gradation of dislodged aggregates. Fourier-Transform Infrared Spectroscopy (FTIR) analysis of the asphalt extracted from HMA samples was performed to observe changes in the functional groups before and after the MiST test.

Statistical analysis showed that seismic modulus and indirect tensile strength were effective in distinguishing poor-performing mixes from the well-performing mixes. Principal component analysis was conducted on the test data, and a reduced set of dimensions that were capable of explaining significant variance in the data was identified. The significant test properties were used to develop machine-learning models with two supervised classification approaches. The k-nearest neighbor model was found to be very accurate in differentiating the mixes. The use of MiST conditioning, specified physical tests, and machine learning methods are recommended for the identification of moisture-susceptible hot mix asphalt.

Contribution of this Work

The major contribution of this work is the creation of a framework or a system that combines appropriate test methods and suitable machine learning models to achieve high accuracy (84%) in predicting the moisture damage potential of Hot Mix Asphalt (HMA)**.** A secondary contribution is that this study, for the first time, combines the principles of Artificial Intelligence (AI), in the form of Machine Learning (ML), with the field of pavement performance, specifically for the evaluation of mixes that are subjected to moisture damage. Finally, the work provides users with a highly accurate ML model as well as an app, which can be used and further improved.

Dedication

I dedicate this dissertation to my parents who were the source of inspiration, guidance and support that enabled me to carry out my research for the Master's and Doctoral programs at the prestigious Worcester Polytechnic Institute. I also dedicate the thesis to my advisors Professor Rajib Mallick and Dr. Aaron Sakulich for their constant guidance, encouragement and support that shaped my professional competency in the field of pavement engineering.

ACKNOWLEDGEMENT

I would like to express my sincerest gratitude to my advisor Prof. Rajib. B. Mallick, for having given me the opportunity to pursue Masters and Doctoral research programs at Worcester Polytechnic Institute. I also thank him and the Civil and Environmental Engineering (CEE) Department for the generous financial support through Research Assistantship and Teaching Assistantship during the entire study period, and also for the support to participate in international conferences organized by the Transportation Research Board (TRB) and the American Society of Civil Engineering (ASCE).

Dr. Aaron Sakulich, my principal advisor, has been a great source of inspiration during the period of my study. He introduced me to the new area of Phase Change Materials. His constant advice, guidance, and support enabled me to understand the properties of phase change materials. Dr. Sakulich's advice from time to time on the characterization of pavement materials created a lot of interest and enthusiasm to pursue research in pavement material characterization. I thankfully acknowledge Dr. Sakulich for all his support, guidance, and advice that shaped me to join the industry with the needed professional knowledge experience and skills.

I would like to thank my dissertation committee members – Prof. Mingjiang Tao, Prof. Xiangnan Kong for their support and guidance from time to time and for monitoring the research to meet the standards of the Ph.D. dissertation. I would also like to thank various researchers – Prof. Soheil Nazarian (Texas-El Paso) and Prof. Paul Mathisen (WPI) for their suggestions and contributions at different stages of this research work. I would like to thank the Maine Department of Transportation for funding the project and providing the material, especially the valuable field mixes for the research work. My sincere thanks go to my lab managers – Mr. Don Pellegrino and Mr. Russ Lang, who were very resourceful in the laboratory. I thank the former department head Prof. Tahar El-Korchi for all his efficient coordination to run the experiments smoothly and for his support for my teaching assistantship (TA). I would also thank all of my TA course professors, Prof. John R Hall, Prof. Paul P. Mathisen, and Prof. Guillermo F. Salazar for their kind support. I would also thank the department office staff - Marylou Horanzy and Cynthia Bergeron, for their extensive help in all the works related to the office.

I thank my fellow students and friends – Nivedya Madankara Kottayi, Uma Maheswar Arepalli, James Vorosmarti, Austen E. Crawford, Wenwen Yao, Ryan Worsman, Mohammed Salhi, Shiva Prasad, and Sravan Katepalli for their help and support at different stages of this long journey.

I would like to thank my parents, caring brother, Ramanan Veeraragavan and my loving wife, Aarthi Ram Kumar for all their love, care, and support. I thank all my friends and relatives for their encouragement and support throughout the period of my study at WPI.

TABLE OF CONTENTS

LIST OF TABLES

LIST OF FIGURES

1.0 INTRODUCTION

1.1 Importance of Studies on Moisture Induced Damage to HMA

Highway infrastructure plays a vital role in the economic development and growth of a nation leading to social benefits. One of the most difficult challenges for the development of any road network is to execute projects in harmony with the concept of sustainable development. It is, therefore, necessary to develop sustainable highway pavements that are highly durable, energy-efficient, and cost-effective for the construction and maintenance of roads.

A majority of highways and airfield pavements throughout the world are surfaced with Hot Mix Asphalt (HMA). The surface layer acts as a "wearing" course and is designed not to be affected significantly during service life by traffic load/tire pressure repetitions and the environment. Generally, this surface HMA layer acts as an 'impermeable' layer to prevent the ingress of water into the pavement structure. This is because water has been identified as the single most destructive element in pavements leading to pavement distresses such as cracking and rutting. Such moisture-related distresses in pavements has been observed since the late 1920s and has been regarded as a national concern. Extensive research conducted by Hicks (1991) has shown that about half of the states in the United States had experienced moisture-related distresses. Moisture-induced damage is therefore regarded as one of the leading causes of premature failures in asphalt pavements and a major concern to the paving industry. Moisture in any form combined with traffic and environmental conditions can cause a significant loss in asphalt pavement strength and durability (Al-Swailmi *et al*. 1994). The mechanisms by which it occurs depends on several factors such as material properties (aggregate and binder properties), mixture properties (voids, permeability, etc.), and external factors (moisture exposure conditions, etc.) (Bagampadde *et al.* 2005, Masad *et al.* 2006, Lottman *et al*. 1978, Read *et al.* 2003).

Over the years, extensive research has been conducted to develop a reliable and practical laboratory test procedure that can simulate field moisture damage conditions, and that can make predictions that correlate well with the field performance. From the literature, it can be concluded that no single laboratory test method can be used to accurately predict the performance of a given

HMA mixture due to various potential mechanisms of moisture damage. Research conducted by the Maine Department of Transportation (MDOT) and other agencies have found the moisture conditioning of HMA samples with the Moisture Induced Stress Tester (MiST) and the use of Indirect Tensile Strength test (ITS) to be effective in screening moisture susceptible HMA mixtures (Arepalli *et al*. 2017, Mallick *et al*. 2001). However, the test results were not found to be sufficiently accurate to justify the use of the MiST and ITS procedures on a regular basis.

Conventional statistical models such as linear regression models or significance tests are generally used to develop relationships among variables such as relating mix properties to performance or screen poor-performing mixes. The main disadvantage of such conventional statistical methods is that they cannot estimate nonlinear and complex relationships accurately (Nivedya *et al.* 2018). Recent advances in statistics and data science have led to the development of Machine Learning (ML) techniques. ML is a sub-field of artificial intelligence that allows the computers to learn without being explicitly programmed. Unlike statistics, ML requires no prior assumptions about the relationships between the variables. The ultimate goal of ML is to develop computer algorithms that can cluster or classify or make predictions and is particularly applicable under the following conditions: There is a multitude of factors that influence the target (of regression) or the outcome (of classification or clustering); and, the relationship between the predictors or the variables to the target or the outcome is not simple – it is very complex, and the assumption of linearity in models is not valid. ML techniques can be used to predict HMA mix properties more accurately than conventional statistical approaches. There is a need for research on accurate prediction of mix performance using ML techniques.

1.2 Objectives

The overall objectives of this study were to determine a suitable set of tests that could be used with a moisture conditioning process and to develop a machine-learning model with appropriate test data to predict the moisture susceptibility of HMA. The specific objectives of the present study are as follows:

1. Development of a framework that considers different test methods to predict the moisture induced damage of Hot Mix Asphalt (HMA).

2. Develop suitable machine learning methods to achieve significantly high accuracy (84%) in predicting the moisture damage potential of Hot Mix Asphalt (HMA).

3. Development of a tool for use by the practicing engineers to identify hot mix asphalt samples that are likely to be affected by moisture induced damage.

1.3 Scope of the Present Study

The scope of the present study is limited to laboratory experiments on hot mix asphalt to study the various factors influencing the moisture induced damage. The findings of the laboratory experiments were validated from samples of hot mix asphalt obtained from the field. The laboratory performance of the HMA samples was validated with field HMA samples. An App has been developed for use by the practicing engineers to identify HMA mixes that are susceptible to moisture induced damages from limited laboratory experiments.

2.0 LITERATURE REVIEW

2.1 Importance of Research on Moisture Induced Damage in HMA

Moisture damage in asphalt pavement is a complex phenomenon involving many factors. It is one of the major causes of distress in HMA and has been considered a national issue (D'angelo, 2003; Epps *et al*., 2003; Little *et al*., 2003). In general, not all damages are caused directly by moisture, but its presence accelerates the extent and severity of different distresses. Moisture damage has been defined as the loss in structural strength and durability of HMA mixtures due to the deterioration caused by the effects of moisture. The existence of moisture in pavement can lead to loss of cohesion within the asphalt binder itself or the loss of interfacial adhesion between binder and aggregates. Figure 2.1(a) and 2.1(b) show typical distresses that may occur due to moisture damage.

(a)

(b)

Figure 2.1(a): Longitudinal Cracking Due to Moisture Induced Damage in HMA Layers

Figure 2.1(b): Alligator Cracks Due to Moisture Induced Damage in HMA Layers

Several factors contribute to moisture induced damages in HMA. The properties of the aggregates, properties of the binder and mixes as well as external factors contribute towards moisture induced damages in HMA (Table 2.1).

Table 2.1: Factors That Can Contribute to Moisture Damage in Pavements (Varveri, 2017)

Aggregate Properties	Binder Properties	Mixture Properties	External Factors
Mineralogy	Rheology	Void content	Rainfall
Surface texture	Physico-chemical properties	Permeability	Humidity
Porosity	Constitution	Asphalt content	Water pH
Dust	Surface free energy	Asphalt film thickness	Presence of salts
Durability		Filler type	Temperature
Surface area		Aggregate grading	Temperature cycling
Surface free energy		Type of mixture	Traffic
Absorption			Design
Moisture content			Workmanship
Shape			Drainage
Weathering			

2.2 Aggregate Properties

Some of the important properties of coarse aggregates that are generally considered during the mix design process are strength, shape, texture, and gradation. Since about 95% of a typical HMA mix is made up of mineral aggregates it is essential to consider their properties such as mineralogy, geometric irregularities, and gradation that can be directly related to pavement performance. In addition, it can be inferred from the literature that moisture sensitivity is affected by aggregate chemistry as well as asphalt chemistry. Hence, there is a need to investigate the mineralogy of aggregates and its effects on the asphalt-aggregate system under different conditions.

Natural aggregates are generally classified into three broad categories: Igneous rocks, sedimentary rocks, and metamorphic rocks. Some of the common types of igneous rocks include granite (commonly found in New England states), diorite, gabbro, etc. Rocks are aggregates with one or more minerals whereas minerals are naturally occurring, inorganic solids with a definite chemical composition and a crystalline structure formed by geological processes. The amount of silica in igneous rocks (acidity) can vary from 75% to less than 45%. Higher percentages of silica have been known to reduce asphalt-aggregate bond strength (adhesive failure). For example, marble and limestone (sedimentary) are known to be basic and have lower percentages of silica whereas sandstone granite and quartzite (metamorphic) are acidic. It is also well known that most siliceous aggregates such as granite are negatively charged in the presence of water indicating that they are hydrophilic aggregates. Figure 2.2 shows the classification of common types of igneous rock.

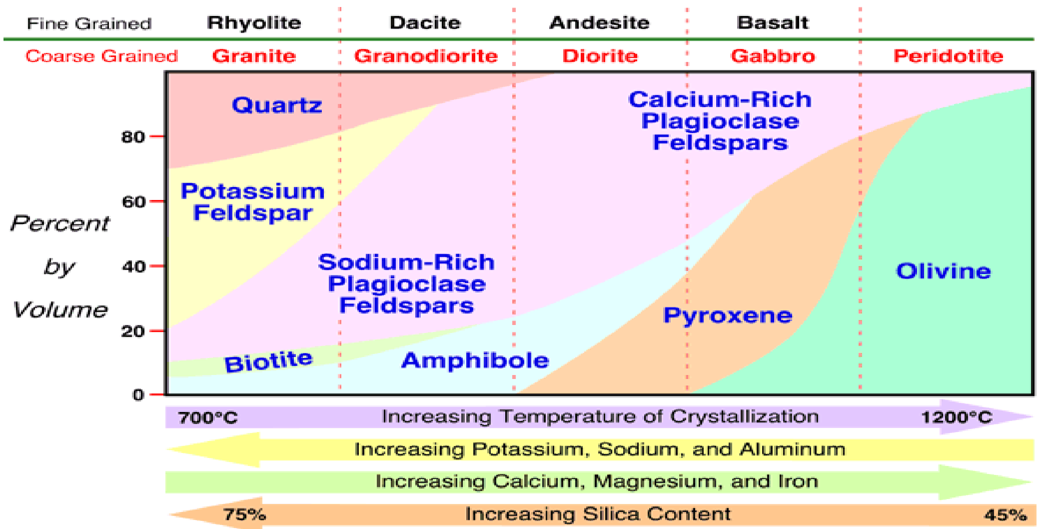

Figure 2.2: Classification of Igneous Rocks

(http://www.physicalgeography.net/fundamentals/10e.html)

Asphalts are highly complex materials. They contain saturated and unsaturated aliphatic and aromatic compounds. These compounds are classified as asphaltenes or maltenes according to their solubility in hexane or heptane solvents. Asphaltenes have high molecular weight species and they are insoluble in these solvents. Maltenes have lower molecular weights and are soluble. Asphalts normally contain between 5% and 25% by weight of asphaltenes. Research work carried out by Ribero (2009) found that some of the minerals like feldspar and biotite contained numerous binding sites where the adsorption of asphaltenes takes place due to the presence of aluminum in the structure of the minerals. On the other hand, quartz with lower aluminum content was found to hinder the interaction between the two materials. Fisher (2013) verified the mechanism using Atomic Force Microscopy (AFM) study. The research done by Bagampadde (2005) found that the higher percentages of both quartz and alkali feldspar in aggregates increased the moisture susceptibility of asphalt mixtures, but higher resistance to moisture damage was found when the quartz content in the aggregate was 100%. Hicks (1991), classified aggregates based on the degree of stripping (i.e. separation of asphalt binder from aggregate surfaces due primarily to the action of moisture) as shown in Table 2.2.

Table 2.2: Classification of Aggregates Based on Degree of Stripping (Hicks, 1999)

Minerals		
Slight stripping	**Moderate stripping**	**Severe stripping**
Biotite	Biotite	Biotite
Hornblende	Hornblende	Hornblende
Feldspars	Feldspars	Feldspars
Labradorite	Oligoclase	Oligoclase
Bytownite	Albite	Albite
Anorthite	Anorthite	Anorthoclase
Chlorite	Garnet	Microcline
Sercite muscovite	Quartz	Perthite
Diopside	Muscovite	Andesite
Olivine		Chalcedony
Pyroxenes		Quartz
Augite		
Calcite		
IGNEOUS ROCKS		
Slight stripping	**Moderate stripping**	**Severe stripping**
Gabbro	Biotite granite	Biotite granite
Basalt	Basalt	Aplite granite
Greenstone	Olivine dolerite with analcite	Pegmatite granite
Quartz dolerite	Quartz diorite	Soda granite
Diabase	Andersite	Granodiorite
Scoria	Diabase	Albitised olivine-diorite
Slight stripping	**Moderate stripping**	**Severe stripping**
Peridotite	Obsidian	Diorite
Scoria		Rhyolite
Peridotite		Trachyte
		Pumice
		Dacite
		Syenite
METAMORPHIC ROCKS		
Slight stripping	**Moderate stripping**	**Severe stripping**
Silicious river sand	Biotite feldspar gneiss	Quartzite
Silicious sand with iron oxide	Feldspar quartz-sercitesnesis	Granite gneiss
Serpentine	Granite quartz-feldspar gnesiss	Quartzite-sericite schist
	Biottie-muscovite schist	Feldspathic-quartzite
	Diabase-hornfeis	Biotite schist
	Hornblende-gneiss	Muscovite schist

Table 2.2: Classification of Aggregates Based on Degree of Stripping (Hicks, 1999) (continued)

SEDIMENTARY ROCKS		
Slight stripping	**Moderate stripping**	**Severe stripping**
Limestone	Limestone	Iron oxide-rich arkose
Dolomite	Dolomite	Chert
Graywacke	Lime rock	Flint
Lime rock	Reed coral	Breccia
	Calcareous sandstone	Feldspadic sandstone
		Sandstone
		Chalk
		Oolitic limestone
		Argillaceous sandstone

Surface texture is known to affect the mechanical bond strength between asphalt and aggregate. Aggregate with rough surface texture and/or high amount of surface porosity will increase the moisture damage resistance of HMA mainly because of the availability of more surface area for the asphalt to bind. Many siliceous aggregates are known to have low porosity or smooth surface texture, but this may not be the case always because, for example, granites do have very high surface texture and can create an excellent mechanical bond but may suffer in chemical bonding. Aggregates like limestone may sometimes contain a high amount of calcite, which is known to interact with calcium carbonate instead of asphalt and may result in a reduced aggregate surface area.

During the aggregate crushing process, dust is generally generated and based on the nature and extent of the dust, it may affect the moisture susceptibility of a mix. The presence of dust coating on the aggregate surface can prevent the asphalt binder from forming a bond directly on the surface of the aggregate. The asphalt layer coated over an aggregate will not allow water to penetrate through it. Water entering through the pores/dust and localized between the binder and surface of the stone can cause stripping. However, this effect is significant only when the aggregate is coated with large amounts of dust. In certain special cases, when a small amount of clay dust particles is coated on the aggregates, it can act as an emulsifier. Similarly, gravel aggregates may have shale. The crushed shale may break down during in-service and may cause a problem of adhesion. Clay has been known to expand in the presence of water, and in the process can strip the asphalt off the surface of aggregate. If this is combined with the action of traffic, the clay will emulsify the asphalt in the mix and can cause severe stripping.

Water absorption rate, amount of water uptake, and the presence of micro cracks in the aggregate surface may have a severe effect on the moisture susceptibility of a mix. It can be said that the aggregates that absorb more water are likely to absorb more asphalt as well. If during the mix design process the percentage of binder added is incorrect without considering the absorption capacity, then more amount of binder would be absorbed by the aggregates and the effective asphalt may be insufficient to bind the aggregates together. This may lead to segregation, raveling, cracking and stripping. Segregation in a hot mix asphalt (HMA) mixture can be defined as the detachment of the coarse aggregate particles in the mix from the rest of the mass, which may be due to insufficient binder in the mix. Raveling is defined as progressive separation and dissociation of fine aggregate particles and binder from the bituminous surface, which is a direct consequence of stripping of the binder from the aggregates as an effect of moisture induced damage. Cracks develop due to either insufficient asphalt content, excessive filler, improper compaction or excessive moisture in the pavement layers. Stripping is a defect which is characterized by the separation of the asphalt film from the surface of the aggregate particles, due to the presence of moisture. Therefore, it can be inferred that moisture in pavement layers cause catastrophic effect and there is a need to understand and quantify the influence of moisture on the performance of asphalt pavements.

2.3 Binder Properties

Asphalt is a viscoelastic material derived from crude oil. Its properties are mainly dependent on the source of the crude oil from which the asphalt is derived. The asphalt binder consists of two principal chemical groups within the binder, the maltenes (saturates, aromatics, and resins) and asphaltenes. These two chemical groups are primarily responsible for the rheology of the asphalt. Hefer *et al*., 2005 conducted a study to understand the relative affinity of aggregate surfaces to the functional groups from asphalt binder and water. Table 2.3 shows the affinity of asphalt functional groups for aggregate surfaces. From the table, it can be inferred that the functional groups of asphalt binder that are significantly adsorbed on the aggregate surface are more prone to being displaced by water. The displacement of the binder by water at the interface region is a chemically favorable phenomenon. Robertson (2000) stated that the overall polarity within the organic molecules promotes the attraction of polar asphalt components to the polar aggregates. He further explains that neither asphalt nor aggregate has a net charge and the components of each form non-uniform charge distributions and behave as if they have charges that attract the opposite. Curtis (1993) had evaluated the asphalt-aggregate interactions in terms of adsorption and desorption and showed that specific functional groups that had the most affinity for the aggregates also tended to have the highest sensitivity to water. He further adds that once the surface of aggregate has been coated with asphalt, their interactions become relatively not significant.

Table 2.3: Affinity of Asphalt Functional Groups for Aggregate Surfaces (Hefer *et al*. 2005)

Plancher *et al*. 1977	Petersen *et al.* 1982	SHRP (Jamieson *et al*.1995)
Most strongly functional groups (decreasing order)		
Carboxylic acids Anhydrides 2-Quinolones Sulfoxides Pyrridine types Ketones	Carboxylic acids Anhydrides Phenols 2-Quinolones Sulfoxides Ketones Pyrridine types Pyrrolic	Carboxylic acids Sulfoxides Pyrridine types Phenolic Pyrrolic Ketones
Susceptibility of adsorbed functional groups for water displacement (decreasing order)		
Carboxylic acids Anhydrides Sulfoxides Pyrridine types 2-Quinolones Ketones	Anhydrides 2-Quinolone types Carboxylic acids Pyrridine types Sulfoxides Ketones Phenolic Pyrrolic	Sulfoxides Carboxylic acids Pyrrolic Ketones Pyrridine types Phenolic

2.4 Surface Energy Theory

According to Surface Energy Theory, adhesive strength can be quantified in terms of adhesive bond energy with the bond being dependent on the surface free energy of the two materials considered (Bhasin *et al.*, 2007). The surface energy can be calculated using the equation:

$\gamma = \gamma^{LW} + \gamma^{+-} = \gamma^{LW} + 2\sqrt{\gamma^{+}\gamma^{-}}$

γ = total surface free energy of the material

γ^{LW} – LW component

γ^{+-} = acid-base component

γ^{-} = Lewis acid component and

γ^{-} = Lewis base component

According to this theory, when a drop of liquid is placed on a horizontal surface, either it can spread on the solid surface, or it can take the shape of a drop with a finite contact angle between solid and liquid phases. This contact angle is commonly used to measure the surface energy of solids based on the relationship between contact angles, the surface energy of solids, wetting of solids and thermodynamic considerations. The properties of these solid-liquid, liquid-vapor, and solid-vapor interfaces can generally be described as a three-phase boundary.

Fig 2.3 shows the two-phase boundary of a liquid on a solid surface in vapor (Readet *et al.*, 2003). In this figure, θ is the angle between solid-liquid interface and the tangent of the liquid-vapor interface.

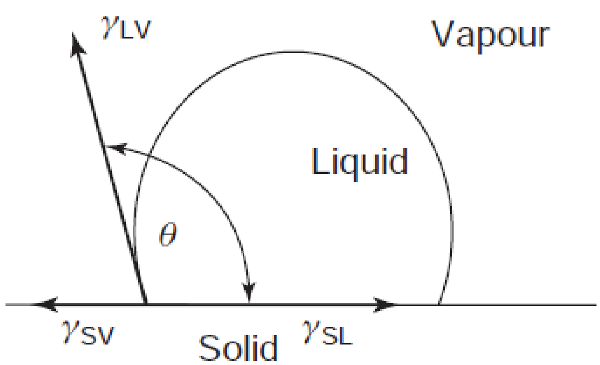

Figure 2.3: Three-Phase Boundary of a Liquid on A Solid Surface in Vapor (Read *et al.*, 2003)

In this figure, the contact angle is greater than 90º, indicating that water does not spread easily over the surface and hence it is a hydrophobic surface. It should be noted that many different theories have been developed to explain adhesion of asphalt to aggregates but none of the theories have provided a completely satisfactory explanation of the true mechanism, which may be a combination of theories (Arno *et al*., 2005).

2.5 Mixture Properties

One of the major factors responsible for the moisture transport in asphalt mixtures is the void structure. It is generally assumed that air voids are not interconnected when the asphalt mixture has 4 to 5% air voids (Choubane *et al*. 2000). Generally, many road construction agencies compact asphalt mixtures to at least 8% in-place air voids during the construction, assuming that the mixture will densify normally under traffic to its final percentage of about 4% air voids over the years due to secondary compaction.

Terrel *et al*. 1993 proposed a concept of pessimum void content in an asphalt mixture that relates to stripping potential. Their research shows that at low percentages of air voids (< 4% to 5%), the voids are not connected and the potential for water intrusion and stripping are low. Also, at higher percentages of air voids (>15% to 20%), the voids are interconnected such that the asphalt mixture is free draining. The percentages of air voids between 5% and 15% is called the pessimum range, where some of the air voids are interconnected, and water may get entrapped in the mixture, thereby increasing the striping potential. Figure 2.4 shows the relation between air voids and retained mix strength.

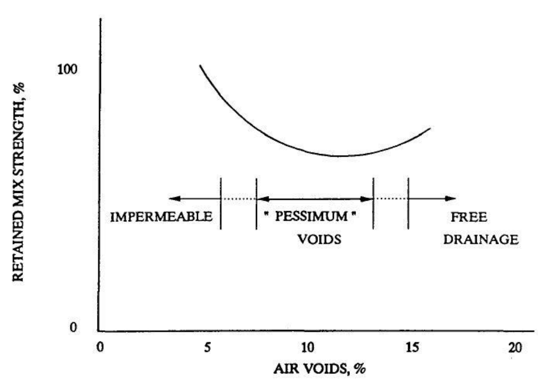

Figure 2.4: Air Voids vs Retained Maximum Strength (Terrel *et al*., 1993)

Unfortunately, most asphalt mixtures are constructed near the pessimum range, causing an increase in the stripping potential during the early pavement life. In addition, it is not always guaranteed that after a few years of construction the asphalt mixture would densify to the impermeable range (4% to 5%). Terrel *et al.* 1993 suggested the adoption of Stone Matrix Asphalt (SMA) and Open Graded Friction Course (OGFC). The SMA mixtures are often densely packed and are impervious after proper compaction. On the other hand, OGFC mixtures are more likely to be outside pessimum air void range allowing adequate drainage. Mohammed (2010) found that the common compaction techniques in asphalt mixtures are prone to generate cracks called checks. These checks are 1 to 4 in. in length and 1 to 3 in. apart. Checks are normally not visible and are generated during the first or second pass of conventional steel-wheel rollers. They had mentioned that these checks promote water transport in isolated areas within the pavement. In addition, they had proposed a new compaction technique that reduces the formation of such cracks.

2.6 Modes of Moisture Transport in Asphalt Mixtures

Moisture can transport in asphalt mixtures by three main modes, the first of which is permeability. Permeability is an important characteristic of pavement materials. It can be defined as the ability of a material to transmit water or fluid through it. Previous research done by Bhattacharjee and Mallick (2002) showed that the permeability is a better indicator of durability than porosity because the permeability indicates the pores that are exposed to water, whereas porosity indicates all the pores, which may or may not be filled with water. There are many existing empirical equations to determine the permeability of asphalt mixtures that cannot be correlated to field performances (Vardanega, 2004).

Capillary rise, the second mode, is more prominent in the region of a saturated gradient combined with ambient conditions at the interface (i.e. low humidity and high temperature). It is generally defined as the rise in the liquid above the level of zero pressure due to the gross upward force produced by the attraction of the water molecules to a solid surface. In asphalt pavements, capillary rise phenomenon allows subsurface water to be transported into the pavement through the capillaries formed by the interconnected voids. The extent to which the water would rise above the saturation surface, as well as the rate of rise, depends on: (1) the geometrical characteristics of the capillaries, (2) the surface tension of water, (3) the density of the water (4) the contact angle between the liquid and solid. Masad et al. (2007) reported that the HMA specimens with high voids showed a rapid increase in the flow of water in the laboratory testing when the contact angle between the water and the particles was lowest. The results were only presented for voids that were equal to or larger than the image resolution of the X-ray computed Tomography equipment. However, it was expected that a greater height of rising took place in smaller voids that were not detected in the images and the aggregate–binder interfaces.

Vapor diffusion through asphalt binder (the third mode) is a slow process because of the molecular structure of the material. The amount of water vapor and the rate at which it accumulates in an asphalt mixture depends on: (1) relative humidity (2) diffusion coefficients (3) storage rate and (4) storage capacity. Vapor diffusion is a cumulative process depending upon the condition of the road (Arambula *et al.*, 2009).

2.7 Test Methods

In general, existing test methods can be classified into two categories: (1) tests on loose mixtures and (2) tests on compacted mix samples. In the past, observation-based rating systems were used to evaluate the moisture susceptibility of loose asphalt mixtures. Some of the tests include the boiling water test (ASTM D3625) and the static immersion test (AASHTO T182). These tests involve visual observation of stripping potential. Such visual based rating systems are currently not in use and have been criticized for subjective visual evaluation and for not accessing moisture potential in compacted asphalt mixtures. Such tests usually focus on moisture-induced adhesive failures without considering cohesive failure within asphalt mastic.

On the other hand, tests on compacted mix samples usually involve dividing the samples into control and moisture-conditioned groups. Both samples are subjected to mechanical testing such as Indirect Tensile Strength (ITS), resilient modulus, and dynamic modulus, as well as wheel tracking tests. Currently, the most widely used mix design test procedure for the evaluation of moisture damage in the U.S. is the AASHTO T283 (AASHTO, 2001) test. The AASHTO T283 procedure requires the samples to be moisture saturated to a level of 70% to 80%. The saturated samples are then subjected to air conditioning at -18°C (-4ºF) for 16 hours followed by a thawing period at 60°C (140ºF) for 24 hours. The specimens are then placed in a water bath at 25°C (77ºF) and tested in indirect tensile mode at 25°C (77ºF). However, a number of researchers have reported the inability of this test procedure to predict the moisture damage potential of HMA mixes accurately. The test does not replicate the high saturation and pore water pressures that are expected in the field and researchers have identified significant variability in test results and the need for alternative tests (Kringos *et al*., 2009). Other test methods under saturated conditions include the Hamburg wheel tracking test (Aschenbrener, 1995) and the saturation ageing tensile stiffness test (Airey *et al*., 2005). Typically, moisture evaluation 'test' procedure refers to a combined system of a conditioning step that simulates field conditions and a characterization test that evaluates the effect of the conditioning. As mentioned before, AASHTO T283 test consists of subjecting a sample to saturation and then to freeze/thaw (generally one cycle).

The environmental conditioning system approach (Al-Swailmi *et al*., 1992) combines these in the sense that tests are conducted within an environmental system that is supposed to simulate field conditions. One of the main criticisms of these conditioning systems is that they cannot simulate the damage caused by the generation of pore water pressure, which occurs due to the effect of tire pressure on fully saturated HMA mixes (Kandhal and Rickards, 2001; Novak *et al*., 2002).

The semi-circular bend (SCB) test was explored by Molenaar (2000) and extensively evaluated through the TPF-5(132) study (Marasteanu *et al*. 2012). SCB test is an important indicator to characterize the cracking resistance of asphalt mixture before and after moisture damage. The post-peak crack energy can be used to characterize the ductility of asphalt mixture. The SCB test was performed according to the AASHTO standard (Al-Qadi *et al*., 2015) at 25ºC. For this test, a semicircular disc of HMA, 150 mm in diameter and 25 mm thick, was tested in a three-point bending mode.

To simulate the generation of pore pressure in HMA in the lab, the MiST was developed (Mallick *et al*., 2003; Buchanan *et al*., 2004;) based on work conducted by Jimenez (1974). The MiST is capable of representing the action of repeated traffic on a saturated asphalt pavement. It uses a hydraulic system to create alternating pressure and vacuum cycles inside the test chamber and hence forces water in and out of the pores of the HMA specimens. It is capable of accommodating any standard HMA sample. Studies have confirmed that high pore water pressures are developed in the upper layers of HMA in the field (Mallick *et al*., 2003), and the MiST is capable of simulating such conditions. The MIST test was designed to simulate stripping damage in fewer than three hours of treatment. The temperature levels are controlled during the test. The pore pressure is generated in the mixture, mimicking temperature, traffic and humidity field conditions. The test is effective for the identification of poor performance HMA (Ahmad *et al*., 2017; Birgisson *et al*., 2007; Mallick *et al*., 2005; Pinkham *et al*.,2013). The MiST is a relatively inexpensive piece of equipment, and the conditioning of the samples can be completed within a reasonable time period (< 24hours).

Image analysis is being increasingly used in the transportation field, due to the ease of obtaining the data and the development of image analysis software (Radopoulou, 2013). This technique continues to be used at a significant level in other areas of pavement engineering, for example in automated identification and analysis of pavement distresses in pavement management systems. The technique is specifically relevant for the topic of moisture damage since it has been reported that if a sample is subjected to moisture conditioning, it is likely that there will be a difference in the color of the sample before and after conditioning, specifically for a moisture susceptible mix. This is because the damage will cause a removal of asphalt from the surface of the aggregates.

The Ultrasonic Pulse Velocity (UPV) test is recommended for the following reasons (University of Texas, 2006):

1. UPV test is nondestructive and can be conducted in a very short period of time;
2. The UPV test has been extensively evaluated, found to be sensitive to key properties of HMA and has been utilized to determine design moduli that could be used in M-E analysis;
3. Seismic modulus data have been previously used successfully to detect moisture susceptible mixes (Birgisson *et al*., 2003; Nazarian *et al*., 2005; Maser *et al*., 2006); and
4. Well-established guidelines have been developed for regular use of this test by the Texas DOT

Fourier transform infrared–attenuated total reflectance (FTIR-ATR) spectroscopy has been widely used by several researchers to characterize the materials used in pavement construction. The equipment is found to be robust and is an accurate noninvasive in situ method to provide data in the shortest possible time to identify various functional groups present in the material. FITR technique has been widely used to examine diffusion in polymers and is found to have wide practical applications.

Seifollah Nasrazadani et. al., (2009) presented the practical applications of Fourier Transform Infrared Spectroscopy (FTIR) in characterizing pavement materials. FTIR technique has been found to be capable of quantifying alkali content in concrete cement. FTIR is found to be useful in the analysis of polymer content in asphalt binders but, it was not found to be a suitable technique to detect and quantify anti-stripping agents in asphalt materials. One of the reasons for this may be because of the low concentration of the antistripping agents and possibly band overlap in the spectra of organic compounds. Howard et.al., (2013) conducted experiments on the aging characteristics of binders using FTIR, while studying the hauling time effects on unmodified, foamed, and additive modified binders used in hot mix asphalt. FTIR can throw light on the specific functional groups of compounds in asphalt. Karmakar et. al., (2018) studied the moisture damage analysis of bituminous mix by Durability index Utilizing waste plastic cup (PC). They conducted FTIR tests on PC-modified bitumen to observe the reduction of carbonyl acid in the bitumen in order to determine the enhanced structural integrity of the bituminous mix. The findings enabled the researchers to quantify the optimal dosage of PC to be added for the improved performance.

Vasconcelos et.al., (2010) measured the water diffusion in asphalt binders using Fourier Transform Infrared – attenuated reflectance spectroscopy (FTIR-ATR) to monitor the diffusion of water into thin films of asphalt binder. Morian et. Al, (2013) studied the effect of binder aging in hot mix asphalt using FTIR. FTIR was used to study the binder kinetics with respect to the carbonyl area measured from the Fourier transform infrared spectroscopy spectra as a function of aging time and temperature and found that effective binder content to be the indicator of the aging characteristics of binders. Lamontagne et. al., (2001) studied the aging characteristics of road bitumen using FTIR.

2.8 Application of Fibers in Hot Mix Asphalt

Researchers are looking for better materials to improve the performance of hot mix asphalt. The addition of fibers in hot mix asphalt is found to improve the fatigue as well as the rutting performance. The addition of fiber also reduces the drain down in case of gap graded asphalt mixes like Stone Matrix Asphalt. It also reduces the temperature susceptibility of the mastic. Fiber incorporation has proved to be a practical and dependable technique for improving the performance of hot mix asphalt. The addition of fiber ensures that the mixes is rich in bitumen. Rich binder will enable better and improved resistance to moisture, aging, fatigue and cracking. (Serfas et al., (1996)

Klinsky et. al., (2018) studied the performance characteristics of fibers modified hot mix asphalt. The addition of fibers has resulted in higher tensile strength; higher resilient modulus; lower permanent strain accumulation and better fatigue resistance. The addition of blended fibers of polypropylene and aramid to hot mix asphalt is found to enhance its mechanical properties and extended the service life. Slebi-Acevedo et. al., (2018) presented a review of the mechanical performance of fibers in hot mix asphalt. The tensile strength, modulus of elasticity, specific gravity and Mohs hardness are the relevant properties to be considered in performance evaluation of asphalt mixes with different fibers. The use of waste fibers and natural fibers like coconut fibers are found to improve the mechanical properties of hot mix asphalt and also improve the performance. Kockal and Kofteci (2016) studied the aggressive environmental effect on polypropylene fiber reinforced hot mix asphalt. The bulk density of the sample and the Marshall stability values improved with the addition of the fibers. Na2SO4 showed most damaging effect on samples under aggressive environment.

Kumar et.al (2009) investigated the laboratory performance of fiber modified asphalt mixes. The indirect tensile strength and Marshall test properties were found to improve with the addition of fibers. As polypropylene fibers get entangled, strength reinforcement of asphalt-binder mastic was found to be necessary. Mufta et. al (2017) carried out a research study to quantify the benefits of using fiber reinforced hot mix asphalt to mitigate the distresses. The researchers have reported that the optimal fiber content recommended by the manufacturer need not be optimal and detailed investigations are needed before field implementation. HMA mixes with higher dosage of fibers had higher fracture energy than control mixes. Rutting and fatigue resistance of the mixes with fibers are found to be higher than control mixes. Alfalah (2020) assessed the impact of fiber type on the performance of fiber reinforced hot mix asphalt. The researchers have found that the fibers affected the volumetric properties, mix durability, and rutting resistance of HMA mixes. The use of fibers was found to improve the rutting and durability performance of asphalt mixtures in the laboratory. However, research studies on improved moisture resistance of hot mix asphalt with fibers is limited and there is a need to investigate the resistance to moisture of HMA with fibers.

2.9 Machine Learning:

Artificial Intelligence (AI) has been defined as the "the science and engineering of making intelligent machines" (McCarthy, 2007). Machine Learning (ML) is a specific way in which AI is implemented in the real world. The aim of ML is to develop algorithms that can receive input data and apply statistical analysis to predict the output within an acceptable range. ML is based on the association of learning with hidden patterns and the theory that computers are able to recognize patterns in such a way as to learn to adjust their responses without human intervention. ML techniques are applicable in classification and regression-type problems with multiple dimensions. They are suitable for nonlinear systems because they can capture non-linear relationships among multivariate datasets – something that is very relevant to the evaluation of moisture susceptibility of HMA. Machine learning techniques can be broadly classified into two categories based on technique that are used to train the model: supervised and unsupervised. Supervised classification models are used to classify the input data into categories if the response variable is discrete. Supervised regression models are applicable in cases where the response variable is continuous. Unsupervised learning models find patterns in the data and develop inferences without any labelled output. The method of clustering is commonly used to find hidden patterns or groupings in the data. Studies have shown that ML models for binary classification outperform regression models that are used for prediction. This is because of the relatively easier process of training when the response variables are categorical and can fall into either one of the two categories.

The k-nearest neighbor method and the Naïve Bayes method are two popular supervised machine-learning techniques that produce nonparametric models. Naïve Bayes Classifiers is a classification based on the Naïve Bayes theorem, while assuming the predictors are independent. In Naïve Bayes classification, it is assumed that the availability of certain feature in a certain class is not related to the presence of any other feature. The algorithm works by counting and conditional probability (Murphy, 2006). The model is a probability table, which is updated depending on training data. Probabilities from the probability table based on the feature values are considered in prediction.

The major advantages of the Naïve Bayes method are it is a fast, easy way to predict a class of dataset for testing. It can also be applied very well in the prediction of a multi class problem. When the assumption of the independence is true, the Naïve Bayes classifier works very well when compared to other models (Richards, 2018). The model requires less training data. The model performs better when the input variables are categorical than the numerical variables. In case of numerical variables, an assumption that the data set follows a normal distribution is to be made.

The limitations of Naïve Bayes algorithm are that it makes an assumption on the shape of the data distribution which may not be true always. The other issues are data scarcity as needed for the model development and validation. The Naïve Bayes Algorithm can be advantageously applied to solve problems in real time prediction, multi-class prediction text classification/sentiment analysis/spam filtering and recommendation systems (Theobald, 2017).

K-Nearest Neighbors (K-NN) is one of the simplest clustering algorithms used to classify new data points in relation to known and nearby data points. It is a non-parametric algorithm, in the sense that there are no underlying assumptions made regarding the distribution of the data (Harrison, 2018). This algorithm can be applied to either regression or to classification problems but is most widely applied in classification problems. When K-NN is used for classification problems, the output may be calculated as the class, which has the highest frequency from the k-most similar instances. In order to identify the K instances in a training dataset, which are most similar to the new input, the distance measurement technique is used. For inputs, which are real values, the most common distance measure is the Euclidean distance. Other distances that can be used include Hamming distance, Manhattan distance, and Minkowski distance. The kind of distance measure can be determined from the data set (Richards, 2018). The goal in K-NN is to determine the K similar data points from a training set, then use them for interpolating the output value, which can be an average for a numeric output, and a majority value for the categorical output. The K parameter is tunable, and should be cross-validated so that the best value can be picked.

K-NN can be used for pattern recognition and statistical estimation. One of the downsides of K-NN is that it can be challenging to apply for high dimensional data (3D and 4D) with multiple features (Theobald, 2017). Measuring multiple data points in a three or four-dimensional space is a burden on taxing resources and complicated to perform accurate classification. Reducing the total number of dimensions, through a descending dimension algorithm such as Principle Component Analysis (PCA) or merging variables, is a common strategy to simplify and prepare a dataset for K-NN analysis (Loria et al., 2008, Bianchini, 2014, Lopes 2016).

The advantages of K-NN algorithm is that it is an excellent algorithm for creating prediction models where the data is very noisy and when the available dataset is large. The limitation of K-NN algorithm is that finding an optimal K would be time consuming. Moreover, the cost of computation is very high, as distance of every query instance to all the training samples is to be found out, although it can be reduced via indexing. It is also not clear as to which distance measure is to be used as well as which are the attributes which should be used in the analysis to produce the results.

2.10 Machine Learning Algorithm (Model) Evaluation Process

In order to evaluate the machine learning algorithm/model and to determine whether it will predict the target results correctly when the present set of data are used as well as when future data are used, the performance of the models is to be evaluated. The process adopted for the model evaluation and validation are as follows.

Overfitting normally occurs when a model has memorized the patterns occurring in training and evaluation data sources, but it has failed to generalize the patterns in data. An overfitted model will perform satisfactorily during the evaluation, but will not be able to make accurate predictions on any unseen data. To avoid an overfitted model, some data are to be preserved for use in validating the performance of the machine learning model. About 60% of the data may be used for training, and 20% of the data can be used for evaluation, and the remaining 20% of the data can be used for validation. Once the model parameters are chosen for the evaluation the second evaluation can be run using the validation data to ensure that the machine-learning model performs satisfactorily. If the test meets the expectations using the validated data, it is not over fitted. If a third set of data are used for the validation, the right machine learning model parameters are to be chosen to prevent overfitting. However, if the data from training process are considered for validation and evaluation, it means that only lesser data will be available for training purpose. This is a problem with using small data sets. It is always good to use a large data set in machine learning. Laboratory-based experiments generally result limited data set. However, if the laboratory-based models are used for field performance prediction, a large data set can be collected and can be used for the validation of the models.

Cross-validation refers to the process of evaluating machine learning models in which several ML models are trained on the subsets of the available input data, then evaluating them on a complementary subset of the data. Cross-validation can be used to detect overfitting. The k-fold cross validation is a common method for cross-validation. In this method, the input data is split into k subsets of data, which are also known as folds. A machine-learning model is then trained on all except one of the data sets; that is, the training is done with k-1 datasets. The evaluation of the model is then done using the subset that was not used for training. The training process is then repeated several times, using a different dataset for evaluation each time. This means the process is repeated k times.

Confusion Matrix also known as error matrix, is one of the ways to evaluate the prediction power of a classification model. Figure 2.5 shows a typical confusion matrix of a binary classification model.

Predicted Class

		Positive	**Negative**	
Actual Class	**Positive**	True Positive (**TP**)	False Negative (**FN**)	Sensitivity TP / (TP+FN)
	Negative	False Positive (**FP**)	True Negative (**TN**)	Specificity TN / (TN+FP)
		Precision TP / (TP+FP)	Negative Predictivity TN / (TN+FN)	Accuracy TP + TN / (TP+TN+FP+FN)

Figure 2.5: Confusion Matrix with Classification Metrics

In the above figure, True Positive (TP) would indicate the total number of correct predictions i.e. the total number of positive class correctly identified as positive by the model. False Negative (FP) would indicate the total number of incorrect predictions made by the model i.e. total number of positive class incorrectly identified as negative (Type II error). False Positive (FP) would also indicate the total number of incorrect predictions made by the model i.e. total number of negative class incorrectly identified as positive (Type I error). True Negative (TN) would indicate the total number of negative predictions i.e. the total number of negative class correctly identified as negative. The sensitivity also known as true positive rate is a measure of positive class identified as positive by the classifier. The specificity also known as true negative rate is a measure of negative class identified as negative by the classifier. In general, there should be high specificity. The precision is the ratio of total number of correctly classified class and the total number of predicted positive class. Accuracy is the proportion of the total number of predictions that the model is capable of identifying correctly.

Principal Component Analysis (PCA) is a technique that is used to find the underlying variables that can best differentiate the data points within a data set. The principal components are the dimensions along which the data points are found to be most spread out. Each principal component is a weighted combination either of different variables, where the weights can be positive, negative, or close to zero. PCA usually works well when the most informative dimensions have the largest spread and is orthogonal to each other. PCA is a multivariate statistical method that can be used for the reduction of high-dimension data to low-dimension and easily comprehensible data (that can be plotted on two or three axes) that retain factors that can explain most of the variance. PCA provides the covariance matrix (how predictors are associated with each other), eigenvectors (how the data are dispersed and the direction of dispersion), and eigenvalues (the relative significance of these directions) (Shlens, 2014)

Limitations of PCA are that the interpretation of the generated components is a challenge and it is very difficult to explain as why the variables are combined in a particular format. The PCA assumes that the dimensions with the largest spread of data points are useful. Moreover, PCA generated orthogonal principal components which would mean that the components are positioned at 90° to each other, which may not be true.

2.11 Conclusions from Literature Review

The following findings are reported in the available literature:

1. Moisture induced damage to the pavement system is due to several factors like binder type, composition, type of the asphalt mix, construction quality, duration of moisture on the pavement, intensity of rainfall, traffic level, pavement profile etc.
2. Several researchers have developed test methods that can be used to predict the moisture induced materials and mixes. The prediction depends on the adopted test method.
3. There is a need to identify suitable accurate method of predicting the moisture induced damage that may be adopted by State Departments of Transportation (DOTs) considering few variables that can be quickly measured in the field.
4. Machine learning can be an effective and useful tool for the identification poor and good performing mixes in terms of moisture induced damages.

3.0 RESEARCH METHODOLOGY AND LABORATORY INVESTIGATIONS

3.1 MATERIALS AND METHODOLOGY

Thirty plant-produced asphalt mixtures were procured from two US state DOTs for use in this study, of which six were good performing mixtures and 24 were poor performing mixes. The details of the asphalt mixes considered in the present investigation are shown in in Table 3.1.

The performance of the mixes was characterized as "good" or "poor" by the DOTs based on their experience and field observations regarding moisture induced damage. The poor mixes had shown premature failures in the field that resulted from moisture-induced damage. The mixes were heated and compacted to produce samples at the desired voids – 20 mixes from one DOT were targeted at 5 ± 1% air voids and ten mixes were targeted at 7 ± 1% air voids, according to the respective DOT specifications.

3.2 Moisture Conditioning

Moisture conditioning was carried out with the MiST. In the MiST conditioning system, a sample is placed inside a chamber that has a built-in bladder. The chamber is filled with water and maintained at the test temperature. The water is forced to flow in and out of the sample by pressurizing and depressurizing the bladder over a desired number of cycles. At the end of the desired number of cycles of pressurization, the sample can be removed and tested, and the test results can be compared with those from unconditioned samples to evaluate the moisture damage potential of the mix. The intensity of moisture-induced damage in MiST is reported to be dependent on the number of cycles and the duration of moisture saturation Tarefder *et al*. (2014). For this study, MiST test was executed at 3,500 cycles at 275 kPa and 60ºC for the PG 64-28 and PG 70-28 mixes and 50ºC for the PG 58-28 mix (ASTM 7870). A 20-hour dwelling period, in which the samples were kept immersed in water at the test temperature, was used prior to cycling in the MiST. The dwelling period was used to simulate the soaking period of water immediately after construction and before the passage of traffic. The use of the dwelling period was based on the work of LaCroix *et al.* (2016) and Varveri *et al*. (2014), who observed that the dwelling period allowed the diffusion of water into the asphalt-aggregate interface. The pre–MiST-conditioned and post–MiST-conditioned samples were subjected to different tests.

Table 3.1: Mix Information

Mix No. /perfor-mance	Nominal Max Agg. Size (NMAS) (mm)	Target construction voids (%)	Binder type	Percentage of binder	Percentage of Reclaimed Asphalt Pavement (RAP)	Additive
1/poor	12.5	5±1	PG 64-28	5.4	20	No
2/poor	12.5	5±1	PG 64-28	5.4	20	No
3/poor	9.5	5±1	PG 64-28	4.5	10	No
4/poor	9.5	5±1	PG 64-28	6.5	20	No
5/Good	9.5	5±1	PG 64-28	4.6	20	Lime
6/Good	12.5	5±1	PG 64-28	5.6	20	No
7/poor	9.5	5±1	PG 64-28	5.7	0	No
8/poor	12.5	5±1	PG 64-28	4.8	20	No
9/Good	9.5	5±1	PG 64-28	5.4	15	No
10/poor	12.5	5±1	PG 64-28	5.9	20	Lime
11/poor	12.5	5±1	PG 58-28	4.4	20	No
12/poor	12.5	5±1	PG 64-28	4.5	20	No
13/poor	12.5	5±1	PG 64-28	5.4	0	No
14/poor	12.5	5±1	PG 64-28	5.4	20	No
15/poor	12.5	5±1	PG 64-28	4.5	10	Lime
16/Good	9.5	7±1	PG 70-28	5.6	20	No
17/Good	9.5	7±1	PG 58-28	4.6	20	No
18/poor	9.5	7±1	PG 64-28	6.5	20	Commerc-ial
19/poor	12.5	7±1	PG 64-28	5.0	20	No
20/poor	12.5	7±1	PG 64-28	4.1	20	No
21/Good	12.5	7±1	PG 64-28	5.0	20	No
22/poor	12.5	7±1	PG 64-28	4.7	20	No
23/poor	12.5	7±1	PG 64-28	5.4	20	No
24/poor	12.5	7±1	PG 64-28	4.9	20	Novagrip
25/Good	12.5	7±1	PG 64-28	4.6	20	
26/poor	12.5	5±1	PG 64-28	5.0	20	PaveGrip
27/poor	12.5	5±1	PG 64-28	5.4	20	Zycosoil
28/poor	9.5	5±1	PG 64-28	5.6	20	No
29/poor	12.5	5±1	PG 64-28	4.6	20	No
30/poor	12.5	5±1	PG 64-28	5.6	20	No
31/poor	12.5	5±1	PG 64-28	5.2	20	No
32/poor	12.5	5±1	PG 64-28	0.9	20	No
33/poor	9.5	5±1	PG 64-28	0.8	10	Zycosoil
34/poor	12.5	5±1	PG 64-28	1.0	0	No
35/poor	12.5	5±1	PG 64-28	0.9	0	No
36/Good	12.5	5±1	PG 64-28	0.9	20	No
37/Good	12.5	5±1	PG 64-28	0.9	20	Zycosoil
38/poor	12.5	5±1	PG 64-28	0.8	20	Zycosoil

3.3 Tests for Characterization of Moisture Conditioned Samples

In order to evaluate the moisture susceptibility of an asphalt mixture, the mechanical capacity and integrity of the material needs to be evaluated pre- and post-moisture conditioning. The test procedures can be broadly classified as destructive versus non-destructive.

3.3.1 Indirect Tensile Strength (ITS)

The indirect tensile test (ASTM D6931) was used to determine the strength of the asphalt mixes. The test was conducted by loading a cylindrical across its vertical diametric plane at a specified rate of deformation (50 mm (2 in.) per minute) and at a test temperature of 25°C (77ºF). The peak load at failure was recorded and was used to calculate the ITS strength of the specimen. Tensile Strength Ratio (TSR) of the conditioned and unconditioned specimens are typically used as a measure of the moisture susceptibility and durability of asphalt mixtures. A higher ratio indicates a more moisture resistant mix.

3.3.2 Ultrasonic Pulse Velocity (UPV)

The UPV test is a method of non-destructive evaluation of an HMA specimen based on wave propagation techniques. Conventionally, UPV test has been extensively used as a measure to evaluate the quality of portland cement concrete mixes. The UPV test has a good potential to detect moisture susceptible HMA mixes because the measured seismic modulus (E_s) is sensitive to both of the deterioration effects of moisture, i.e. due to the effect of pore pressure because of presence of water in the pores after moisture conditioning, and due to the loss of integrity of the mix, as a result of loss in its cohesion or adhesion (Birgisson *et al*., 2003, Nazarian, 2005). The UPV test is based on the idea that the speed of compressional waves (P waves) passing through a medium depends on the medium's elastic properties and density. The time the wave travels through the specimen is measured as t_v, which is then used to calculate the samples bulk-constrained modulus and also bulk density (r). The seismic modulus (E_s) and design modulus of the sample can be derived from the calculated bulk-constrained modulus. The loss in E_s can be used utilized to detect moisture susceptibility, and the E_s values can also be transformed to design modulus (E_d)

to estimate the loss in structural capacity or service life as a result of moisture damage, with the help of available data/relationships as mentioned below.

The specimen dimensions were determined for each sample, and the compression wave (P-wave) Velocity, V_p was then calculated from the equation:

$$v_P = \frac{H}{t_v} \tag{3.1}$$

Where H is the height of the specimen and t_v is the corresponding travel time (mean of four transmission time readings per sample). The constraint modulus, M_V, was then calculated using:

$$M_v = \rho \times V_P^2 \tag{3.2}$$

Where ρ is the bulk density of the specimen in g/cc. The constraint modulus was then converted to Young's modulus, E_V, through a theoretically corrected relationship in the form of

$$E_v = M_V \times \frac{(1+\mu)\times(1-2\mu)}{(1-\mu)} \tag{3.3}$$

Where E_v is Young's modulus and μ is Poisson's ratio. The Poisson's ratio for all mixes was assumed to be 0.35. The E_v measured in this way is known as the seismic modulus, or E_s, which can be used to estimate the design modulus, E_d (Aouad *et al.*, 1993; Li, Y., & Nazarian, 2006).

$$E_d = \frac{E_s}{3.2 \times Temperature\ Correction\ Factor} \tag{3.4}$$

3.3.3 Semi-Circular Bending (SCB):

Fracture energy concepts have been widely used to link pavement cracking performance with an asphalt mix's mechanical properties. Fracture tests can be conducted in either single mode or mixed-mode conditions (tension, shear, or both). At present most of the current test procedures focus on the tensile model (Mode-I) where peak load is used to determine the fracture toughness of the material and the area under the load-displacement curve provides the fracture energy. This test was carried out according to the University of Illinois Method (AASHTO TP-124, Al-Qadi *et al.* 2005). Before conducting the test, a notch was cut using a tile saw blade at the center for all samples for a depth of 15 mm from the flat face of the specimen to initiate the crack propagation. The test was performed by imposing a small contact load of 0.1 ± 0.01 kN and then by loading at a rate of 50 mm/min. The test was stopped once the load dropped below 0.1 kN. The total work of fracture W_f was calculated by dividing the load-displacement data into two parts, that is, the curve prior to peak load and the curve after the peak load, and then numerically integrating the total area under the two parts. The total work of fracture is calculated using the integral equation

$$W_f = \int_0^{u_0} P_1(u)du + \int_{u_0}^{u_{final}} P_2(u)du \qquad (3.5)$$

Where U_{final} is the displacement at 0.1 kN cut-off load and U_0 is the displacement at peak load (kN). The fracture energy G_f was then found by dividing the work of fracture by the ligament area of the SCB specimen prior to testing.

$$G_f = \frac{W_f}{Area_{lig}} \times 10^6 \qquad (3.6)$$

Where:

G_f = fracture energy (Joules/m^2)

W_f = work of fracture (Joules)

P =load (kN)

Area $_{lig}$ = ligament length x×t, where t is the specimen thickness (mm)

The Flexibility Index (FI) is calculated from the parameters obtained from the load displacement curve.

$$FI = \frac{G_f}{|m|} \times A \qquad (3.7)$$

Where

FI= Flexibility Index

|m|= absolute value of post-peak load slope m (kN/mm)

A= 0.01

Figure 3.1 and 3.2 show the SCB testing and schematics of the test parameters calculated.

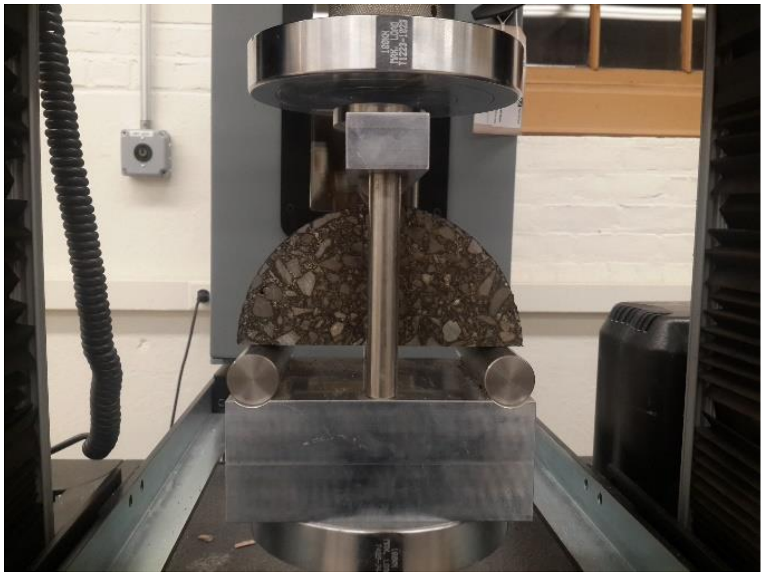

Figure 3.1: Semi-Circular Bending (SCB) Sample Test Setup

Fig 3.2 shows the schematic of the various parameters showing the displacement in the specimen with the load level.

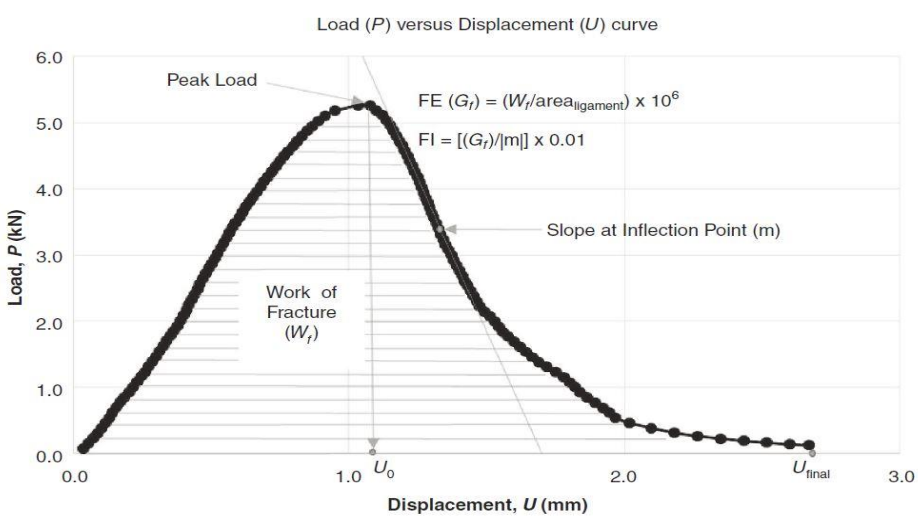

Figure 3.2: Schematic of Fracture Energy and Flexibility Index Parameters

3.4 Effluent Analysis

From the past moisture damage studies (Arepalli *et al.* 2017, Mallick *et al.* 2019) using MiST it has been reported that there is erosion of fine materials with increasing pressure cycles and also that there are traces of leached asphalt in water effluent after MiST conditioning. Field studies conducted by Maine DOT have reported loss of materials (both aggregates and asphalt) associated with moisture damage in HMA pavements (personal communication with Derek Nenerplante, Maine DOT, undated). Therefore, an effort has been made in this study to evaluate the type and the amount of both aggregate and asphalt binder lost from each sample during moisture damage conditioning using MiST equipment. For obtaining Dissolved Organic Carbon (DOC) DOC and Loss of materials (LOM) the ITS samples were individually tested using the Moisture Induced Stress Tester (MiST) and the effluent from the MIST were collected.

The effluent consisted of water, aggregates (broken, coated, and uncoated), and asphalt binder. The LOM was obtained by passing the effluent through 75 μm sieves followed by oven drying the sieves at 45°C (113ºF) for four hours. The weight of the material retained on this sieve was then measured in milligrams. The remaining fraction of the effluent was then subjected to filtration with 45-μm sieve and the DOC analysis was conducted to determine the amount of dissolved hydrocarbon present in the effluent. For DOC analysis a Shimadzu TOC-5000A analyzer was used, which works on the principle of oxidizing the carbon in the effluent to CO_2 and analyzing with a non-dispersive infrared (NDIR) gas detector to quantify the total carbon present. Similar research was performed by Zoftka *et al*. (2014), who found through spectroscopic analysis that results from MIST effluent contained peaks corresponding to asphalt as well as aggregates.

3.5 Image Analysis

Image analysis is a process of extracting meaningful information from a digital image using computer algorithms. The image analysis was performed in this study to quantify the impact of Moisture Induced Stress Tester (MIST) on the laboratory prepared HMA sample. For this, a two-dimensional image processing software named “Pixels” was used. The software enables determination of the number of black pixels before and after MIST testing. Images of the asphalt sample before and after MIST were taken using a high-resolution (16 megapixel) digital single-lens reflex (DSLR) camera under standard lighting conditions and camera settings. All the digital images taken were in RGB (Red-Green-Blue), which means that each individual pixel of that image had their own intensity of each color. Since asphalt is black in color and has a low RGB value, a threshold value of 50 was selected as inputs for the red, blue, and green in this software. An external image-editing software (Photoshop) was used to manually crop the pre-and post-MIST images to remove any background noise. The cropped pre-and post-MIST images of the same sample were uploaded to the software. The software then determined the total number of black pixels in each image with RGB values less than 50 and gave the total number of counted black pixels as output. Figure 3.3 shows the picture of the Pixels software that was developed at WPI specifically for this purpose. The output (i.e. the total number of black pixels in each image) is displayed at the bottom of the software. The percentage change in the black pixels was then calculated for each sample by finding the difference between the pre-MIST and the post-MIST black pixels.

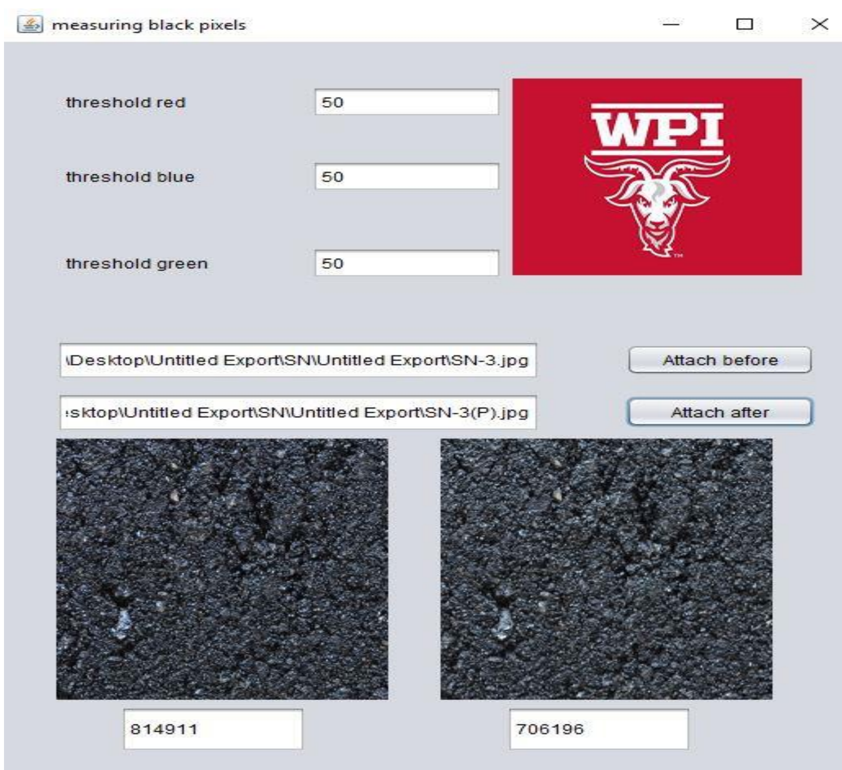

Figure 3.3: Pixels-Image Analysis Software

3.6 Fourier Transform-Infrared Spectroscopy (FTIR)

Asphalt essentially consists of a very large number of different hydrocarbons, heteroatoms (nitrogen, oxygen and sulfur) and/or metal traces (e.g. iron, vanadium and nickel). The heteroatoms form functional groups such as phenolics, pyrrolics, pyridinics, 2-quinolones, sulfoxides, ketones, carboxylic acids and anhydrides. Such functional groups play a major role in the interaction of asphalt and aggregate surfaces, thus determining the resistance of mixtures to damage to moisture. The strength of the interfacial bond depends on the relative tendency of the functional groups to adsorb on aggregate surfaces and relative water desorption. In general, the most adsorbed polar compounds (such as carboxylic acids and anhydrides) have been reported to be most easily displaced by water (Bagampadde 2005). Phenolics, ketones, and nitrogen bases (especially pyridinics) were associated with the highest resistance to water displacement. Asphalt rheology appears to influence the moisture sensitivity of bituminous mixtures during mixing and compaction. Viscosity must be sufficiently low to allow for proper wettability of the asphalt aggregate. High viscosity during service provides better resistance to damage to moisture than conversely. A high concentration of polar viscosity building asphalt components may increase moisture resistance. Carbonyls are typically found on the spectrum at 1700cm^{-1} and sulfoxides at 1030cm^{-1}in the FTIR spectrum. In this study, the carbonyl and sulfoxide groups are focused on, due to their ability to indicate stripping and aging in asphalt (Dony *et al.* 2016). In most asphalt binders, development of carbonyl and sulfoxide groups can be used to quantitatively assess the chemical interaction that has happened during the aging process. Determining carbonyl or sulfoxide indices (I_{CO} and I_{SO} respectively) by FTIR spectroscopy is used as a scientific tool in assessing the binder properties towards ageing of bituminous mixtures (Petersen *et al.* 2009, Hofko *et al.* 2018). Moisture damage in asphalt mixtures can cause stripping of asphalt materials, which in turn can increase the surface area to oxidation thereby increasing the I_{co} and I_{so} indices.

FTIR testing was carried out using a PerkinElmer Spectrum Two spectrometer with a universal Attenuated Total Reflectance (ATR) accessory. Figure 3.4 shows the FTIR spectrometer used for the FTIR testing. Before carrying out the experiments using the FTIR, a background scan was performed to remove unwanted peaks from the sample spectrum. In this study, 17 mixes were selected and the asphalt binders for these mixes were extracted using solvent extraction method (ASTM D5404).

Figure 3.4: Fourier-Transform Infrared Spectrometer (FTIR)

Around 0.1g of the extracted asphalt was rolled into a small ball and placed on the FTIR crystal as shown in Figure 3.5.

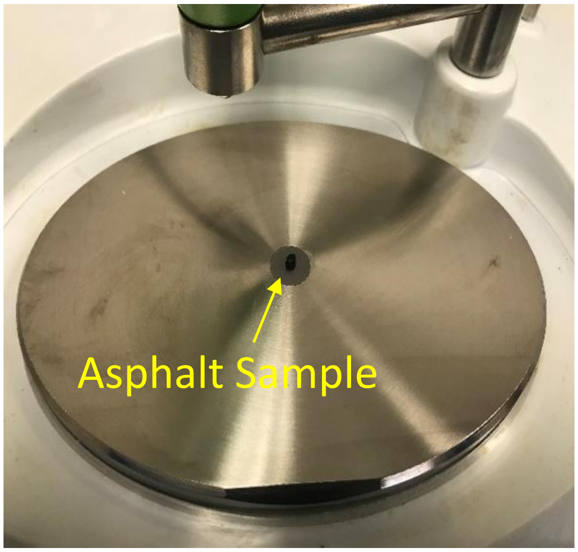

Figure 3.5: Extracted Asphalt Binder on ATR Crystal

The ATR detector was then lowered to scan and the absorption spectrum was acquired. The absorption spectrum data collected was in the wavelength range of 2000 cm^{-1} to 500cm^{-1}. The experiment was repeated thrice using different samples to check the repeatability in the test results. The results of the FTIR spectra are shown in Appendix A.

4.0 TEST RESULT AND ANALYSIS

4.1 Statistical Analysis

The average and standard deviation values of the different test results are presented in Table 4.1. For further analysis, the pre- and post-conditioned data from each test were used to calculate a ratio. The ratios are indicated in percentages for the ITS and the Es, and as absolute values for the other test properties.

Table 4.1: Average Values (Standard Deviation) of Various Test Parameters

DOC=Dissolved Organic Carbon; LOM=Loss of Material; BP=Black Pixel; FE=Fracture Energy; FI=Flexibility Index

Mix No	PreMiST E_s (MPa)	PostMiST E_s (MPa)	PreMiST ITS (kPa)	PostMiST ITS (kPa)	PreMiST FE ITS (J/m^2)	PostMiST FE ITS (J/m^2)	PreMiST FE SCB (J/m^2)	PostMiST FE SCB (J/m^2)	PreMiST FI	PostMiST FI	Effluent FM	DOC (mg)	LOM (mg)	PreMiST BP	PostMiST BP
1	13112 (1486)	13128 (635)	852 (53)	743 (128)	2087 (193)	2990 (386)	2587 (1232)	4681 (1860)	14.6 (8.5)	34.1 (13)	2.4 (0.7)	1.8 (2.3)	82.9 (45.6)	1063208 (69009)	1041372 (82148)
2	13167 (593)	12893 (337)	1074 (33)	991 (27)	3534 (571)	3936 (233)	4851 (2106)	7240 (2105)	16.4 (7.1)	45.7 (11.5)	2.4 (0.3)	9 (9.1)	99.4 (43.4)	1051937 (39056)	960522 (30532)
3	12309 (499)	10864 (451)	688 (85)	593 (43)	2360 (198)	3322 (192)	4483 (1387)	7251 (996)	20.7 (7.2)	95.9 (29.3)	2.1 (0.2)	6.7 (5.8)	113.3 (28.4)	1045671 (36253)	992049 (23633)
4	12610 (285)	11778 (712)	780 (98)	738 (140)	2294 (288)	3034 (261)	3209 (1613)	5303 (1001)	15.5 (9)	35.3 (15.2)	3 (1)	11.6 (1.3)	130.7 (24.5)	789592 (97652)	751128 (69122)
5	12397 (555)	11227 (421)	670 (57)	591 (31)	2131 (226)	2567 (154)	3461 (547)	3928 (499)	34 (4.8)	47.9 (19.8)	3.2 (0.6)	10.8 (0.9)	145 (37.8)	776914 (100174)	692640 (67104)
6	14575 (263)	13449 (284)	697 (21)	534 (19)	2109 (210)	2386 (9)	5505 (1498)	4865 (1897)	56.2 (31.9)	71.2 (63.7)	3.5 (0.6)	10.3 (2.2)	138 (29.7)	937804 (46491)	922528 (35054)
7	11384 (463)	8223 (255)	694 (44)	371 (20)	2343 (104)	1798 (250)	4407 (466)	2103 (337)	23 (8.8)	30.8 (6.5)	2.3 (1.1)	132 (29.2)	530.7 (320.3)	1128147 (31354)	1057240 (74015)
8	13125 (195)	13251 (261)	852 (229)	770 (87)	2577 (105)	3949 (94)	4384 (503)	10105 (444)	15.7 (4.1)	69.8 (13.7)	2.8 (0.1)	11 (13.6)	104.9 (57)	1128147 (37009)	1057240 (59697)
9	12094 (20)	10651 (2)	683 (76)	584 (25)	2428 (168)	3442 (224)	4380 (343)	8712 (437)	40.3 (5.2)	128.8 (34.5)	2.4 (0.1)	9.5 (0.3)	77.5 (18.7)	1081764 (103213)	1031301 (45152)
10	12390 (341)	12302 (847)	610 (79)	539 (22)	1820 (44)	2643 (137)	2825 (867)	5579 (1552)	12.8 (3.9)	42.6 (7.7)	3.3 (0.7)	11.5 (1.6)	200.9 (78.4)	1155357 (40011)	936062 (33197)
11	11642 (816)	11674 (155)	754 (66)	722 (3)	2437 (92)	3102 (14)	2700 (275)	5116 (1456)	15 (3.3)	40.1 (33.2)	2.7 (1.3)	10.5 (1.7)	278.7 (129)	1193266 (280976)	1093430 (43029)
12	9474 (111)	12142 (596)	692 (2)	563 (8)	2015 (100)	2871 (306)	4146 (1453)	6403 (1009)	21.6 (5.9)	44.5 (19)	2.6 (0.8)	15.6 (0.6)	96.5 (63.9)	1526461 (284257)	1391515 (206206)

Table 4.1: Average Values (Standard Deviation) of Various Test Parameters (Continued)

Mix No	PreMiST E_s (MPa)	PostMiST E_s (MPa)	PreMiST ITS (kPa)	PostMiST ITS (kPa)	PreMiST FE ITS (J/m²)	PostMiST FE ITS (J/m²)	PreMiST FE SCB (J/m²)	PostMiST FE SCB (J/m²)	PreMiST FI	PostMiST FI	Effluent FM	DOC (mg)	LOM (mg)	PreMiST BP	PostMiST BP
13	13471 (1342)	12901 (1034)	716 (5)	684 (7)	2089 (31)	3412 (306)	3812 (1719)	9889 (1429)	27.3 (13.1)	89.9 (31.7)	2.2 (0.6)	14.8 (0.6)	184.7 (174)	1053014 (110123)	1145165 (37727)
14	13213 (613)	12562 (327)	720 (119)	684 (26)	1700 (47)	2754 (4)	3297 (732)	6649 (559)	11.3 (4.5)	37.6 (8.1)	3.6 (0.1)	10.9 (1.1)	334.9 (321.9)	1141154 (13203)	1217756 (57331)
15	13056 (253)	10345 (281)	588 (216)	433 (2)	1885 (16)	2347 (129)	7598 (1040)	9162 (873)	45.6 (8.7)	93.5 (17.4)	3 (0.1)	11 (2.6)	104.9 (90)	1128147 (31354)	1057240 (74015)
16	13727 (534)	14714 (721)	932 (49)	931 (76)	2912 (46)	3921 (364)	4118 (441)	6649 (559)	24.5 (4.9)	37.6 (8.1)	3.1 (1.1)	12.1 (1.5)	190.9 (35.3)	1113326 (54664)	1086906 (52219)
17	12057 (259)	11287 (414)	546 (54)	405 (16)	1932 (101)	2504 (132)	4753 (386)	6226 (567)	47.4 (6.6)	90.1 (48.8)	2.6 (0.5)	8.3 (0.9)	308.4 (209.2)	1042742 (58201)	992659 (25024)
18	11694 (569)	11143 (494)	541 (99)	484 (28)	1622 (80)	2067 (160)	1548 (456)	2119 (141)	11.3 (1.8)	25.6 (5.9)	2.5 (0.2)	9.9 (3.1)	155.3 (19)	1106379 (38458)	977332 (61942)
19	11697 (523)	10054 (637)	400 (160)	308 (2)	1688 (28)	2259 (157)	1793 (98)	4045 (633)	23.8 (3)	83.3 (47.7)	2.7 (0.6)	10.2 (3.8)	130.9 (42.6)	1193434 (73273)	1209652 (51956)
20	12290 (317)	11275 (414)	647 (11)	550 (22)	2265 (149)	2549 (406)	2116 (170)	4414 (2479)	15.9 (3.8)	28.9 (8.5)	3 (0.2)	10.1 (0.7)	50.5 (8.8)	1118450 (52473)	920488 (75030)
21	12479 (308)	11301 (234)	650 (8)	525 (34)	2192 (140)	3209 (106)	2066 (149)	3969 (1645)	12 (1.1)	42.9 (7.3)	2.6 (0.3)	10.5 (1.2)	65.1 (18.5)	1190532 (28745)	1148747 (9819)
22	13895 (790)	12734 (606)	641 (85)	622 (54)	2399 (21)	2972 (231)	2403 (300)	4269 (513)	17.2 (2.1)	92.7 (36.5)	2.3 (0.4)	17.5 (1.7)	474.9 (69.2)	1068219 (31375)	1021573 (41909)
23	11856 (242)	11410 (437)	504 (136)	397 (14)	2151 (217)	2902 (210)	2005 (259)	3077 (404)	25.7 (8.1)	69.2 (27.5)	2.6 (0.2)	11.1 (0.5)	102.6 (16.1)	1184374 (78605)	1193382 (71180)
24	12245 (450)	11525 (571)	801 (29)	750 (34)	2350 (92)	3207 (86)	1540 (205)	2251 (125)	7.1 (2.3)	17.8 (1.9)	2.8 (0.3)	10.8 (0.7)	96.2 (27)	1128147 (31354)	1057240 (74015)
25	12229 (647)	12806 (342)	603 (100)	504 (80)	2035 (160)	3085 (261)	2152 (451)	3050 (764)	11 (6.3)	39.9 (22.5)	3.2 (0.2)	17.8 (0.8)	103.2 (43.4)	1238704 (67104)	1258733 (46491)

Table 4.1: Average Values (Standard Deviation) of Various Test Parameters (Continued)

Mix No	PreMiST E_s (MPa)	PostMiST E_s (MPa)	PreMiST ITS (kPa)	PostMiST ITS (kPa)	PreMiST FE ITS (J/m^2)	PostMiST FE ITS (J/m^2)	PreMiST FE SCB (J/m^2)	PostMiST FE SCB (J/m^2)	PreMiST FI	PostMiST FI	Effluent FM	DOC (mg)	LOM (mg)	PreMiST BP	PostMiST BP
26	12376 (836)	13341 (338)	950 (31)	883 (16)	3862 (231)	4432 (414)	2825 (327)	5116 (615)	12.8 (4.5)	40.1 (12.4)	2.4 (0.1)	20.1 (0.2)	111.5 (320.3)	1245242 (57331)	1165598 (103213)
27	10928 (332)	11547 (234)	688 (28)	581 (22)	2903 (250)	3646 (234)	3209 (494)	5116 (982)	15.5 (1.3)	30.8 (34.4)	3 (0.6)	10.4 (2.3)	121.8 (18.7)	1275936 (75030)	1221627 (54664)
28	12180 (342)	11955 (425)	614 (149)	585 (20)	1910 (210)	3198 (100)	3683 (437)	2175 (1014)	9.8 (3.2)	30.9 (55.4)	3.1 (0.9)	8.6 (0.9)	92.5 (63.9)	1190931 (69122)	1069193 (100174)
29	10737 (435)	10621 (321)	608 (66)	520 (21)	2112 (168)	3123 (46)	1992 (229)	1895 (871)	10.5 (5.2)	16.7 (17.6)	2.9 (0.7)	12.8 (1.7)	89.6 (19)	1121847 (57331)	1075040 (284257)
30	12032 (433)	11231 (232)	660 (98)	701 (94)	2491 (46)	3167 (217)	1579 (160)	1779 (516)	10 (1.3)	9.7 (65.3)	2.4 (0.5)	18.5 (1.1)	132.9 (69.2)	1025832 (41909)	1064303 (52473)
31	11492 (342)	11411 (326)	728 (92)	682 (46)	2151 (119)	2574 (94)	2119 (100)	3297 (817)	15.9 (2.8)	21.6 (43.8)	2.8 (0.6)	15.2 (0.8)	180.6 (27)	1137560 (31354)	1120041 (67104)
32	11577 (143)	12719 (625)	925 (86)	845 (20)	2778 (168)	3268 (4)	1689 (149)	2011 (715)	5.9 (8.5)	11.1 (15.4)	2.3 (0.1)	12.3 (0.9)	116.9 (18.3)	1234734 (103213)	1064744 (57331)
33	10388 (69)	11652 (394)	985 (22)	982 (86)	3456 (166)	4579 (244)	6820 (633)	7743 (717)	18.6 (4.2)	27.85 (43.6)	3.1 (0.3)	7.5 (0.7)	165.2 (16.1)	1125671 (28745)	982149 (9819)
34	12352 (512)	11835 (83)	846 (62)	729 (27)	2448 (94)	3794 (2232)	4185 (652)	6650 (595)	11.62 (3.4)	37.61 (33.5)	2.7 (0.4)	12.4 (0.5)	157.8 (18.7)	947814 (31375)	952518 (46491)
35	12165 (294)	11705 (545)	755 (26)	616 (44)	2481 (311)	3903 (330)	5503 (342)	2685 (943)	15.1 (5.4)	11.19 (23.7)	3.2 (0.6)	9.5 (1.2)	120.4 (18.5)	1256357 (78605)	916032 (54664)
36	11690 (278)	12207 (24)	849 (28)	859 (39)	3096 (1816)	4339 (2552)	4844 (537)	7032 (842)	13.4 (4.3)	48.5 (25.4)	2.1 (0.2)	11.4 (0.8)	86.25 (63.9)	1218603 (67104)	1258732 (41909)
37	11356 (39)	12631 (439)	960 (134)	887 (150)	3228 (1912)	3472 (2130)	5102 (519)	7140 (759)	15.2 (5.6)	45.2 (28.5)	2.3 (0.7)	15.351 (2.3)	90.153 (43.4)	1236560 (57331)	1220240 (71180)
38	10914 (554)	12702 (231)	1004 (37)	896 (41)	3197 (149)	4541 (245)	4293 (236)	5871 (854)	12.6 (2.6)	38.7 (45.5)	2.1 (0.9)	11.364 (1.7)	111.9 (320.3)	1221647 (69122)	1175139 (103213)

4.2 Discussion

The average values of pre-MiST seismic modulus ranged from 14,547 MPa (14.547 GPa) to 9,474 MPa (9.474 GPa) with mix no. 6 showing the highest value and mix no. 12 showing the lowest value. The standard deviation was higher for mix no.1, which is a poor mix compared to mix no. 9, which is a good mix. For the post-MiST seismic modulus, the average values ranged from 14,714 MPa to 8,223 MPa. mix no. 16 had the highest value and mix no.7 had the lowest value. The variance of the post-MiST seismic value was the highest for poor mix no.13 and lowest for good mix no.9. The mean pre-MiST ITS values ranged from 1074 kPa to 400 kPa. mix no. 2 had the highest pre-MiST ITS value and the mix 19 had the lowest value. The standard deviation ranged from 229.0 for mix 8 to 2.0 for mix 12 both of which are poor mix. The mean for the post MiST ITS value ranged from 991 to 308 with the highest post-MiST ITS value for mix 2 and lowest being for mix 19. The standard deviation for the mixes ranged from 140.0 for mix 4 and 2.0 for mix 19 both of which are poor mixes. For the pre-MiST ITS the average values for the mixes ranged from 3,862 J/m^2 to 1,622 J/m^2 with mix 26 having the higher value and mix 18 having the lower value. The standard deviation for the mixes were in between 571 and 16. In the post-MiST FE ITS property we can see that mean was varying between 4,432 J/m^2 to 1,798 J/m^{2}for mixes 26 and 7, respectively, both being poor mixes. The standard deviation in this test property was in between 4 and 414 In the pre-MiST SCB-FE, the average values were in between 7,598 J/m^2 to 1,540 J/m^2, with the highest value corresponding to mix 15 and the lowest corresponding to mix 18. The standard deviation for this test property ranged from 2,106 for mix 2 to 98 for mix 9. For the post-MiST SCB-FE, the mean was from 10,105 J/m^2 to 1,779 J/m^2 with the maximum value corresponding to mix 8 and the lowest value corresponding to mix 30.

4.3 FTIR Data Average Values and Discussions

The FTIR spectra of all the extracted samples were carried out and absorption spectrum data collected was in the wavelength range of 2000 cm^{-1} to 500 cm^{-1}. A sample spectrum of VTP2 (poor performing mix) sample before and after conditioning is shown in Figure 4.1 and peaks of carbonyl and sulfoxide groups are highlighted. The carbonyl or sulfoxide indices (I_{CO} and I_{SO}

respectively) were determined from the FTIR spectrum using equations as shown below (Equation 4.1 and 4.2).

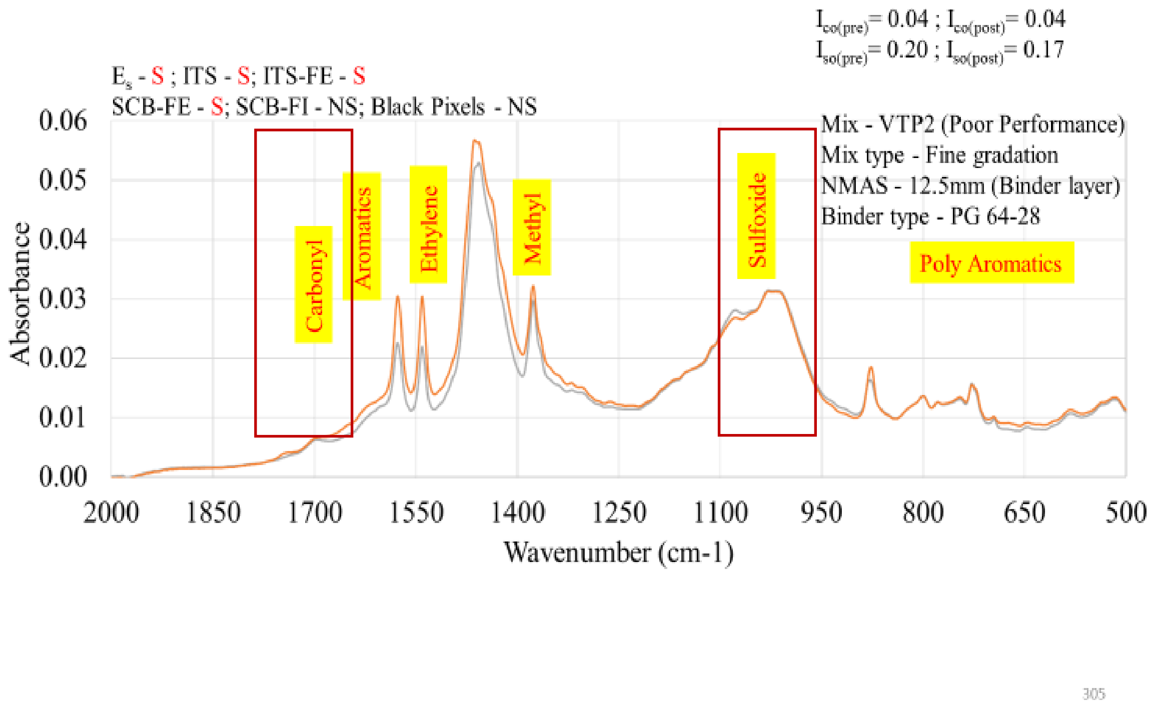

Figure 4.1 A Sample FTIR Spectra with Peaks at Carbonyl and Sulfoxide Groups (Highlighted)

I_{CO} is calculated according to the following equation (Dony *et al.* 2016):

$$I_{co} = \frac{A_1}{A_0} \tag{4.1}$$

A_1 is the peak area of carbonyl group at 1700 cm^{-1}, A_o is the area of peaks referred to ethylene and methyl groups selected as reference peaks and centered at 1460 and 1375 cm^{-1} respectively. I_{SO} is calculated according to the following equation (Dony *et al.* 2016):

$$I_{so} = \frac{A_2}{A_0} \tag{4.2}$$

A_2 is the peak area of sulfoxide group at 1030 cm^{-1}. Table 4.2 represents the calculated I_{CO} and I_{SO} indices for all the 17 mixes used for the study.

Table 4.2 Indices from FTIR (I_{co} and I_{so})

Mix	I_{CO}		I_{SO}	
	Pre-MiST	Post-MiST	Pre-MiST	Post-MiST
1	0.06	0.05	0.24	0.13
2	0.06	0.05	0.15	0.11
3	0.09	0.05	0.10	0.12
4	0.07	0.08	0.28	0.27
5	0.05	0.07	0.08	0.16
6	0.07	0.05	0.10	0.14
7	0.07	0.11	0.21	0.26
8	0.06	0.04	0.20	0.12
9	0.07	0.08	0.33	0.38
10	0.04	0.04	0.09	0.08
11	0.04	0.04	0.20	0.17
12	0.06	0.08	0.18	0.24
13	0.07	0.04	0.16	0.14
14	0.06	0.09	0.24	0.25
15	0.08	0.08	0.25	0.26
16	0.10	0.09	0.28	0.28
17	0.06	0.03	0.17	0.14

The following observations are made:

1. I_{SO} values were found to be higher compared to I_{CO} values for all the samples.
2. For mixes seven and twelve, the Post MiST indices were found to be higher. These mixes were poor performance mixes and the slight increase in the indices can be attributed to the aging due to moisture conditioning.

Statistical analysis such as Analysis of Valiance (ANOVA) was carried out using the two indices. It can be seen from the statistical analysis in Table 4.3, that in most of the mixes no significant change was observed between the pre-MiST and the post MiST I_{co} and I_{so} indices. Thus, it can be inferred that moisture damage did not cause enough aging so as to see an increase in the I_{CO} and I_{SO} indices.

4.4 Statistical Analysis and Results Including FTIR Data

The results from all tests were analyzed using Analysis of Valiance (ANOVA) to detect significant difference between the pre- and post-MiST samples. The hypothesis was that poor mixes will show significant differences whereas good mixes will not. Table 4.3 shows a summary of these tests. The results show that significant differences were found between the mixes when the FTIR data were analyzed. There is no single test that is consistently accurate for detecting both good and poor mixes. It can be inferred from Table 4.4 that the properties can be listed in terms of their effectiveness., as: (from high to low): SCB-FI, SCB-FE, E_s, ITS, ITS-FE, and BP. The prediction accuracy was computed as the sum of number of true positives (TP) and true negatives (TN) divided by the number of true positives, true negatives, false positives, and false negatives (Total Observations).

$$Accuracy = \frac{(True\ Positive\ (TP) + True\ Negative\ (TN)}{Total\ Observations\ (n)} \qquad (4.3)$$

For Example, from Table 4.3 the accuracy for Es is calculated as follows:
The total number of True Positive (TP) = 6; (i.e. good mixes identified as good mixes by statistics)
The total number of True Negative (TN) = 9; (i.e. poor mixes identified as poor mixes by statistics)
Total number of observations (n) =38

$$E_s\ Accuracy = \frac{6+9}{38} = 39.5\% \qquad (4.4)$$

Table 4.3: Statistical Analysis Results

(YES and NO indicates presence and absence of significant difference, respectively)

Mix	E_s	ITS	ITS – FE	Black Pixels	SCB-FE	SCB-FI	FT-IR		Performance
							Carbonyl	Sulfoxide	
1	NO	NO	YES	NO	NO	YES	NO	NO	POOR
2	NO	YES	NO	YES	NO	YES	NO	NO	POOR
3	YES	NO	YES	YES	YES	YES	NO	NO	POOR
4	NO	NO	YES	NO	YES	NO	NO	NO	POOR
5	YES	NO	NO	NO	NO	NO	NO	YES	GOOD
6	NO	NO	NO	NO	NO	NO	NO	NO	GOOD
7	NO	NO	YES	NO	NO	YES	NO	NO	POOR
8	YES	YES	YES	YES	YES	YES	YES	NO	POOR
9	NO	NO	YES	NO	YES	YES	YES	YES	GOOD
10	NO	NO	YES	NO	YES	YES	YES	NO	POOR
11	NO	NO	YES	NO	YES	YES	YES	YES	POOR
12	NO	NO	YES	NO	NO	NO	NO	NO	POOR
13	NO	NO	YES	NO	YES	YES	NO	NO	POOR
14	NO	NO	YES	NO	YES	YES	NO	NO	POOR
15	NO	NO	YES	NO	YES	YES	NO	NO	POOR
16	YES	YES	YES	NO	NO	YES	NO	NO	GOOD
17	YES	YES	YES	NO	YES	NO	YES	YES	GOOD
18	NO	NO	YES	NO	YES	NO	NO	NO	POOR
19	YES	YES	YES	NO	NO	YES	NO	NO	POOR
20	NO	NO	YES	NO	NO	YES	NO	NO	POOR
21	NO	YES	YES	NO	NO	NO	YES	NO	GOOD
22	NO	NO	YES	NO	NO	NO	NO	NO	POOR
23	YES	YES	NO	YES	NO	YES	NO	NO	POOR
24	YES	YES	NO	NO	NO	NO	NO	NO	POOR
25	NO	NO	YES	NO	NO	YES	-	-	GOOD
26	YES	NO	YES	NO	NO	YES	-	-	POOR
27	YES	NO	YES	NO	YES	YES	-	-	POOR
28	NO	NO	YES	NO	YES	NO	-	-	POOR
29	NO	NO	YES	NO	NO	NO	-	-	POOR
30	NO	NO	YES	NO	NO	YES	-	-	POOR
31	NO	NO	YES	NO	NO	YES	-	-	GOOD
32	YES	NO	YES	NO	YES	YES	-	-	POOR
33	YES	NO	YES	NO	YES	NO	-	-	POOR

Table 4.3: Statistical Analysis Results (Continued)

Mix	E_s	ITS	ITS – FE	Black Pixels	SCB-FE	SCB-FI	Carboxyl	Sulfoxide	Performance
34	NO	YES	NO	NO	NO	**YES**	-	-	POOR
35	NO	YES	**YES**	NO	NO	**YES**	-	-	POOR
36	NO	NO	**YES**	NO	NO	**YES**	-	-	GOOD
37	NO	NO	NO	NO	NO	**NO**	-	-	GOOD
38	NO	YES	**YES**	NO	NO	**NO**	-	-	POOR

The following accuracies were obtained for each of the properties.

Table 4.4: Statistical Accuracy

No	Test Property	Accuracy (%)
1	SCB-FI	65.8
2	SCB-FE	52.6
3	Es	39.5
4	ITS	36.8
5	ITS-FE	73.7
6	BP	34.2

4.5 Use of Radar Chart to Evaluate Multiple Criteria Based on Multiple Test Properties

The multi variate data can be displayed ina graphical form using a radar chart. The radar chart may display three or more variables that can be quantified. The axes for the variables start from the same point. In the graphical representation, the relative position as well as the angle of the axes are not important. The relative position of the points reveal the distinct correlations and other information which can be used to compare the importance of the different variable influencing the dependent variable.

Since no individual property was found to have a high degree of accuracy, one option could be the use of multiple properties using radar charts, and comparing a radar chart of a good mix to any other mix in question. The radar chart was prepared to understand the relative difference between the mixes, by normalizing the values with respect to those of the best performing mix

(mix 16). Such a chart can be utilized by DOTs on a regular basis for comparative evaluation of mixes. For example, Figure 4.2 shows two radar charts – one for a good mix (mix 21) and another for a poor mix (mix 7).

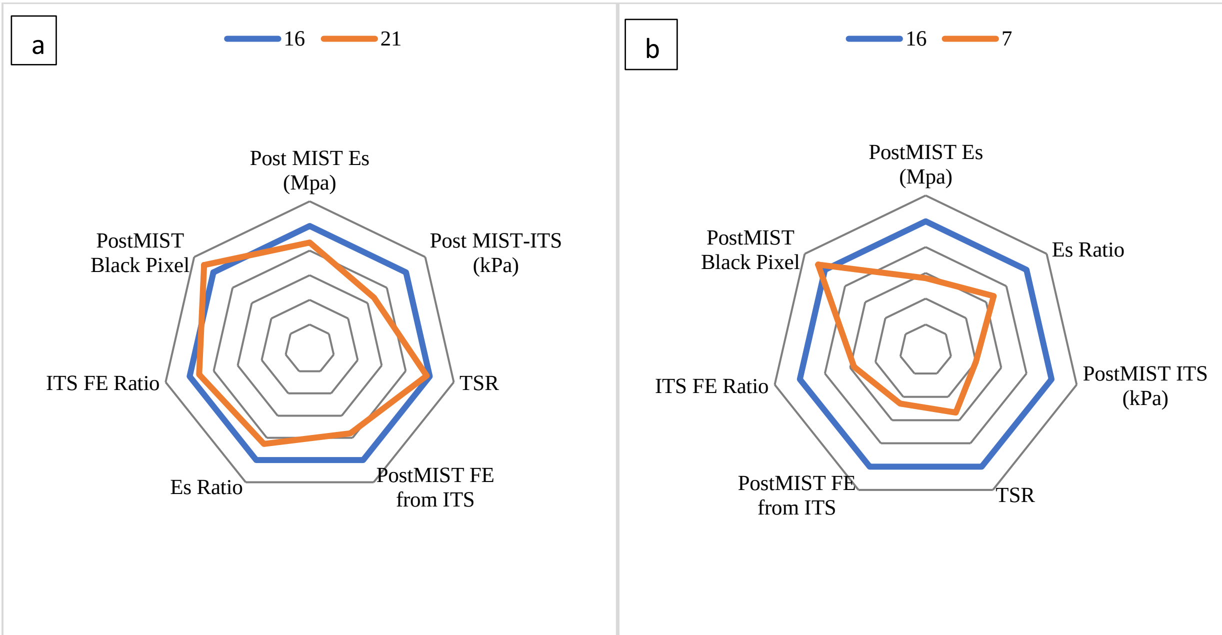

Figure 4.2: Radar Chart a) Good Mix; b) Poor Mix

It can be inferred from the figure that the imprints on the charts are different for the two mixes. The good mix 21 has post MiST black pixels, Es ratio, TSR, ITS-FE ratio properties similar to mix 16, whereas the poor mix 7 has lower values for the same properties in comparison to mix 16.

5.0 APPLICATION OF MACHINE LEARNING IN MOISTURE INDUCED DAMAGE PREDICTION IN HOT MIX ASPHALT

5.1 Study Approach

The approach adopted in this research is illustrated with a flowchart in Figure 5.1.

Step 1: A dataset of test properties of mixes and classifications were collected according to their field performance: In this step, the data on test properties of mixes and materials, and their performance, related parameters or actual performance in the field were compiled. This step forms the backbone of the entire process. The bigger the dataset, the more robust and reliable will be the predictions.

Step 2: A correlation analysis was performed on the experimental dataset to isolate uncorrelated (relevant) properties: To identify the relevant variables, the test properties collected in Step 1 were subjected to a correlation analysis and pairs of properties whose correlation coefficient exceeds 0.8 were identified. For each of these pairs, the test property, which can be obtained relatively easily, was retained for further analysis.

Step 3: A Principal Component Analysis (PCA) was performed. The purpose of the analysis is to reduce the dimensions and identification of the first three PCs that can identify most of the variance in the data.

Step 4: Using the PCAs as predictors and performance as target, appropriate ML methods were used to identify the best model, with the highest accuracy

Step 5: The ML model was developed in step 4 by building an App with features to check the quality of the mix with input parameters from the user.

Step 6: The mixes were classified as "good" by the ML model, as a possible option for the designer to accept or reject a mix.

Figure 5.1 shows the overall framework for the application of Machine Learning technique to identify mixes that are susceptible to moisture induced damages.

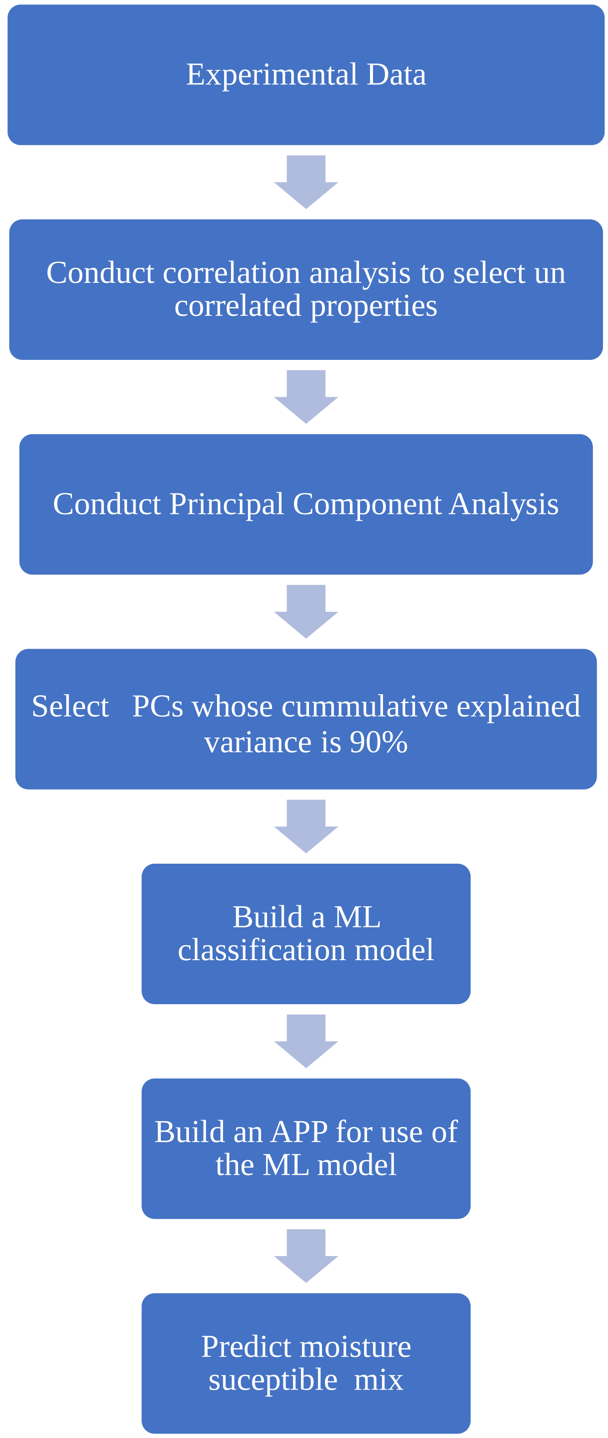

Figure 5.1: Flowchart of ML Framework Steps

5.2 Results of ML Analysis

5.2.1 Correlation Analysis

The test data were first subjected to a correlation analysis to determine whether there are factors that are strongly correlated to each other. Figure 5.2 shows the results of the analysis where a higher correlation (R = 0.66) between the FE SCB Ratio and FI ratio was found. Therefore, in further analysis, only FI ratio was utilized.

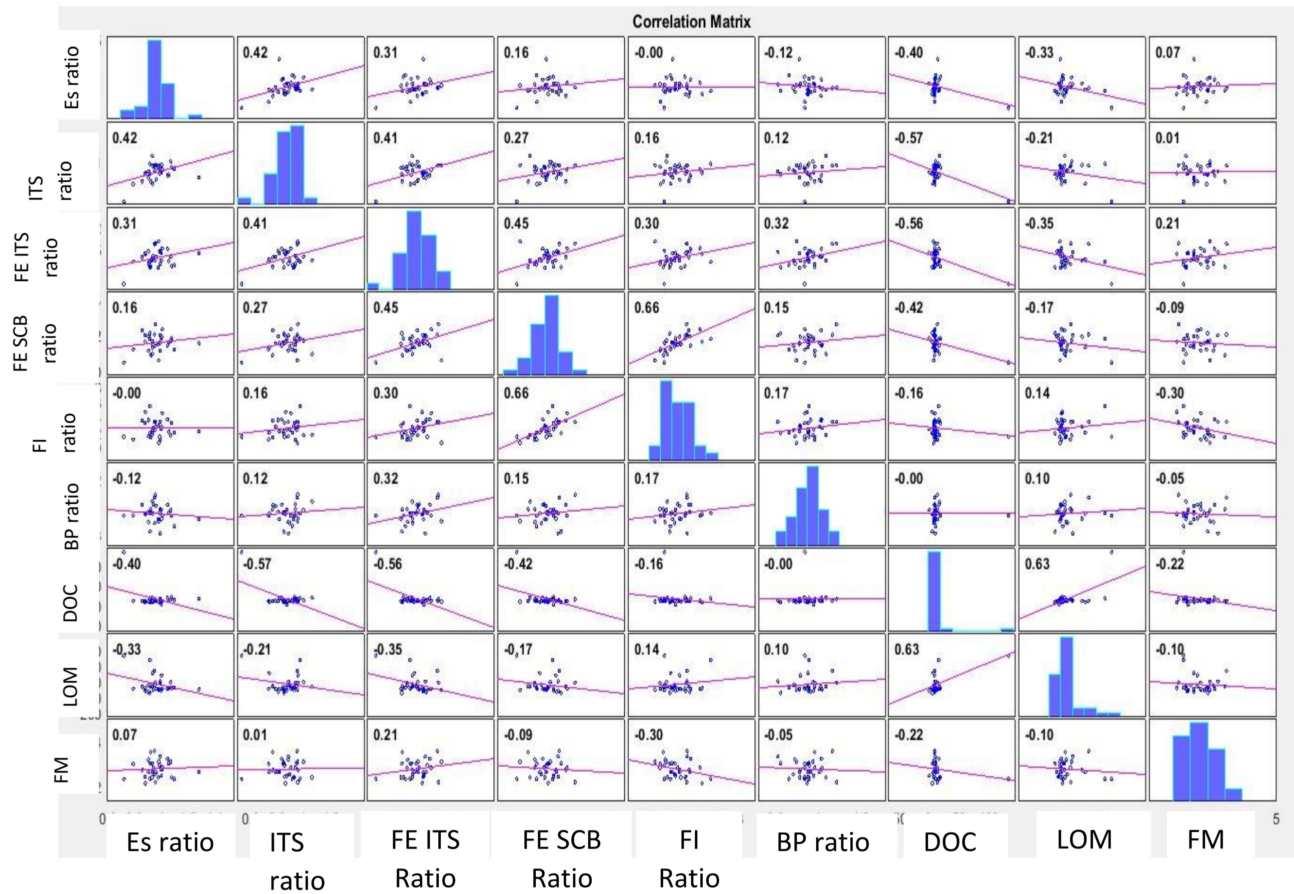

Figure 5.2: Correlation of Variables

A number of variables were explored in this study, and it was necessary to determine which of them were important and which could be eliminated from further analyses without causing a significant loss of quality of the data. This was accomplished with PCA. First, PCA was carried out with all of the test property variables: E_s ratio, ITS ratio, FE ITS ratio, FI ratio, BP ratio, DOC, LOM, and FM. Figure 5.3 shows the results of PCA in the form of a Pareto chart, which highlights the most important set of factors that explain the effects. The x-axis shows the seven principal components obtained after the analysis, the bars show the individual variance, and the line shows the cumulative variance. The chart shows that the first three PCs can explain 70% of variance in the data. The coefficients of principal components 1, 2, and 3 can be seen in Table 5.1. A contribution value was calculated by summing the products of the variance of each principal component with the coefficients of each of the variables.

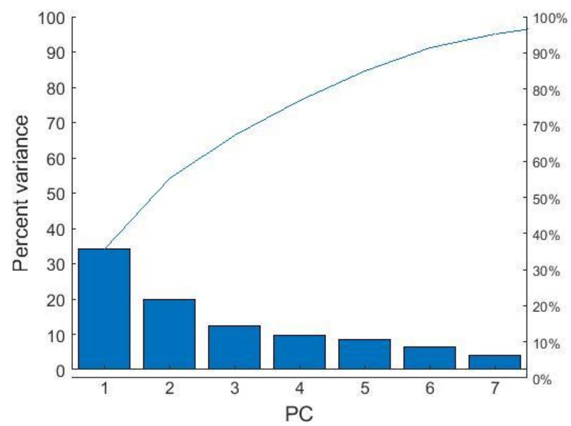

Figure 5.3: Pareto Chart Showing the Percent of Variance in The Data Explained by The First Six Principal Components (PC)

Table 5.1: Coefficients for the Different Predictors for PC 1, PC 2, and PC 3

PC	Es ratio	ITS ratio	FI ratio	BP ratio	DOC	LOM	FM
1	-0.37	-0.43	-0.46	-0.11	-0.07	0.53	0.39
2	-0.16	0.14	0.23	0.62	0.50	0.07	0.31
3	-0.33	-0.15	0.31	-0.22	0.55	0.02	0.10

Next, a contribution value was calculated by summing the products of the variance of each principal component with the coefficients of each of the variables (as shown in Table 5.1). The contribution value of each variable toward the composite principal component is shown in Figure 5.4. This shows that E_s ratio, DOC, ITS, BP ratio are the most significant variables in that they explain most of the variances in the data.

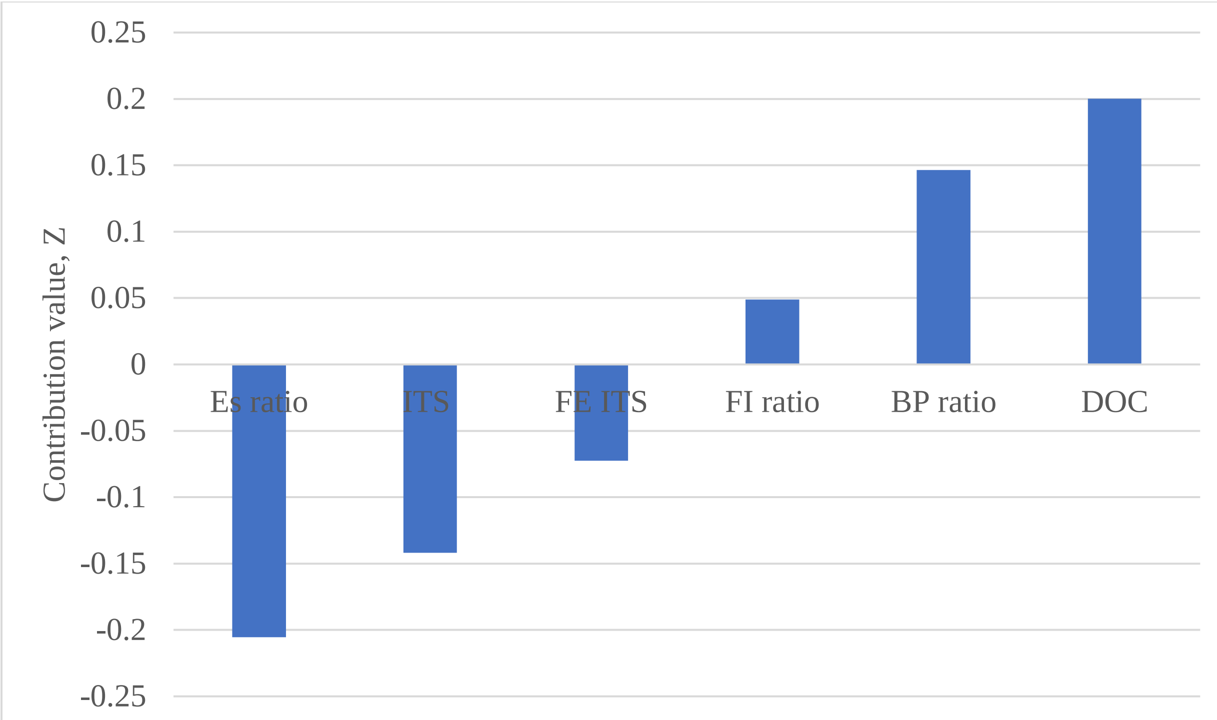

Figure 5.4: Contribution of the Different Variables Towards the Composite Principal Component

Next, PCA was carried out again with only E_s ratio, ITS ratio, DOC, and BP ratio as the variables. The Pareto chart (Figure 5.5) shows that principal components 1, 2, and 3 can explain 90% of the variance. The coefficients of the first three principal components are shown in Table 5.2. These coefficients were used to calculate the contributions of each of the variables, which are shown in Figure 5.6.

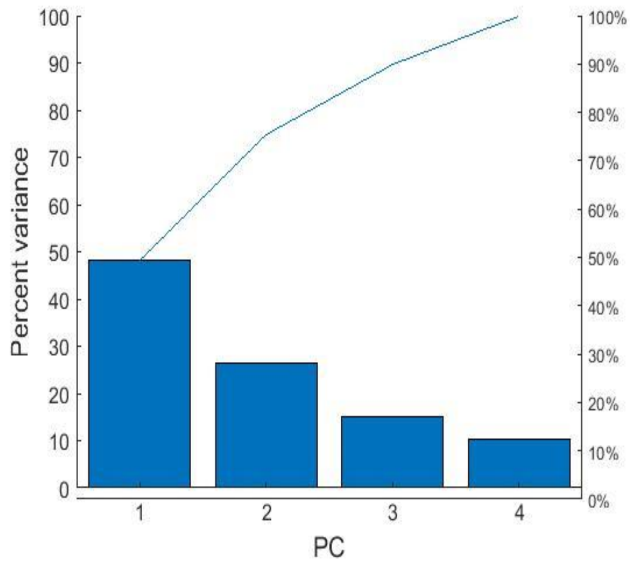

Figure 5.5: Pareto Chart showing the Percent of Variance in the Data Explained by the First Four Principal Components (PC)

Table 5.2: Coefficients for the Different Predictors for PC 1, PC 2 and PC 3

PC	Es ratio	ITS ratio	FE ITS ratio	BP ratio	DOC
1	-0.42	-0.52	-0.50	-0.12	0.54
2	-0.42	-0.06	0.32	0.84	0.11
3	0.76	0.00	-0.18	0.38	0.50

Figure 5.6 shows the contribution value of each variable. The contribution values were then used to estimate the composite scores of the mixes by multiplying the normalized value by the contribution value as shown in Figure 5.7. Also, a high value of composite score was found for mix 17, which exhibited good performance in the field.

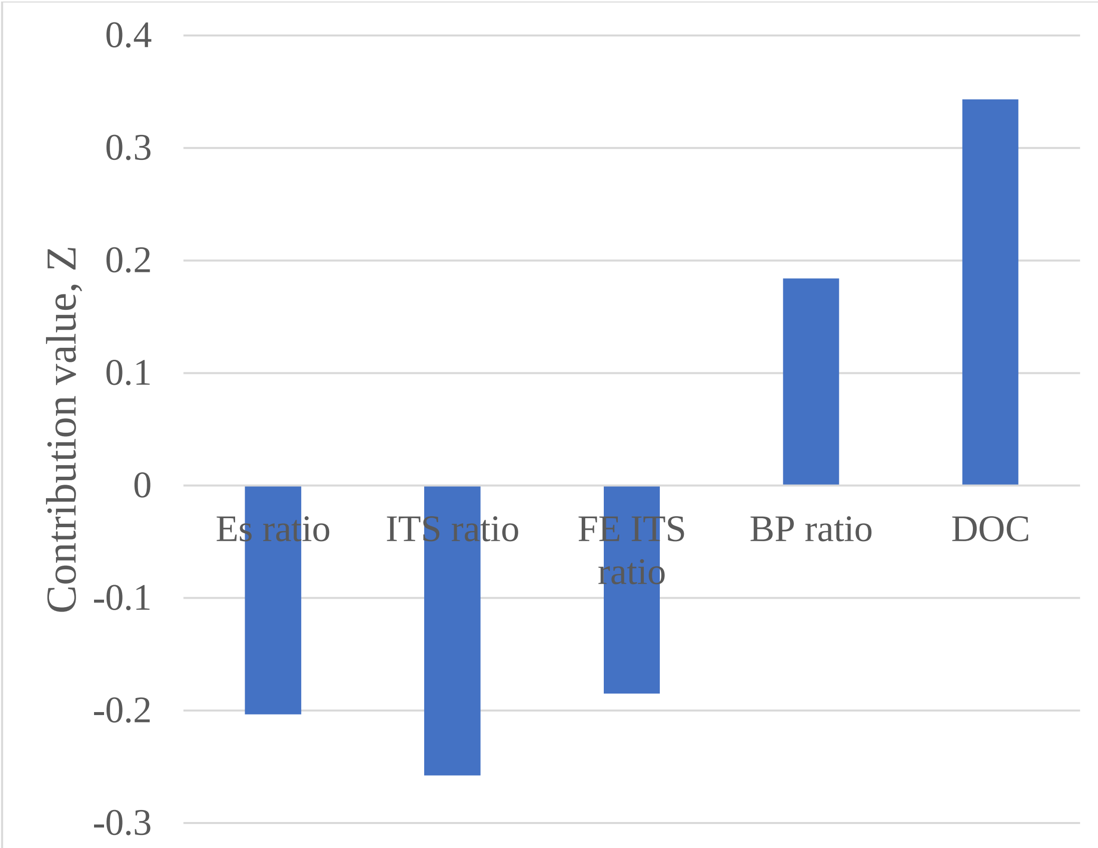

Figure 5.6: Contribution of the Different Variables Towards the Composite Principal Component

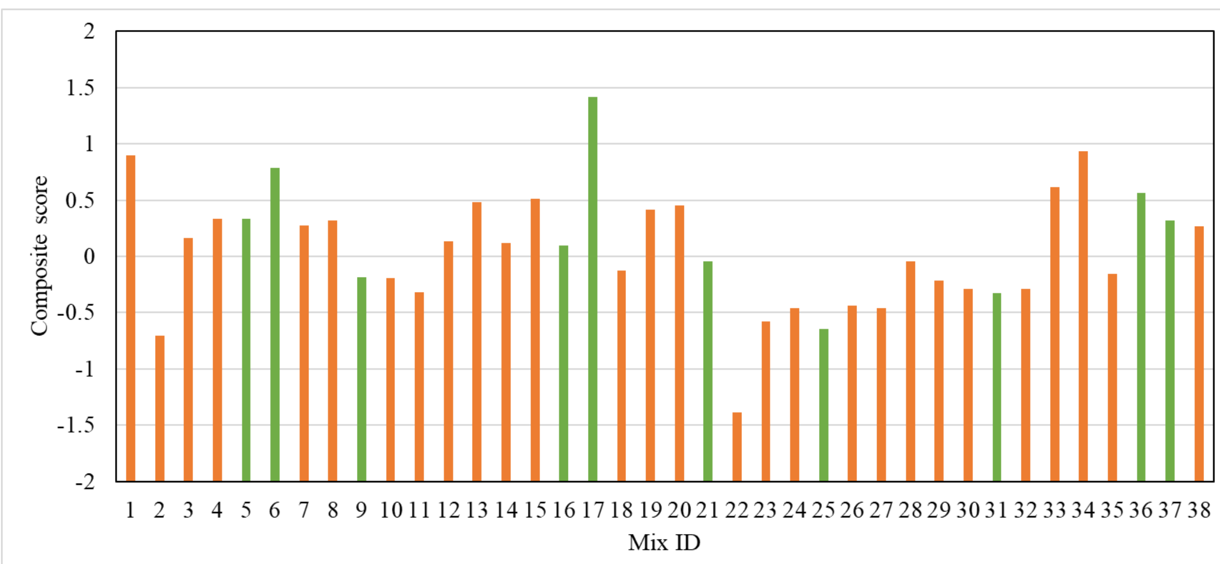

Figure 5.7: Composite Score of Each of the 38 Mixes with Green Bars Indicating Good Mixes

While the use of ITS ratio is shown to be significant in this study, one concern is that poor-performing mixes may show a high ITS ratio in spite of having actually low tensile strengths (both pre- and post-MiST). As has been done in prior studies (e.g, Choubane et al. 2000), an additional criterion of a minimum conditioned ITS can be utilized. For example, a study of field mixes from the Maine DOT (Arepalli et al. 2017; Veeraragavan et al. 2018) showed that moisture-susceptible mixes exhibit a post conditioning ITS value of <500 kPa, while those that are not moisture-susceptible show a post conditioning ITS value of>500 kPa. Therefore, a minimum post conditioning ITS value of 500 kPa can be used, along with the suggested method, to ensure adequately moisture-resistant mixes.

5.3 Application of Machine Learning Techniques:

The most significant variables identified from the results of PCA (E_s ratio, ITS ratio, FE ITS ratio BP ratio and DOC) were used to develop ML models to predict the performance of the mixes. A set of supervised machine learning algorithms based on the k-nearest neighbor and naïve Bayes methods were used in this study.

5.3.1 K-Nearest Neighbor (K-NN) Method

The data were divided into training and testing sets. The training data set consisted of 60% of the data, and k-fold validation was carried out. The model was run several times to get an optimized set of parameters by minimizing the validation error. Both k-fold and distance parameters were varied for the different models. The validation error was found to be minimized when the number of nearest neighbors was set at six. The optimized set of parameters for the k-nearest neighbor model obtained from the results are as follows: number of nearest neighbors, six; distance, standardized Euclidean distance; distance weight, squared inverse; k-fold, three. The confusion matrix for the prediction from this optimized model showed an accuracy of 83% as shown in Figure 5.8.

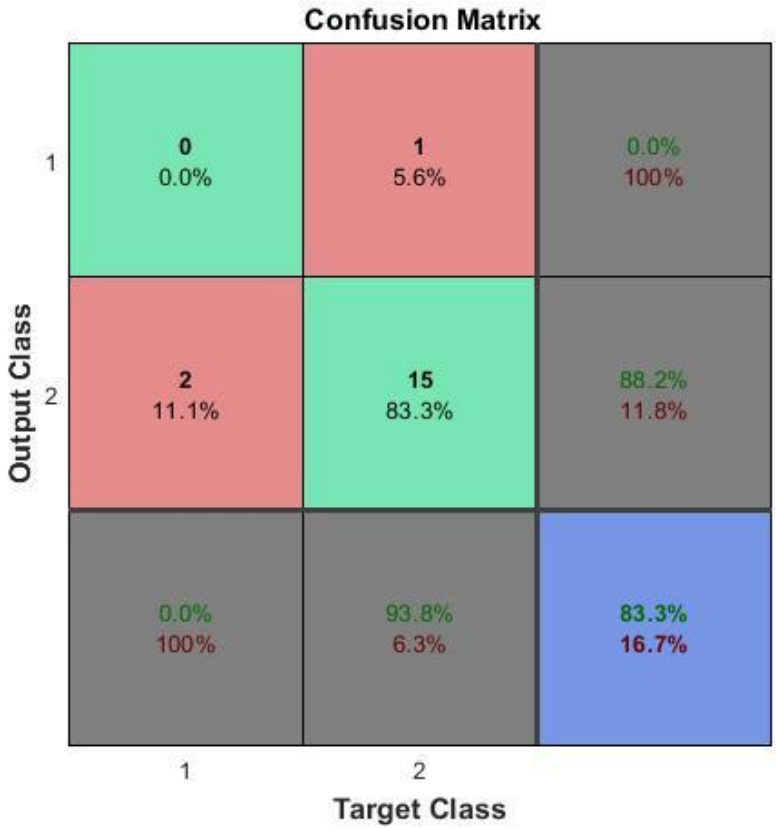

Figure 5.8: Confusion Plot for NN Method

5.3.2 Naïve Bayes (NB) Method

The naïve Bayes method is commonly used for analyzing small data sets with many parameters. The process assumes that the features in a class are not related to each other. The training data set consisted of 60% of the data, and k-fold validation was also carried out. The model that gave the best accuracy was used to predict the test data. The confusion plot (Figure 5.9) showed an accuracy of 59%.

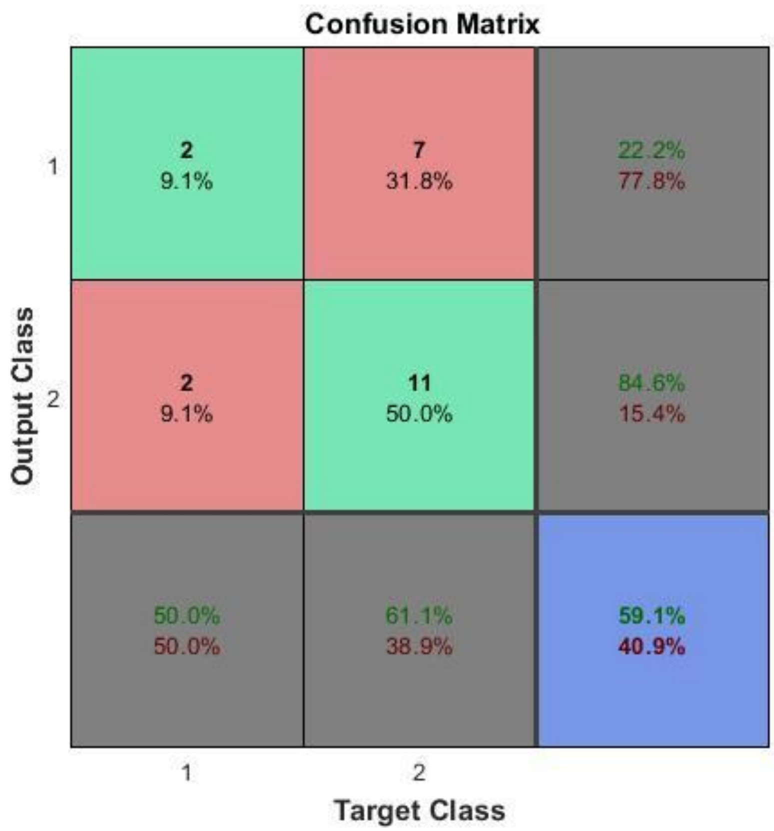

Figure 5.9: Confusion Plot for NB Method

5.4 Application (APP) For the Use of ML Model:

A Graphical User Interface (GUI) application was developed as a way for the user to provide complex instructions to communicate with the machine easily. MATLAB application offers a self-contained GUI program that is capable of executing complex machine learning predictions calculations without the need to learn computer coding (Pueyo, 2015). In order to build the application, MATLAB offers a variety of tools, one of them is the app designer tool (https://www.mathworks.com/products/matlab/app-designer.html). Figure 5.10 shows the app designer interface layout to design the app. The app designer interface consists of three columns namely component library at the left region, the canvas at the center and component properties on the right. Following are the steps followed for developing the app.

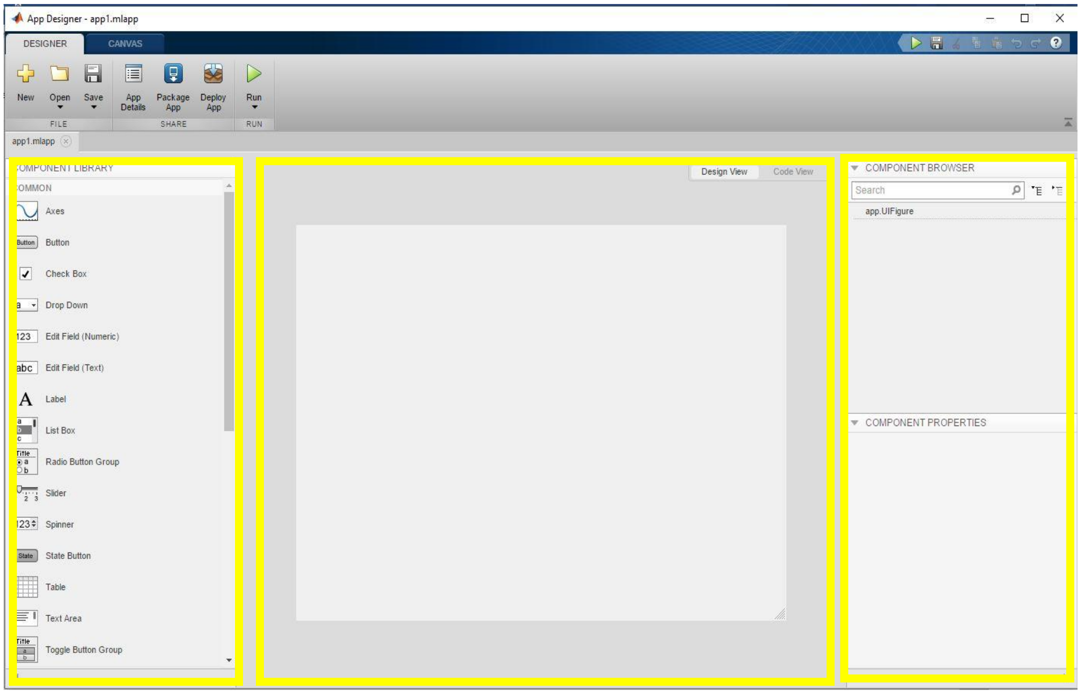

Figure 5.10: Layout of MATLAB App Designer Interface

Step 1: For Designing a user interface using, various components are aligned in the design canvas to get the layout of the app. Various inputs such as E ratio, ITS ratio, FE ITS ratio, BP ratio and DOC are identified as the inputs to be provided by the user. The equations used to calculate the ratios are as follows:

$$E_s\ ratio = \frac{Post\ MIST\ E_s}{Pre\ MIST\ E_s} \tag{5.1}$$

$$ITS\ ratio = \frac{Post\ MIST\ ITS}{Pre\ MIST\ ITS} \tag{5.2}$$

$$FE - ITS\ ratio = \frac{Post\ MIST\ FE\ ITS}{Pre\ MIST\ FE\ ITS} \tag{5.3}$$

$$BP\ ratio = \frac{Post\ MIST\ BP}{\text{Pre MIST BP}} \tag{5.4}$$

Step 2: Standard components such as buttons and text fields are used from the library of the APP designer in MATLAB. Along with the input components, a 'Classify' button and a field 'Performance' is used to show the predicted response.

Step 3: Callback functions are added that will execute the machine learning model, in this case KNN model, when the user uses the 'Classify' button. Thus, as per the input given by the user and the saved ML Model, performance of the mix is shown as 'Good' or 'Poor'. The detail code used as the call back function is given in the Appendix B.

Step 4: The app can be shared with other MATLAB users. A freely available single MATLAB application installation file will enable others to access the application and use it for predicting the performance of the asphalt mixes

For this App development from the PCA analysis run on the data, Es ratio, ITS ratio, FE ITS ratio BP ratio and DOC have been used as the significant variables which are necessary as inputs to classify a mix performance. From the PCA analysis the K-NN model was found to have a higher accuracy of 84%. Five inputs were therefore placed on the canvas for each individual ratio as inputs from the user, and a classify button was used to assign and run the K-NN machine learning model. The final predictor or the output from the model is displayed under performance. Figure 5.11 shows the MATLAB application user interface with Es ratio, ITS ratio, FEITS ratio, BP ratio and DOC as inputs and the performance of the mix predicted as the final output.

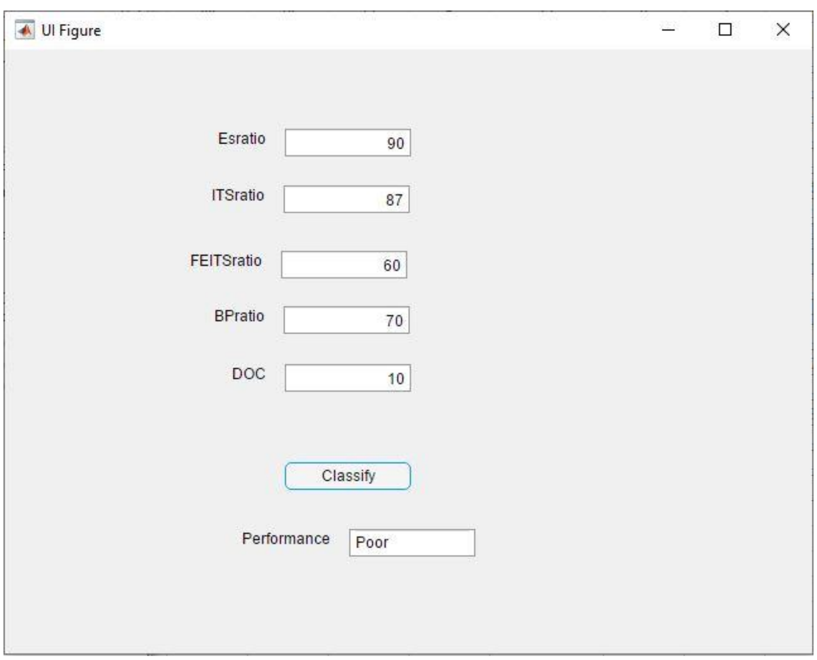

Figure 5.11: MATLAB Application Interface to Classify Mix Performance

6.0 EVALUATION OF USE OF FIBERS FOR THE ENHANCEMENT OF RESISTANCE AGAINST MOISTURE DAMAGE

6.1 Fibers in HMA for Improved Performance

Several technologies have been developed over the years to improve the moisture susceptibility of HMA. It is reported that fibers when added to HMA can result in reduced moisture induced damages to the HMA. The fiber is likely to enhance bonding between the aggregates and the binder into a dense mix resulting in reduced moisture induced damages. Researchers have used polymers and glass fibers in their research investigations. Few researchers have also used natural fibers like coir, jute etc. In the present study, High Tenacity Polypropylene Fiber (HTPP), a synthetic fiber, is used. These polypropylene fibers are typically used in concrete mixes and are generally cheap and readily available (Kalbskopf *et al.*, 2003). HTPP fibers have demonstrated an increase in tensile strength in concrete and hence an attempt is made in the present study to explore the benefits of reduced moisture induced damage in HMA. HTPP fibers are found to have a higher melting point, between 160°C (320ºF) and 170°C (338ºF) (Qin, Y. et al., 2019), which is the above the mixing temperature adopted for most commonly used HMA. The specific fibers used in this study were purchased from Staint Gobain Brazil and are 10 mm (0.39 in) in diameter and 12 μm (4.7 x 10^{-4} in) in length.

Table 6.1 shows the physical properties of the HTPP fibers.

Table 6.1. Physical Properties of HTPP Fibers

Description	Property values
Titer	2, 8 to 6 dtex
Cut-Length	40-120 mm
Tenacity	3,8-5,4 cN/dtex
Elongation	>40%->80%
Specific Weight	0.91 g/cm3
Melting point	163℃
Color	White

In the present investigation, one poor performing mix no. 3 was chosen. The dosage of HTPP fibers at 0.25% of total mass was added. If the dosage of the fibers is high, it was observed that non-uniform distribution of the fibers occurred in the mix resulting in wide variation in the obtained bulk densities. The mix was heated to 150°C (302ºF) for 2 hours. The hot mix was blended with 0.25% fibers in a mechanical mixer for 1 minute. Later the mix was conditioned in an over for 30 min and remixed in the mixer for one minute again and compacted. Figure 6.1 shows the pre- and post-MIST ITS results with and without HTPP fibers.

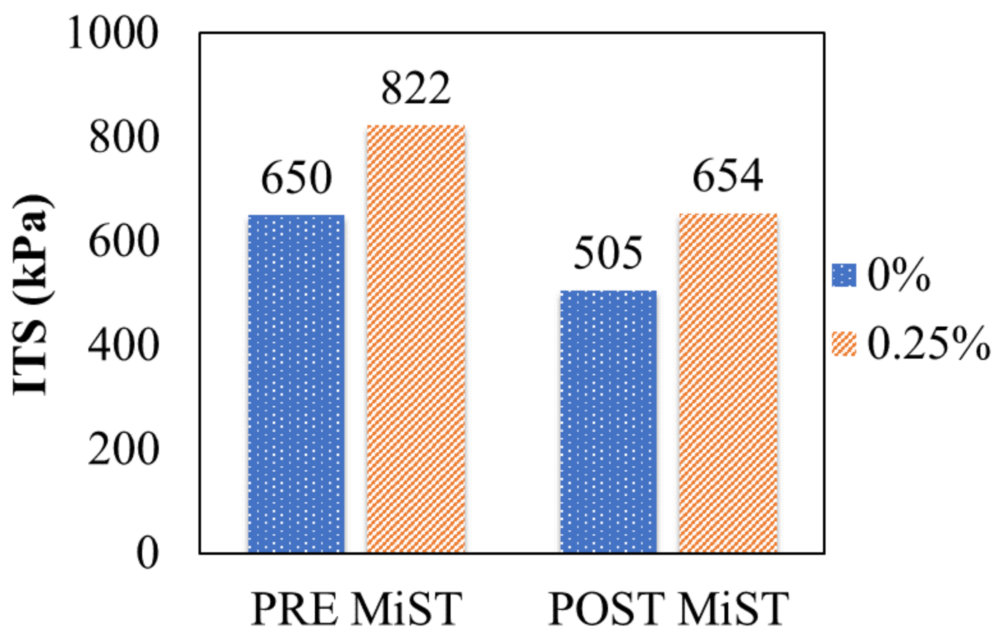

Figure: 6.1: Pre-MiST and Post-MiST ITS Results with 0% and 0.25% HTPP Fibers

The findings from this part of the study are as follows.

1. Higher ITS strength of about 21% was obtained for the samples with 0.25% fibers, tested without moisture conditioning when compared with those without fibers.
2. The retained ITS strength was about 79.6% (approx. 80%) after the post MiST conditioning. The desirable minimum retained ITS strength in the field is 80%
3. It was found that the samples prepared without the addition of the fibers showed a lower ITS strength of only 67.9% and hence they do not meet the minimum required retained ITS strength.

4. The ITS strength increased by 22.78% for the post MiST samples with 0.25% fibers, when compared to the samples without fiber.

The addition of fibers resulted in increased resistance to moisture induced damage in the HMA.

7.0 CONCLUSIONS AND RECOMMENDATIONS

7.1 Conclusions

1. MiST conditioning process with the 20-hour dwell period prior to 3,500 pressure cycling at 275 kPa was found to be able to simulate field moisture damage conditions in the laboratory.
2. Poor mixes are found to lose more finer aggregates during the MiST conditioning process than good mixes.
3. Non-destructive testing using ultrasonic pulse velocity was able to identify moisture susceptible mixes. Seismic modulus and indirect tensile strength tests, used in conjunction with a MiST conditioning process consisting of a dwelling period followed by pressure cycles, have good potential for identifying moisture-susceptible HMA
4. Test properties such as seismic modulus and indirect tensile strength after moisture conditioning can be used by agencies to predict the moisture damage potential of HMA. Statistical analyses of the seismic modulus and ITS of pre- and post-conditioned samples were able to differentiate between good- and poor-performance mixes with moderate accuracy.
5. Principal component analysis identified the following properties as the primary factors that could explain most of the variance in the data: seismic modulus, indirect tensile strength, black pixels, and fracture energy from indirect tensile strength.
6. The models developed with two machine learning techniques, the K-Nearest Neighbor and Naïve Bayes (NB) method show excellent accuracy for classification of mixes into good and poor performing in terms of potential of moisture damage.
7. The nearest neighbor model, a supervised machine learning technique, classified the good and poor mixes with 84% accuracy.
8. The use of machine learning techniques and the app could help agencies to detect moisture susceptible asphalt mixtures and can be used to develop appropriate specifications that could be used to build moisture resistant pavement.
9. Although most of the mixes showed a decrease in black pixels content after moisture conditioning and the poor-performance mixes tended to show a higher change, statistical

analysis of the BP content of samples of these mixes failed to differentiate between good- and poor-performance mixes with high accuracy.

10. The machine learning model developed can be used for classification of good and poor performing HMA. The application of artificial intelligence in prediction of moisture susceptible asphalt mixtures and the App developed as an outcome of the present research work will help the state agencies identifying the good and poor mixes before construction.

7.2 Recommendations

Recommendations are made for utilizing the suite of tests identified in this research work along with models developed from machine learning techniques, to classify mixes in terms of their moisture susceptibility. A minimum value of post conditioned indirect tensile strength may also be used to identify good and poor mixes. The use of the indirect tensile strength test along with the ultrasonic pulse velocity test is recommended.

7.3 Scope for Future Work

It is acknowledged that the data used for this study are limited, and that the developed models could be improved significantly with more data, i.e., from a number of mixes with known field performance and laboratory test properties. Therefore, the developed method is proposed as a framework, which can be expanded and improved, by agencies and researchers with additional performance data.

REFERENCES

- AASHTO (American Association of State Highway and Transportation Officials) (2001) AASHTO T283-89: Resistance of Compacted Bituminous Mixture to Moisture Induced Damage. Standard Specifications for Transportation Materials and Methods and Sampling and Testing. Part II: Tests. AASHTO, Washington, DC, USA.
- AASHTO T 283 (2014) Standard method of test for resistance of compacted asphalt mixtures to moisture-induced damage. AASHTO, Washington, DC.
- Abadi, M., Agarwal, A., Barham, P., Brevdo, E., Chen, Z., Citro, C., & Ghemawat, S. (2016). Tensorflow: Large-scale machine learning on heterogeneous distributed systems. arXiv preprint arXiv:1603.04467.
- Abtahi, S. M., Sheikhzadeh, M., & Hejazi, S. M. (2010). Fiber-reinforced asphalt-concrete–a review. Construction and Building Materials, 24(6), 871-877.
- Ahmad, M., Mannan, U. A., Islam, M. R., & Tarefder, R. A. (2018). Chemical and mechanical changes in asphalt binder due to moisture conditioning. Road Materials and Pavement Design, 19(5), 1216-1229.
- Airey, G. D., Masad, E., Bhasin, A., Caro, S., & Little, D. N. (2007, December). Asphalt mixture moisture damage assessment combined with surface energy characterization. In International conference on advanced characterisation of pavement and soil engineering materials (pp. 739-748).
- Airey GD, Choi YK, Collop AC, Moore AJ and Elliott RC (2005). Combined laboratory ageing/moisture sensitivity assessment of high modulus base asphalt mixtures (with discussion). Journal of the Association of Asphalt Paving Technologists 74.
- Alfalah, A., Offenbacker, D., Ali, A., Decarlo, C., Lein, W., Mehta, Y., & Elshaer, M. (2020). Assessment of the Impact of Fiber Types on the Performance of Fiber-Reinforced Hot Mix Asphalt. Transportation Research Record, 0361198120912425.
- Al-Qadi, I. L., Ozer, H., Lambros, J., El Khatib, A., Singhvi, P., Khan, T., ... & Doll, B. (2015). Testing protocols to ensure performance of high asphalt binder replacement mixes using RAP and RAS. Illinois Center for Transportation/Illinois Department of Transportation.

- Al-Swailmi S and Terrel RL (1994). Water Sensitivity of Asphalt– Aggregate Mixtures: Test Selection. Strategic Highway Research Program, National Research Council, Washington, DC, USA, SHRP-A-403.
- Al-Swailmi S, Scholz TV and Terrel RL (1992). Development and evaluation of test system to induce and monitor moisture damage to asphalt concrete mixtures. Transportation Research Record 1353: 39–45.
- Aouad, M. F., Stokoe, I. I., Kenneth, H., & Briggs, R. C. (1993). Stiffness of asphalt concrete surface layer from stress wave measurements. Transportation Research Record, (1384).
- Anastasio, S., et al. Laboratory Testing Methods for Evaluating the Moisture Damage on the Aggregate-Asphalt System. in 8th RILEM International Symposium on Testing and Characterization of Sustainable and Innovative Bituminous Materials. 2016. Springer
- Arambula, E., S. Caro, and Masad, E., Experimental measurement and numerical simulation of water vapor diffusion through asphalt pavement materials. Journal of Materials in Civil Engineering, 2009. 22(6): p. 588-598.
- Arepalli UM (2018) A study of moisture induced material loss of hot mix asphalt (HMA). Ph.D.
- Arepalli UM, Mallick R. B, Methisen P et al. (2017). Study of hot-mix asphalt susceptible to moisture-induced material loss. In Proceedings of the 96th Transportation Research Board Annual Meeting. The National Academies of Sciences, Engineering, and Medicine, Washington, DC, USA.
- Aschenbrener T (1995). Evaluation of Hamburg wheel-tracking device to predict moisture damage in hot mix asphalt. Transportation Research Record 1492: 193–201.
- ASTM (2013) D 7870/D 7870M: Standard practice for moisture conditioning compacted asphalt mixture specimens by using hydrostatic pore pressure. ASTM International, West Conshohocken, PA, USA.
- ASTM (2016) C 597: Standard test method for pulse velocity through concrete. ASTM International, West Conshohocken, PA, USA.
- Bagampadde U, Isacsson U, Kiggundu B (2005). Influence of aggregate chemical and mineralogical composition on stripping in bituminous mixtures. Int J Pavement Eng 6(4):229–239.

- Behiry AEAE-M (2013). Laboratory evaluation of resistance to moisture damage in asphalt mixtures. Ain Shams Eng J4(3):351–363.
- Bhasin A, Little DN, Vasconcelos KL and Masad, E. (2007). Surface free energy to identify moisture sensitivity of materials for asphalt mixes. Transportation Research Record 2001: 37–45.
- Bhattacharjee, S., & Mallick, R. B. (2002). An alternative approach for the determination of bulk specific gravity and permeability of hot mix asphalt (HMA). International Journal of Pavement Engineering, 3(3), 143-152.
- Bianchini, A. (2014). Pavement maintenance planning at the network level with principal component analysis. Journal of Infrastructure Systems, 20(2), 04013013.
- Birgisson B, Roque R, Page G and Wang J (2007). Development of new moisture-conditioning procedure for hot-mix asphalt. Transportation Research Record 2001: 46–55.
- Bishop CM (2006). Pattern recognition and machine learning. Springer, New York.
- Bonnin, R. (2016). Building Machine Learning Projects with TensorFlow. Packt Publishing Ltd.
- Brown, E. R., Hainin, M. R., Cooley, A., & Hurley, G. (2004). Relationships of HMA in-place air voids, lift thickness, and permeability NCHRP web document 68 (Project 9-27), Vol. Vol. 1, 2004.
- Brown, E. R., Hainin, M. R., Cooley, A., & Hurley, G. (2004). Relationships of HMA in-place air voids, lift thickness, and permeability. NCHRP web document 68 (Project 9-27), Vol. Vol. 2, 2004.
- Brown, E. R., Hainin, M. R., Cooley, A., & Hurley, G. (2004). Relationships of HMA in-place air voids, lift thickness, and permeability. NCHRP web document 68 (Project 9-27), Vol. Vol. 3, 2004.
- Brown, E. R., Hainin, M. R., Cooley, A., & Hurley, G. (2004). Relationships of HMA in-place air voids, lift thickness, and permeability. NCHRP web document 68 (Project 9-27). NCHRP web document, Vol. Vol. 4, 2004.
- Buchanan MS, Moore V, Mallick R. B, O'Brien S and Regimand A (2004). Accelerated moisture susceptibility testing of hot mix asphalt (HMA) mixes. In Proceedings of the 83rd Transportation Research Board Annual Meeting. The National Academies of Sciences, Engineering, and Medicine, Washington, DC, USA.

- Canestrari F, Cardone F, Graziani A, Santagata F and Bahia HU (2010). Adhesive and cohesive properties of asphalt-aggregate systems subjected to moisture damage. Road Materials and Pavement Design 11: 11–32.
- Cedergren, H. R. (1974). Drainage of highway and airfield pavements.
- Carman, P. C. (1938). Determination of the specific surface of powders I. Transactions. J. Soc. Chemical Industries., 57, 225-234.
- Caro S, Masad, E., Bhasin A and Little DN (2008). Moisture susceptibility of asphalt mixtures, part 1: mechanisms. International Journal of Pavement Engineering 9(2): 81–98.
- Chen, C., Yin, F., Turner, P., West, R. C., & Tran, N. (2018). Selecting a laboratory loose mix aging protocol for the NCAT top-down cracking experiment. Transportation Research Record, 2672(28), 359-371.
- Choubane, B., Page, G. C., & Musselman, J. A. (2000). Effects of water saturation level on resistance of compacted hot-mix asphalt samples to moisture-induced damage. Transportation Research Record, 1723(1), 97-106.
- Cooley Jr, L., Brown, E. R., & Maghsoodloo, S. (2001). Developing critical field permeability and pavement density values for coarse-graded superpave pavements. Transportation research record, 1761(1), 41-49.
- Copeland, A. R., Kringos, N., Youtcheff Jr, J. S., & Scarpas, T. (2007). Measurement of aggregate–mastic bond strength in presence of moisture: Combined experimental-computational study (No. 07-1829).
- Crawford, A. E. (2019). Understanding the Effects of Moisture on Hot Mix Asphalt (HMA).
- Cui, S., et al., Durability of asphalt mixtures: Effect of aggregate type and adhesion promoters. International Journal of Adhesion and Adhesives, 2014. 54: p. 100-111.
- Curtis CW, Ensley K and Epps J (1993). Fundamental Properties of Asphalt–Aggregate Interactions including Adhesion and Absorption. National Research Council, Washington, DC, USA.
- D'angelo, J. and R. Anderson. Material production, mix design, and pavement design effects on moisture damage. in Moisture Sensitivity of Asphalt Pavements-a National Seminar. 2003.
- Dawson, A. (Ed.). (2008). Water in road structures: movement, drainage & effects (Vol. 5). Springer Science & Business Media.
- Darcy, H. (1856). Fontaines publiques de la ville de Dijon (Libraire des Corps).

- Deng J, Dong W, Socher R et al. (2009). ImageNet: a large-scale hierarchical image database. In Proceedings of the 2009 IEEE Conference on Computer Vision and Pattern Recognition. Institute of Electrical and Electronics Engineers, Piscataway, NJ, USA, pp. 248–255.
- Epps, J., E. Berger, and J.N. Anagnos. Treatments. in Moisture Sensitivity of Asphalt Pavements-A National Seminar. 2003.
- Fischer, H.R., E. Dillingh, and C. Hermse, On the interfacial interaction between bituminous binders and mineral surfaces as present in asphalt mixtures. Applied Surface Science, 2013. 265: p. 495-499.
- Gatys LA, Ecker AS and Bethge M (2016). Image style transfer using convolutional neural networks. In Proceedings of the 2016 IEEE Conference on Computer Vision and Pattern Recognition. Institute of Electrical and Electronics Engineers, Piscataway, NJ, USA, pp. 2414–2423.
- Goodfellow I, Bengio Y and Courville A (2016). Deep Learning. MIT Press, Cambridge, MA, USA.
- Grenfell J, Ahmad N, Liu Y et al. (2014). Assessing asphalt mixture moisture susceptibility through intrinsic adhesion, asphalt stripping and mechanical damage. Road Materials and Pavement Design 15(1): 131–152.
- Hainin, M. R., Cooley Jr, L. A., & Prowell, B. D. (2003). An investigation of factors influencing permeability of Superpave mixes. International Journal of Pavements, 2(2), 41-52.
- Hamzah MO, Kakar MR, Hainin MR (2015). An overview of moisture damage in asphalt mixtures. Jurnal Teknologi (Sciences & Engineering) 73(4):125–131.
- Harrison, O. (2018). Machine Learning Basics with the K-Nearest Neighbors Algorithm. Towards Data Science. September, 10.
- Hazen, A. (1892). Some physical properties of sands and gravels: with special reference to their use in filtration, publisher not identified.
- He, K., Zhang, X., Ren, S., & Sun, J. (2016). Deep residual learning for image recognition. In Proceedings of the IEEE conference on computer vision and pattern recognition (pp. 770-778).
- Hicks RG (1991). Moisture damage in asphalt concrete. NCHRP Synthesis of Highway Practice 175, Transportation Research Board, Washington, DC.
- Hicks RG (1991). Moisture Damage in Asphalt Concrete. Transportation Research Board, Washington, DC, USA.

- Hofko, B., Porot, L., Cannone, A. F., Poulikakos, L., Huber, L., Lu, X., ... & Grothe, H. (2018). FTIR spectral analysis of bituminous binders: reproducibility and impact of ageing temperature. Materials and Structures, 51(2), 45.
- Howard, I. L., Baumgardner, G. L., Jordan III, W. S., Menapace, A. M., Mogawer, W. S., & Michael Hemsley Jr, J. (2013). Haul time effects on unmodified, foamed, and additive-modified binders used in hot-mix asphalt. Transportation research record, 2347(1), 88-95.
- Huang G, Liu Z, Weinberger KQ and van der Maaten L (2017). Densely connected convolutional networks. In Proceedings of the 2017 IEEE Conference on Computer Vision and Pattern Recognition. Institute of Electrical and Electronics Engineers, Q26 Piscataway, NJ, USA, vol. 1,p. 3.
- Huang, B., Li, G., Vukosavljevic, D., Shu, X., & Egan, B. K. (2005). Laboratory investigation of mixing hot-mix asphalt with reclaimed asphalt pavement. Transportation Research Record, 1929(1), 37-45.
- Jimenez RA (1974). Testing for debonding of asphalts from aggregates. Transportation Research Record 515: 1–17.
- Kandhal, P.S., Moisture susceptibility of HMA mixes: identification of problem and recommended solutions. 1992, National Asphalt Pavement Association.
- Kandhal PS, Lubold CW, Roberts FL (1989). Water damage to asphalt overlays: case histories. National Center for Asphalt Technology, Nashville.
- Kandhal PS and Rickards IJ (2001). Premature Failures of Asphalt Overlays from Stripping: Case Histories. National Center for Asphalt Technology, Auburn, AL, USA, NCAT Report 01-01.
- Kanitpong, K., Benson, C. H., & Bahia, H. U. (2001). Hydraulic conductivity (permeability) of laboratory-compacted asphalt mixtures. Transportation Research Record, 1767(1), 25-32.
- Karmakar, S., Majhi, D., Roy, T. K., & Chanda, D. (2018). Moisture damage analysis of bituminous mix by durability index utilizing waste plastic cup. Journal of Materials in Civil Engineering, 30(9), 04018216.
- Klinsky, L. M. G., Kaloush, K. E., Faria, V. C., & Bardini, V. S. S. (2018). Performance characteristics of fiber modified hot mix asphalt. Construction and Building Materials, 176, 747-752.

- Kiggundu BM, Roberts FL (1988). Stripping in HMA mixtures: state-of-the-art and critical review of test methods. National Center for Asphalt Technology, Auburn.
- Koçkal, N. U., & Köfteci, S. (2016). Aggressive Environmental Effect on Polypropylene Fibre Reinforced Hot Mix Asphalt. Procedia engineering, 161, 963-969.
- Kozeny, J. (1927). Uber kapillare leitung der wasser in boden. Royal Academy of Science, Vienna, Proc. Class I, 136, 271-306.
- Kringos N, Scarpas A (2008). Physical and mechanical moisture susceptibility of asphaltic mixtures. Int J Solids Struct 45(9):2671–2685.
- Kringos N and Scarpas A (2005). Raveling of asphaltic mixes due to water damage: computational identification of controlling parameters. Transportation Research Record 1929: 79–87.
- Kringos N, Azari H and Scarpas A (2009). Identification of parameters related to moisture conditioning that cause variability in modified Lottman test. Transportation Research Record 2127: 1–11.
- Kumar, P., Mehndiratta, H. C., & Immadi, S. (2009). Investigation of fiber-modified bituminous mixes. Transportation research record, 2126(1), 91-99.
- Lamontagne, J., Dumas, P., Mouillet, V., & Kister, J. (2001). Comparison by Fourier transform infrared (FTIR) spectroscopy of different ageing techniques: application to road bitumens. Fuel, 80(4), 483-488.
- Loria, L., Sebaaly, P. E., & Hajj, E. Y. (2008). Long-term performance of reflective cracking mitigation techniques in Nevada. Transportation research record, 2044(1), 86-95.
- Lopes, M., Mouillet, V., Bernucci, L., & Gabet, T. (2016). The potential of Attenuated Total Reflection imaging in the mid-infrared for the study of recycled asphalt mixtures. Construction and Building Materials, 124, 1120-1131.
- Li, Y., Moraes, R., Lyngdal, E., & Bahia, H. (2016). Effect of polymer and oil modification on the aging susceptibility of asphalt binders. Transportation Research Record, 2574(1), 28-37.
- Li, Y., & Nazarian, S. (1995). Evaluation of aging of hot-mix asphalt using wave propagation techniques. In Engineering Properties of Asphalt Mixtures and the Relationship to Their Performance. ASTM International.

- Little DN & Jones DR (2003). Chemical and mechanical processes of moisture damage in hot-mix asphalt pavements. Proceedings of Moisture Sensitivity of Asphalt Pavements – A National Seminar, San Diego, CA, USA, pp. 37–70.
- Little DN, Petersen JC (2005). Unique effects of hydrated lime filler on the performance-related properties of asphalt cements: physical and chemical interactions revisited. J Mater Civ Eng 17(2):207–218.
- Liu, Y., et al., Examination of moisture sensitivity of aggregate–asphalt bonding strength using loose asphalt mixture and physico-chemical surface energy property tests. International Journal of Pavement Engineering, 2014. 15(7): p. 657-670.
- Logaraj, S. Chemistry of asphalt-aggregate interaction–Influence of additives. in Moisture Damage Symposium, Laramie, Wyoming. 2002
- Lottman, R. P. (1982). Laboratory test methods for predicting moisture-induced damage to asphalt concrete. Transportation Research Record, (843).
- Lottman, R. P. (1978). PREDICTING MOISTURE--INDUCED DAMAGE TO ASPHALTIC CONCRETE (No. Final Rpt.).
- Lu, Q. & J. Harvey, Long-term effectiveness of antistripping additives: Laboratory evaluation. Transportation Research Record: Journal of the Transportation Research Board, 2006(1970): p. 14-24.
- Mallick, R. B., Gould, J. S., Bhattacharjee, S., Regimand, A., James, L. H., & Brown, E. R. (2003). Development of a rational procedure for evaluation of moisture susceptibility of asphalt paving mixes. Transportation Research Board, Washington, DC.
- Mallick, R. B., Pelland‖, R., & Hugo#, F. (2005). Use of accelerated loading equipment for determination of long term moisture susceptibility of hot mix asphalt. International Journal of Pavement Engineering, 6(2), 125-136.
- Mallick, R. B., Cooley, L. A., Teto, M., & Bradbury, R. (2001). Development of a simple test for evaluation of in-place permeability of asphalt mixes. International Journal of Pavement Engineering, 2(2), 67-83.
- Mallick, R. B., Madankara Kottayi, N., Veeraragavan, R. K., Dave, E., DeCarlo, C., & Sias, J. E. (2019). Suitable Tests and Machine Learning Approach to Predict Moisture Susceptibility of Hot-Mix Asphalt. Journal of Transportation Engineering, Part B: Pavements, 145(3), 04019030.

- Masad, E., *et al*., Nondestructive measurements of moisture transport in asphalt mixtures. Asphalt Paving Technology-Proceedings, 2007. 76: p. 919
- Masad, E., Castelblanco, A., & Birgisson, B. (2006). Effects of air void size distribution, pore pressure, and bond energy on moisture damage. Journal of testing and evaluation, 34(1), 15-23.
- Masad, E., Al-Omari, A., & Lytton, R. (2006). Simple method for predicting laboratory and field permeability of hot-mix asphalt. Transportation Research Record, 1970(1), 55-63.
- Maupin Jr, G. W. (2001). Asphalt permeability testing: specimen preparation and testing variability. Transportation research record, 1767(1), 33-39.
- McLaughlin, J. F., & Goetz, W. H. (1955). Permeability, void content, and durability of bituminous concrete. In Highway Research Board Proceedings (Vol. 34).
- McCarthy, J. What is artificial intelligence? http://jmc.stanford.edu/articles/whatisai/whatisai.pdf, accessed June 17, 2018.
- Mejias de Pernia, Y., Metz, J., Gunaratne, M., Nash, T., & Musselman, J. (2016). Application of image analysis techniques to develop a quality control tool for automated optimum binder content determination of open-graded friction course mixtures. Transportation Research Record, 2575(1), 48-60.
- Miguel-Hurtado, O., Guest, R., Stevenage, S. V., Neil, G. J., & Black, S. (2016). Comparing machine learning classifiers and linear/logistic regression to explore the relationship between Hand dimensions and demographic characteristics. PloS one, 11(11).
- Morian, N., Hajj, E. Y., & Sebaaly, P. E. (2013). Significance of mixture parameters on binder aging in hot-mix asphalt mixtures. Transportation research record, 2370(1), 116-127.
- Morian, N., Hajj, E. Y., Glover, C. J., & Sebaaly, P. E. (2011). Oxidative aging of asphalt binders in hot-mix asphalt mixtures. Transportation research record, 2207(1), 107-116.
- Murphy, K. P. (2006). Naive bayes classifiers. University of British Columbia, 18, 60.
- Nasrazadani, S., Mielke, D., Springfield, T., & Ramasamy, N. (2010). Practical applications of FTIR to characterize paving materials (No. FHWA/TX-11/0-5608-1).
- Nataatmadja, A. (2010, October). The use of hyperbolic function for predicting critical permeability of asphalt. In ARRB Conference, 24th, 2010ARRB.

- Noorvand, H., Salim, R., Medina, J., Stempihar, J., & Underwood, B. S. (2018). Effect of synthetic fiber state on mechanical performance of fiber reinforced asphalt concrete. Transportation Research Record, 2672(28), 42-51.
- Nsengiyumva, G., Haghshenas, H. F., Kim, Y. R., & Kommidi, S. R. (2020). Mechanical-Chemical Characterization of the Effects of Type, Dosage, and Treatment Methods of Rejuvenators in Aged Bituminous Materials. Transportation Research Record, 0361198120909110.
- Nivedya MK, Mallick R.B. (2018) Accurate prediction of laboratory permeability of hot mix asphalt using machine learning techniques, In: Proceedings of Advances in Materials and Pavement Performance Prediction. Doha, Qatar.
- Nivedya, M. K., & Mallick, R. B. (2018, July). Accurate prediction of laboratory permeability of hot mix asphalt using machine learning techniques. In Advances in Materials and Pavement Prediction: Papers from the International Conference on Advances in Materials and Pavement Performance Prediction (AM3P 2018), April 16-18, 2018, Doha, Qatar (p. 133). CRC Press.
- Novak, M., Birgisson, B., & McVay, M. C. (2002, January). Effects of permeability and vehicle speed on pore pressure in hot mix asphalt pavements. In Transportation Research Board Meeting, Washington, DC.
- Petersen, J. C., Plancher, H., Ensley, E. K., Venable, R. L., & Miyake, G. (1982). Chemistry of asphalt-aggregate interaction: relationship with pavement moisture-damage prediction test. Transportation Research Record, (843).
- Petersen, J. C. (2009). A review of the fundamentals of asphalt oxidation: chemical, physicochemical, physical property, and durability relationships. Transportation Research Circular, (E-C140).
- Pinkham, R. E., Cote, S. A., Mallick, R. B., Tao, M., Bradbury, R. L., & Regimand, A. (2012). Use of moisture induced stress testing to evaluate stripping potential of hot mix asphalt (HMA) (No. 43077). Maine. Dept. of Transportation.
- Plancher, H., Dorrence, S. M., & Petersen, J. C. (1977). Identification of chemical types in asphalts strongly adsorbed at the asphalt-aggregate interface and their relative displacement by water.[Moisture damage to roads] (No. CONF-770216-1). Energy Research and Development Administration, Laramie, WY (USA). Laramie Energy Research Center.

- Pueyo, L. G. (2015). Image Processing Software Developed with MATLAB®(Graphic Design Software-GDS) (Doctoral dissertation, Universitat Politècnica de Catalunya. Escola Tècnica Superior d'Enginyeria de Telecomunicació de Barcelona. Departament de Teoria del Senyal i Comunicacions, 2015 (Màster universitari en Enginyeria Electrònica).
- Rad, F. Y., Elwardany, M. D., Castorena, C., & Kim, Y. R. (2018). Evaluation of chemical and rheological aging indices to track oxidative aging of asphalt mixtures. Transportation Research Record, 2672(28), 349-358.
- Read, J. & D. Whiteoak, *The shell asphalt handbook*. 2003: Thomas Telford.
- Regimand, A., James, L. H., Muse, P. D., Landreth, K., & He, T. (2012). U.S. Patent No. 8,312,776. Washington, DC: U.S. Patent and Trademark Office.
- Regimand, A., James, L. H., Muse, P. D., & He, T. (2004). U.S. Patent No. 6,799,471. Washington, DC: U.S. Patent and Trademark Office.
- Ribeiro, R.C., J.C.G. Correia, and P.R. Seidl, The influence of different minerals on the mechanical resistance of asphalt mixtures. Journal of Petroleum Science and Engineering, 2009. 65(3): p. 171-174.
- Richards, K. (2018). Machine Learning: For Beginners—Your Starter Guide For Data Management, Model Training. Neural Networks. CreateSpace Independent Publishing Platform, Machine Learning Algorithms.
- Robertson, R. E. (2000). Chemical properties of asphalts and their effects on pavement performance (No. 499). Transportation Research Board, National Research Council.
- Sasaki, I., *et al*., New test method for moisture permeation in bituminous mixtures. Journal of the Japan Petroleum Institute, 2006. 49(1): p. 33-37.
- Santucci, L. (2002). Moisture sensitivity of asphalt pavements. Tech topics.
- Shakiba, M., Darabi, M. K., & Little, D. N. (2017). Effect of pore water pressure on response of asphalt concrete. Transportation Research Record, 2631(1), 114-122.
- Shlens, J. (2014). A tutorial on principal component analysis. arXiv preprint arXiv:1404.1100.
- Simonyan, K., & Zisserman, A. (2014). Very deep convolutional networks for large-scale image recognition. arXiv preprint arXiv:1409.1556.
- Slebi-Acevedo, C. J., Lastra-González, P., Pascual-Muñoz, P., & Castro-Fresno, D. (2019). Mechanical performance of fibers in hot mix asphalt: A review. Construction and Building Materials, 200, 756-769.

- Smith, B. T., & Howard, I. L. (2018). Short-and longer-term effects of short-term aging on asphalt mixture properties. Journal of Materials in Civil Engineering, 30(3), 04018005.
- Solaimanian, M., & Harrigan, E. (2002). Improved conditioning procedure for predicting the moisture susceptibility of HMA pavements. In Proceedings of moisture damage symposium, Laramie, Wyoming, USA.
- Solaimanian, M., Harvey, J., Tahmoressi, M., & Tandon, V. (2003). Test methods to predict moisture sensitivity of hot-mix asphalt pavements. In Moisture Sensitivity of Asphalt Pavements-A National Seminar California Department of Transportation; Federal Highway Administration; National Asphalt Pavement Association; California Asphalt Pavement Alliance; and Transportation Research Board.
- Song, Y. R., Wang, C. X., & Zhang, Y. Z. (2011). Determination of the chemical composition in asphalt aqueous solutions by SPE and GC/MS. Petroleum science and technology, 29(15), 1590-1595.
- Syunyaev, R. Z., Balabin, R. M., Akhatov, I. S., & Safieva, J. O. (2009). Adsorption of petroleum asphaltenes onto reservoir rock sands studied by near-infrared (NIR) spectroscopy. Energy & Fuels, 23(3), 1230-1236.
- Taylor, M. A., & Khosla, N. P. (1983). Stripping of asphalt pavements: State of the art (discussion, closure) (No. 911).
- Tarefder, R. A., White, L., & Zaman, M. (2005). Neural network model for asphalt concrete permeability. Journal of Materials in Civil Engineering, 17(1), 19-27.
- Theobald, O. (2017). Machine learning for absolute beginners.
- Vivar, E., & Haddock, J. E. (2007). Hot-mix asphalt permeability and porosity. Journal of the Association of Asphalt Paving Technologists, 76.
- Vardanega, P. J. (2014). State of the art: Permeability of asphalt concrete. Journal of Materials in Civil Engineering, 26(1), 54-64.
- Varveri, A., Avgerinopoulos, S., & Scarpas, A. (2016). Experimental evaluation of long-and short-term moisture damage characteristics of asphalt mixtures. Road Materials and Pavement Design, 17(1), 168-186.
- Vasconcelos, K. L., Bhasin, A., & Little, D. N. (2010). Measurement of Water Diffusion in Asphalt Binders Using Fourier Transform Infrared–Attenuated Total Reflectance. Transportation research record, 2179(1), 29-38.

- Veeraragavan, R. K., Nivedya, M. K., Mallick, R. B., Tao, M., Dave, E., Daniel, J. S., ... & Nener-Plante, D. (2018). Use of the Moisture-Induced Stress Tester (MIST), Appropriate Tests, and Analyses for Evaluation of Moisture Susceptibility of Asphalt Mixture (No. 18-05403).
- Villegas-Villegas, R. E., Baldi-Sevilla, A., Aguiar-Moya, J. P., & Loria-Salazar, L. (2018). Analysis of asphalt oxidation by means of accelerated testing and environmental conditions. Transportation Research Record, 2672(28), 244-255.
- Waters, T. (2004). A study of water infiltration through asphalt road surface materials. In ROAD SYSTEM AND ENGINEERING TECHNOLOGY FORUM, 2004, BRISBANE, QUEENSLAND, AUSTRALIA.
- Weigel, S., & Stephan, D. (2018). Bitumen characterization with Fourier Transform Infrared Spectroscopy and multivariate evaluation: prediction of various physical and chemical parameters. Energy & fuels, 32(10), 10437-10442.
- Westerman, J. R. (1998, January). AHTD's experience with superpave pavement permeability. In Arkansas Superpave Symposium (Vol. 21, No. 2, pp. 82-99).
- Williams, B. A., Bausano, J. P., & Williams, R. C. (2007). Criterion Test for Method Selection in Determining the Bulk Specific Gravity of Hot-Mix Asphalt. Journal of ASTM International, 4(1), 1-10.
- Yi J, Shen S, Wang D, Feng D and Huang Y (2016). Effect of testing conditions on laboratory moisture test for asphalt mixtures. Journal of Testing and Evaluation 44(2): 856–867.
- Yilmaz, A. and S. Sargin, Water effect on deteriorations of asphalt pavements. Online J. of Sci. and Tech, 2012. 2(1)
- Zhang J, Apeagyei AK, Airey GD and Grenfell JR (2015). Influence of aggregate mineralogical composition on water resistance of aggregate–asphalt adhesion. International Journal of Adhesion and Adhesives 62: 45–54.
- Zofka A, Maliszewski M and Bernier A (2014). Alternative moisture sensitivity test. Proceedings of the 9th International Conference on Environmental Engineering, Vilnius, Lithuania.

APPENDIX A

Appendix A consists of plots comparing FTIR absorption spectrum before and after MiST testing for each of the 17 extracted binders. The calculated Ico and Iso indices results are also presented as tables at the end of the plots.

A 1.1: FTIR Test Plots

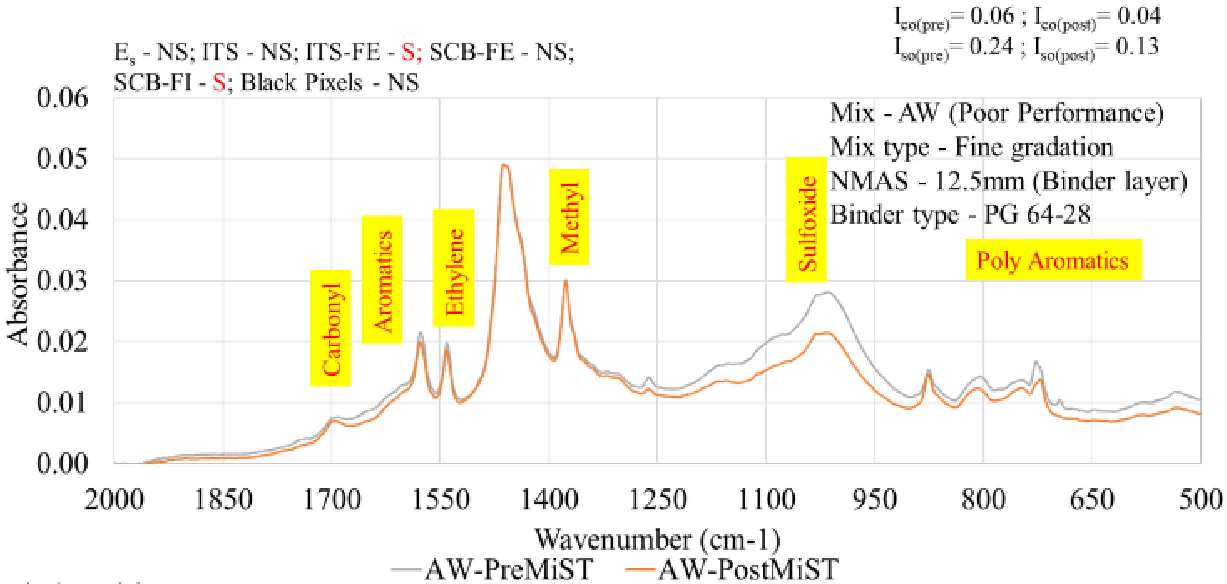

Es -Seismic Modulus;
ITS-FE -Indirect Tensile strength Fracture Energy
SCB-FE -Semi Circular Bending test Fracture Energy
SCB-FI -Semi Circular Bending test Flexibility Index

S -Significant;
NS -Not significant 290

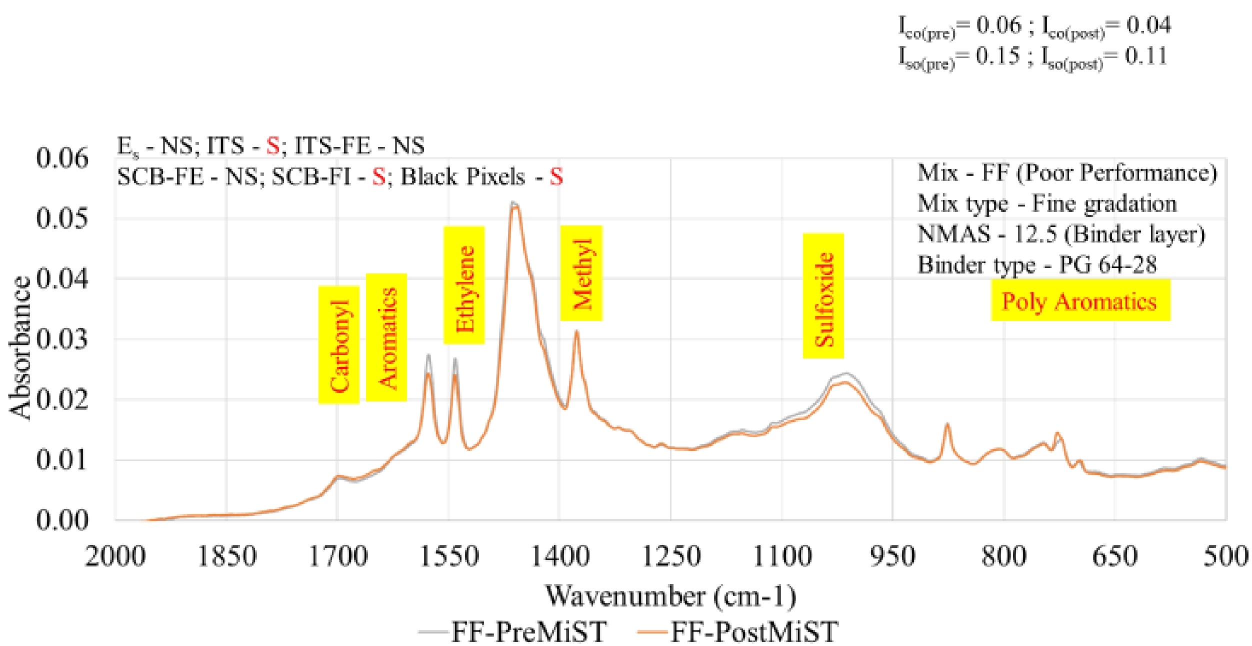

291

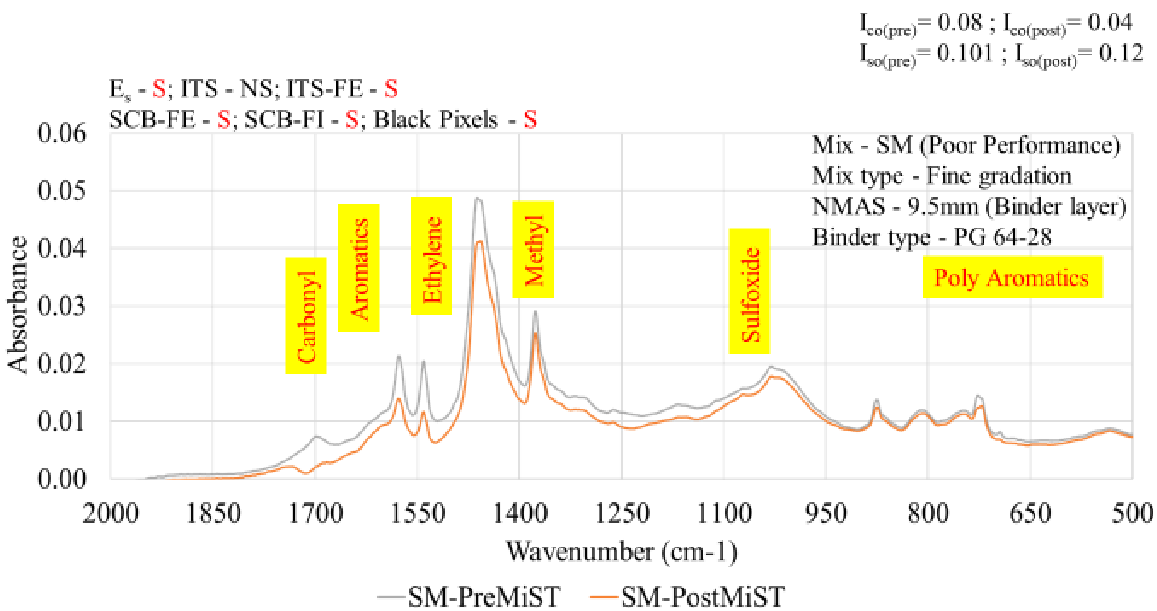
$I_{co(pre)}$ = 0.08 ; $I_{co(post)}$ = 0.04
$I_{so(pre)}$ = 0.101 ; $I_{so(post)}$ = 0.12
E_s - S; ITS - NS; ITS-FE - S
SCB-FE - S; SCB-FI - S; Black Pixels - S
Mix - SM (Poor Performance)
Mix type - Fine gradation
NMAS - 9.5mm (Binder layer)
Binder type - PG 64-28
Carbonyl
Aromatics
Ethylene
Methyl
Sulfoxide
Poly Aromatics
Absorbance
Wavenumber (cm-1)
SM-PreMiST
SM-PostMiST

292

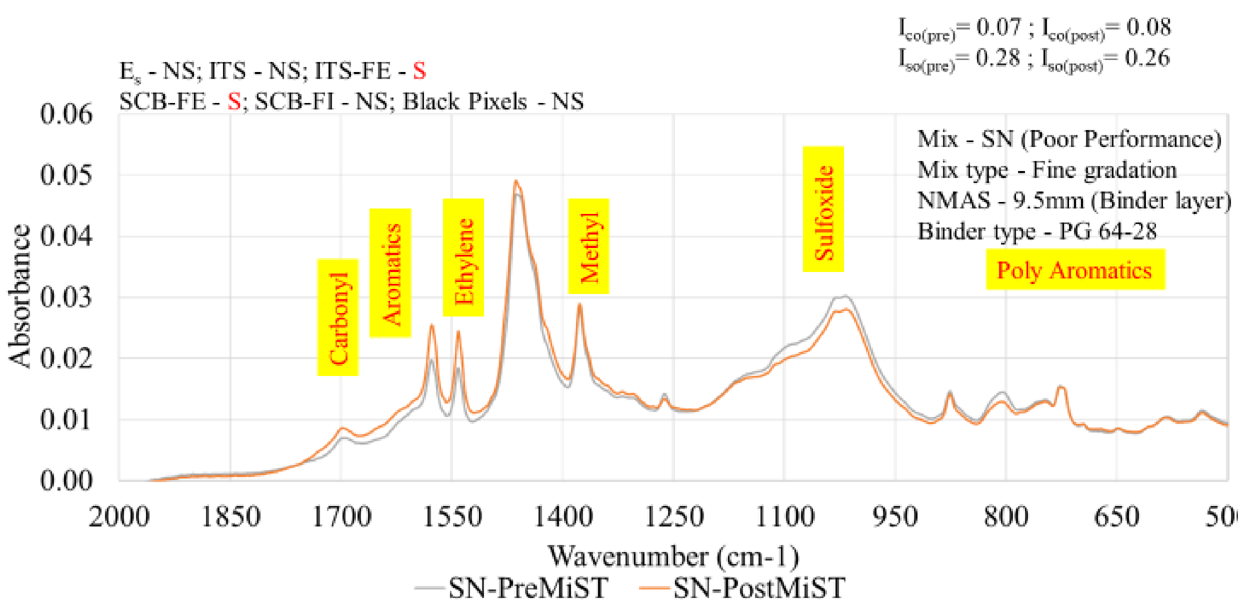
$I_{co(pre)}$ = 0.07 ; $I_{co(post)}$ = 0.08
$I_{so(pre)}$ = 0.28 ; $I_{so(post)}$ = 0.26
E_s - NS; ITS - NS; ITS-FE - S
SCB-FE - S; SCB-FI - NS; Black Pixels - NS
Mix - SN (Poor Performance)
Mix type - Fine gradation
NMAS - 9.5mm (Binder layer)
Binder type - PG 64-28
Carbonyl
Aromatics
Ethylene
Methyl
Sulfoxide
Poly Aromatics
Absorbance
Wavenumber (cm-1)
SN-PreMiST
SN-PostMiST

293

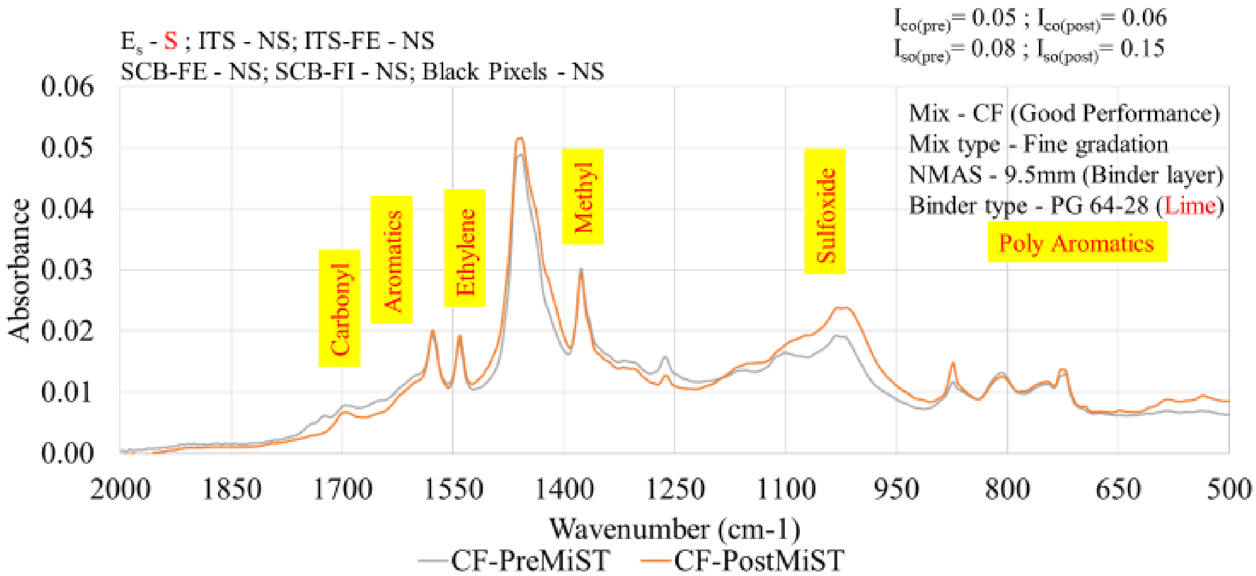

$I_{co(pre)}$= 0.05 ; $I_{co(post)}$= 0.06
$I_{so(pre)}$= 0.08 ; $I_{so(post)}$= 0.15
E_s - S ; ITS - NS; ITS-FE - NS
SCB-FE - NS; SCB-FI - NS; Black Pixels - NS
Mix - CF (Good Performance)
Mix type - Fine gradation
NMAS - 9.5mm (Binder layer)
Binder type - PG 64-28 (Lime)
Poly Aromatics
Carbonyl
Aromatics
Ethylene
Methyl
Sulfoxide
Absorbance
Wavenumber (cm-1)
CF-PreMiST
CF-PostMiST

294

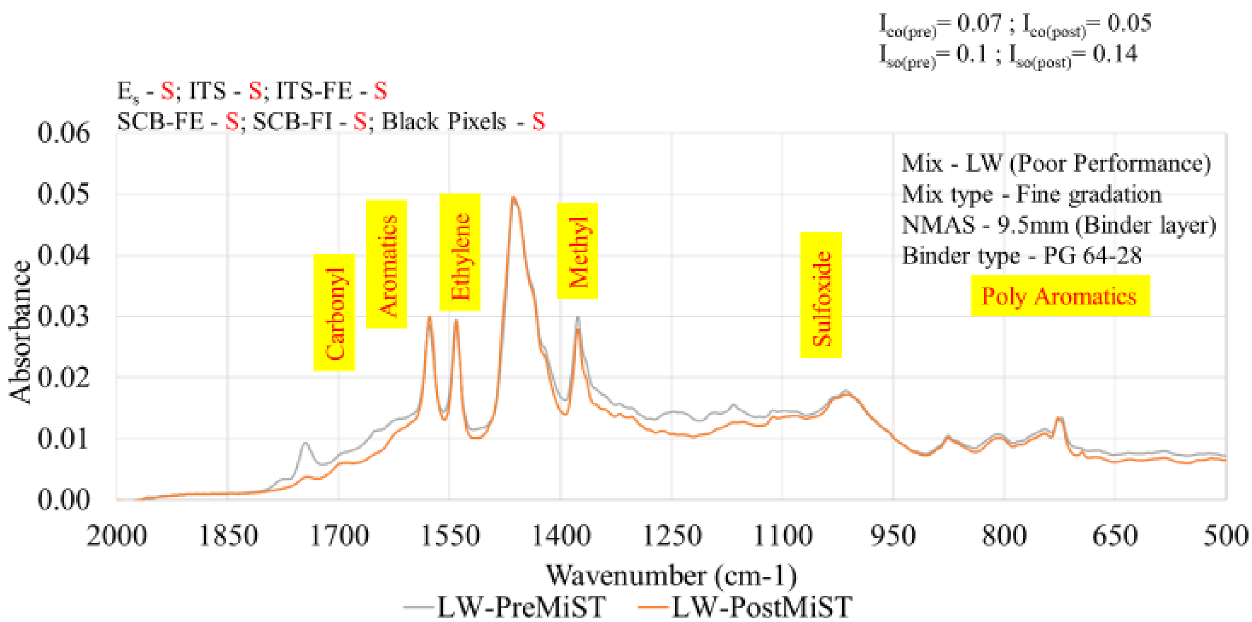

$I_{co(pre)}$= 0.07 ; $I_{co(post)}$= 0.05
$I_{so(pre)}$= 0.1 ; $I_{so(post)}$= 0.14
E_s - S; ITS - S; ITS-FE - S
SCB-FE - S; SCB-FI - S; Black Pixels - S
Mix - LW (Poor Performance)
Mix type - Fine gradation
NMAS - 9.5mm (Binder layer)
Binder type - PG 64-28
Poly Aromatics
Carbonyl
Aromatics
Ethylene
Methyl
Sulfoxide
Absorbance
Wavenumber (cm-1)
LW-PreMiST
LW-PostMiST

295

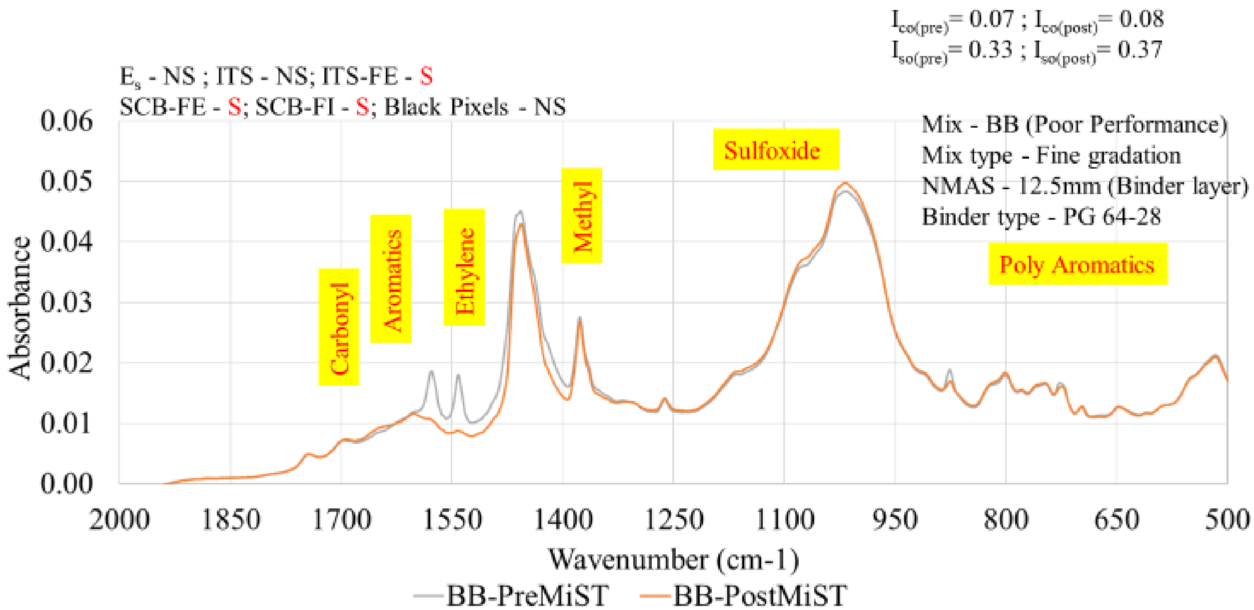

$I_{co(pre)}$= 0.07 ; $I_{co(post)}$= 0.08
$I_{so(pre)}$= 0.33 ; $I_{so(post)}$= 0.37
E_s - NS ; ITS - NS; ITS-FE - S
SCB-FE - S; SCB-FI - S; Black Pixels - NS
Mix - BB (Poor Performance)
Mix type - Fine gradation
NMAS - 12.5mm (Binder layer)
Binder type - PG 64-28
Carbonyl
Aromatics
Ethylene
Methyl
Sulfoxide
Poly Aromatics
Absorbance
Wavenumber (cm-1)
BB-PreMiST
BB-PostMiST

296

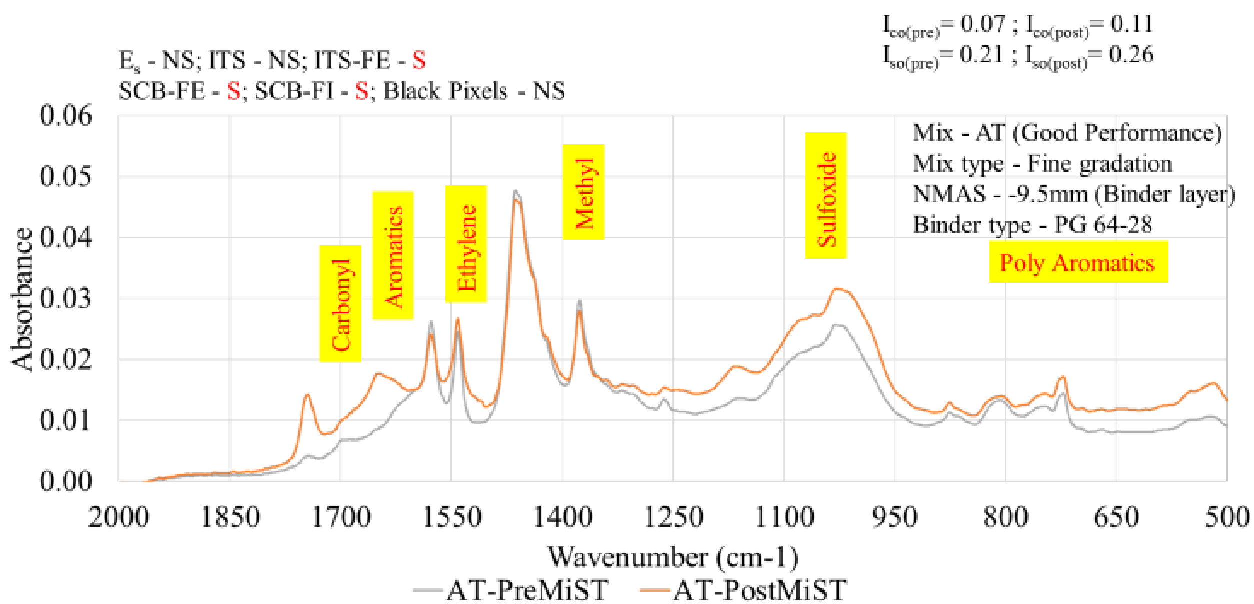

$I_{co(pre)}$= 0.07 ; $I_{co(post)}$= 0.11
$I_{so(pre)}$= 0.21 ; $I_{so(post)}$= 0.26
E_s - NS; ITS - NS; ITS-FE - S
SCB-FE - S; SCB-FI - S; Black Pixels - NS
Mix - AT (Good Performance)
Mix type - Fine gradation
NMAS - -9.5mm (Binder layer)
Binder type - PG 64-28
Carbonyl
Aromatics
Ethylene
Methyl
Sulfoxide
Poly Aromatics
Absorbance
Wavenumber (cm-1)
AT-PreMiST
AT-PostMiST

297

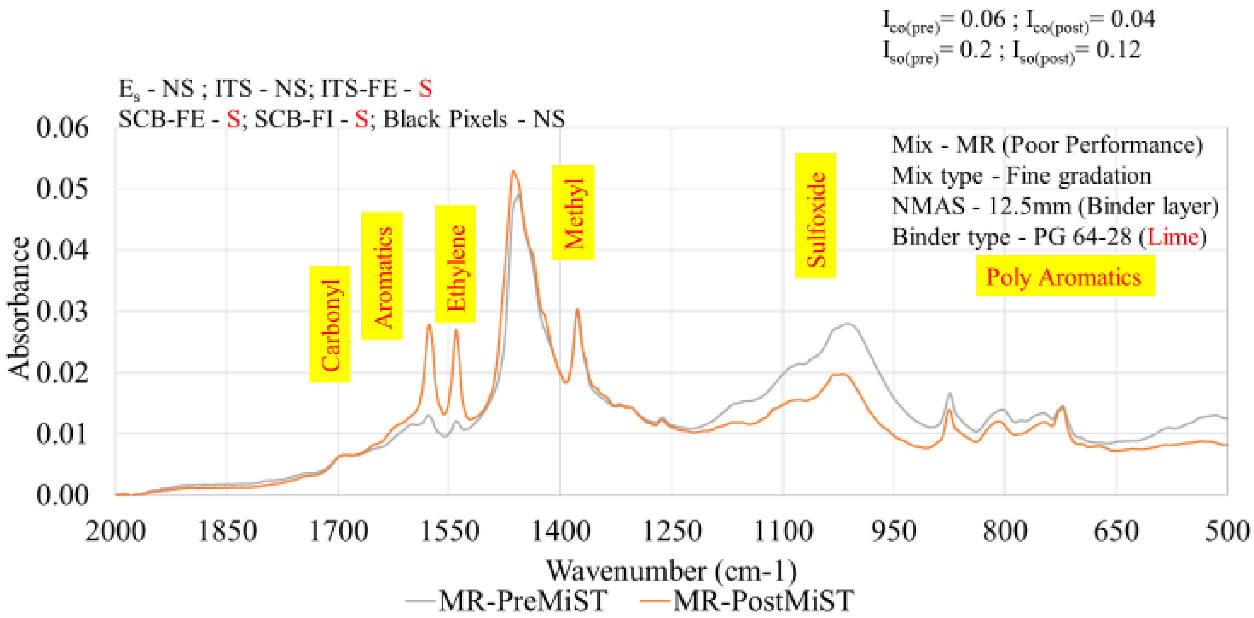

$I_{co(pre)}$= 0.06 ; $I_{co(post)}$= 0.04
$I_{so(pre)}$= 0.2 ; $I_{so(post)}$= 0.12
E_s - NS ; ITS - NS; ITS-FE - S
SCB-FE - S; SCB-FI - S; Black Pixels - NS
Mix - MR (Poor Performance)
Mix type - Fine gradation
NMAS - 12.5mm (Binder layer)
Binder type - PG 64-28 (Lime)
Poly Aromatics
Carbonyl
Aromatics
Ethylene
Methyl
Sulfoxide
Absorbance
Wavenumber (cm-1)
MR-PreMiST
MR-PostMiST

298

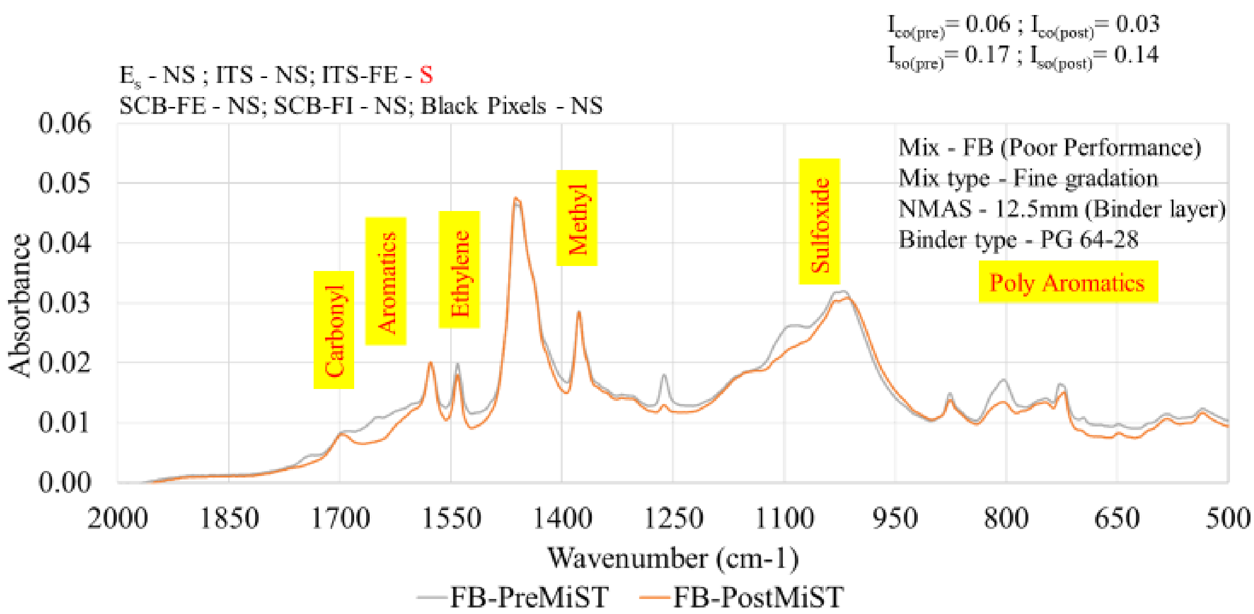

$I_{co(pre)}$= 0.06 ; $I_{co(post)}$= 0.03
$I_{so(pre)}$= 0.17 ; $I_{so(post)}$= 0.14
E_s - NS ; ITS - NS; ITS-FE - S
SCB-FE - NS; SCB-FI - NS; Black Pixels - NS
Mix - FB (Poor Performance)
Mix type - Fine gradation
NMAS - 12.5mm (Binder layer)
Binder type - PG 64-28
Poly Aromatics
Carbonyl
Aromatics
Ethylene
Methyl
Sulfoxide
Absorbance
Wavenumber (cm-1)
FB-PreMiST
FB-PostMiST

299

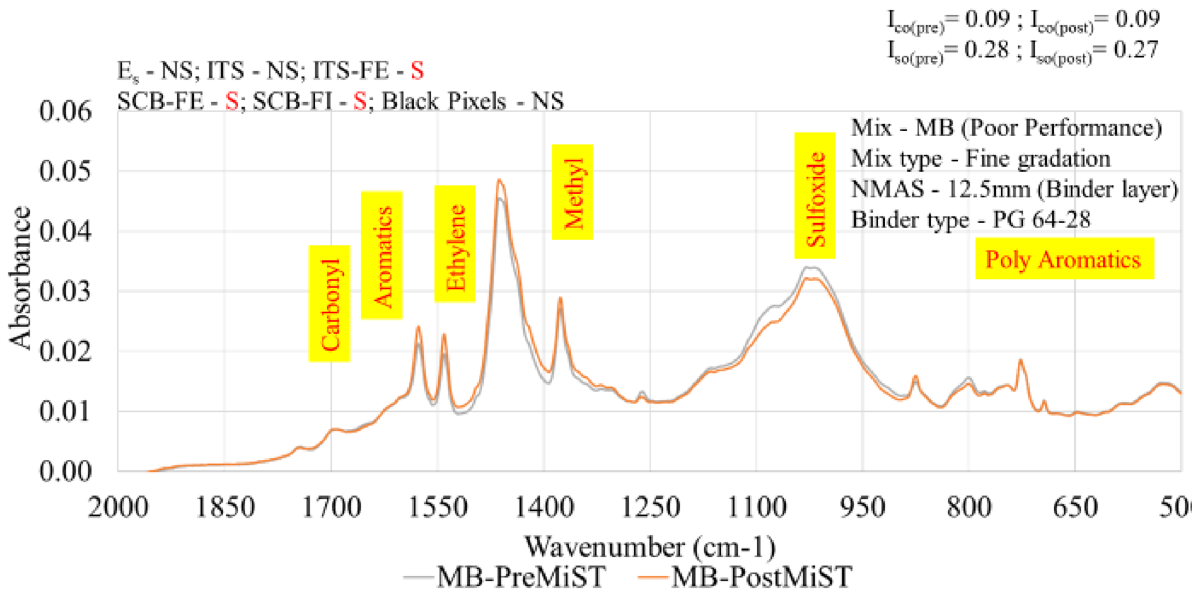

$I_{co(pre)}$= 0.09 ; $I_{co(post)}$= 0.09
$I_{so(pre)}$= 0.28 ; $I_{so(post)}$= 0.27
E_s - NS; ITS - NS; ITS-FE - S
SCB-FE - S; SCB-FI - S; Black Pixels - NS
Mix - MB (Poor Performance)
Mix type - Fine gradation
NMAS - 12.5mm (Binder layer)
Binder type - PG 64-28
Carbonyl
Aromatics
Ethylene
Methyl
Sulfoxide
Poly Aromatics
Absorbance
Wavenumber (cm-1)
MB-PreMiST
MB-PostMiST

300

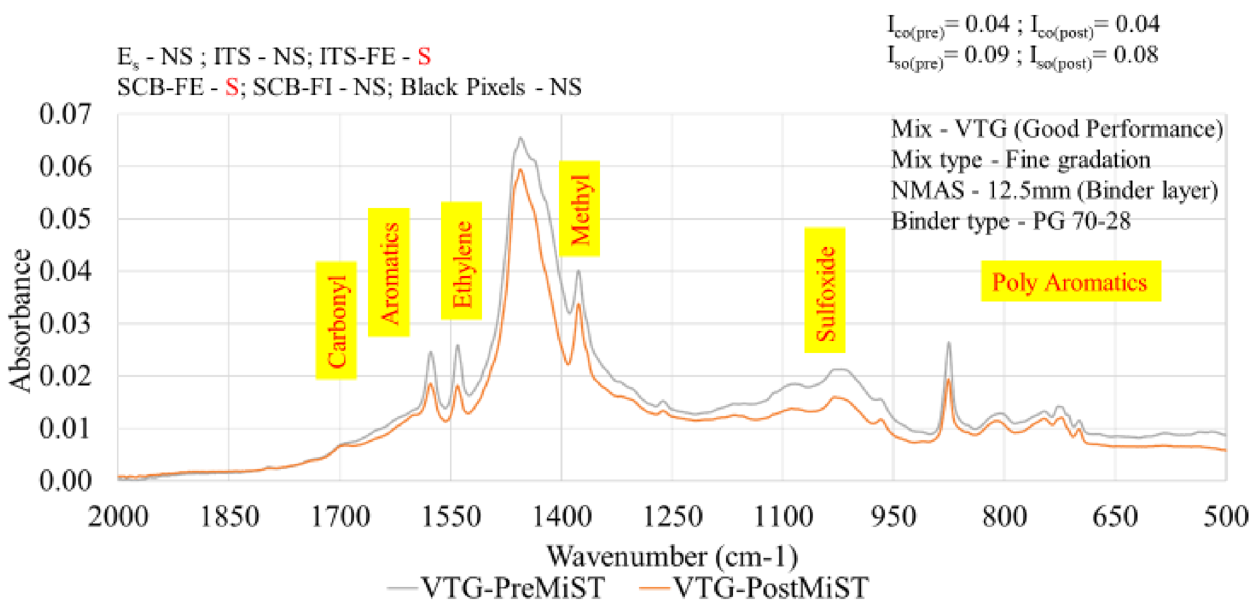

$I_{co(pre)}$= 0.04 ; $I_{co(post)}$= 0.04
$I_{so(pre)}$= 0.09 ; $I_{so(post)}$= 0.08
E_s - NS ; ITS - NS; ITS-FE - S
SCB-FE - S; SCB-FI - NS; Black Pixels - NS
Mix - VTG (Good Performance)
Mix type - Fine gradation
NMAS - 12.5mm (Binder layer)
Binder type - PG 70-28
Carbonyl
Aromatics
Ethylene
Methyl
Sulfoxide
Poly Aromatics
Absorbance
Wavenumber (cm-1)
VTG-PreMiST
VTG-PostMiST

301

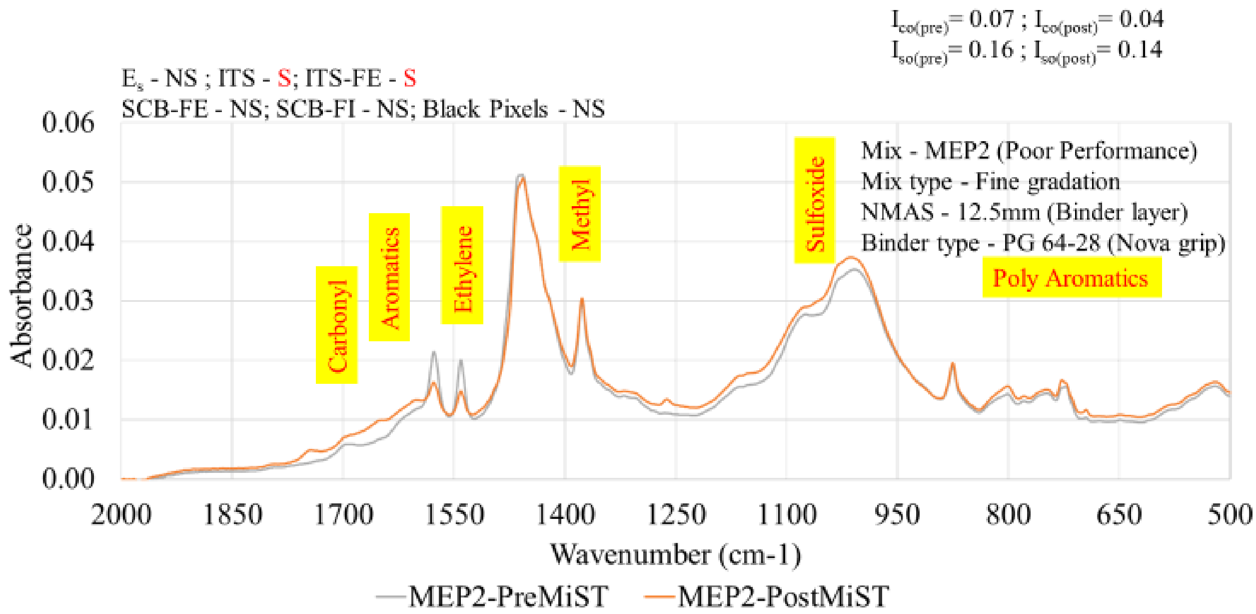

$I_{co(pre)}$= 0.07 ; $I_{co(post)}$= 0.04
$I_{so(pre)}$= 0.16 ; $I_{so(post)}$= 0.14
E_s - NS ; ITS - S; ITS-FE - S
SCB-FE - NS; SCB-FI - NS; Black Pixels - NS
Mix - MEP2 (Poor Performance)
Mix type - Fine gradation
NMAS - 12.5mm (Binder layer)
Binder type - PG 64-28 (Nova grip)
Poly Aromatics
Carbonyl
Aromatics
Ethylene
Methyl
Sulfoxide
Absorbance
0.06
0.05
0.04
0.03
0.02
0.01
0.00
2000
1850
1700
1550
1400
1250
1100
950
800
650
500
Wavenumber (cm-1)
MEP2-PreMiST
MEP2-PostMiST

302

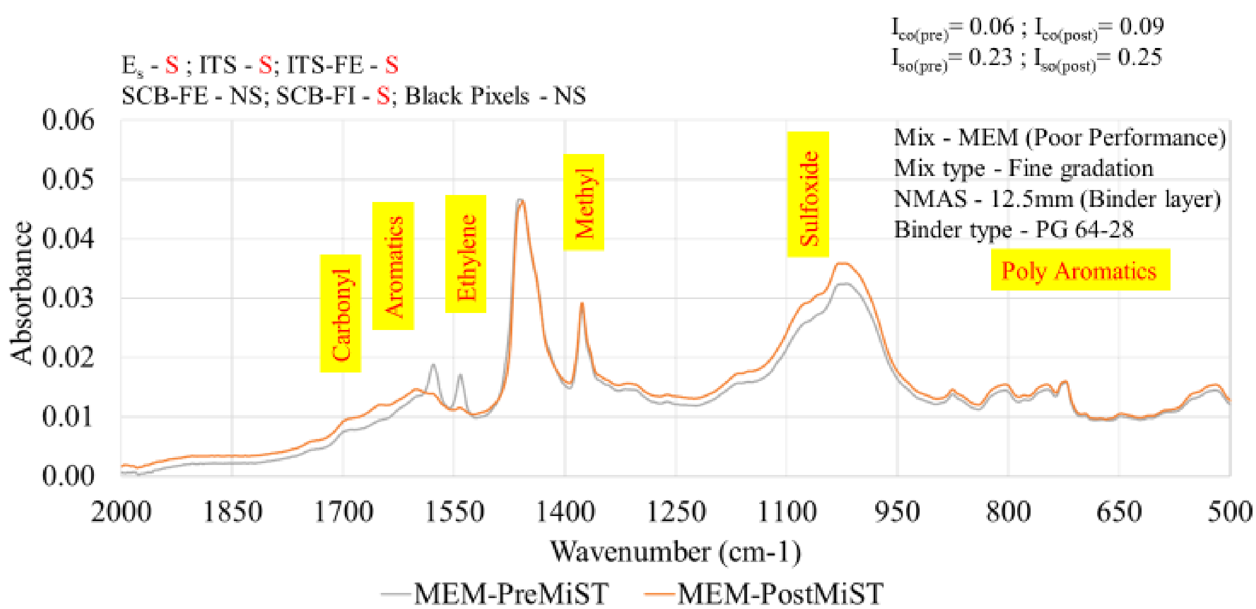

$I_{co(pre)}$= 0.06 ; $I_{co(post)}$= 0.09
$I_{so(pre)}$= 0.23 ; $I_{so(post)}$= 0.25
E_s - S ; ITS - S; ITS-FE - S
SCB-FE - NS; SCB-FI - S; Black Pixels - NS
Mix - MEM (Poor Performance)
Mix type - Fine gradation
NMAS - 12.5mm (Binder layer)
Binder type - PG 64-28
Poly Aromatics
Carbonyl
Aromatics
Ethylene
Methyl
Sulfoxide
Absorbance
0.06
0.05
0.04
0.03
0.02
0.01
0.00
2000
1850
1700
1550
1400
1250
1100
950
800
650
500
Wavenumber (cm-1)
MEM-PreMiST
MEM-PostMiST

303

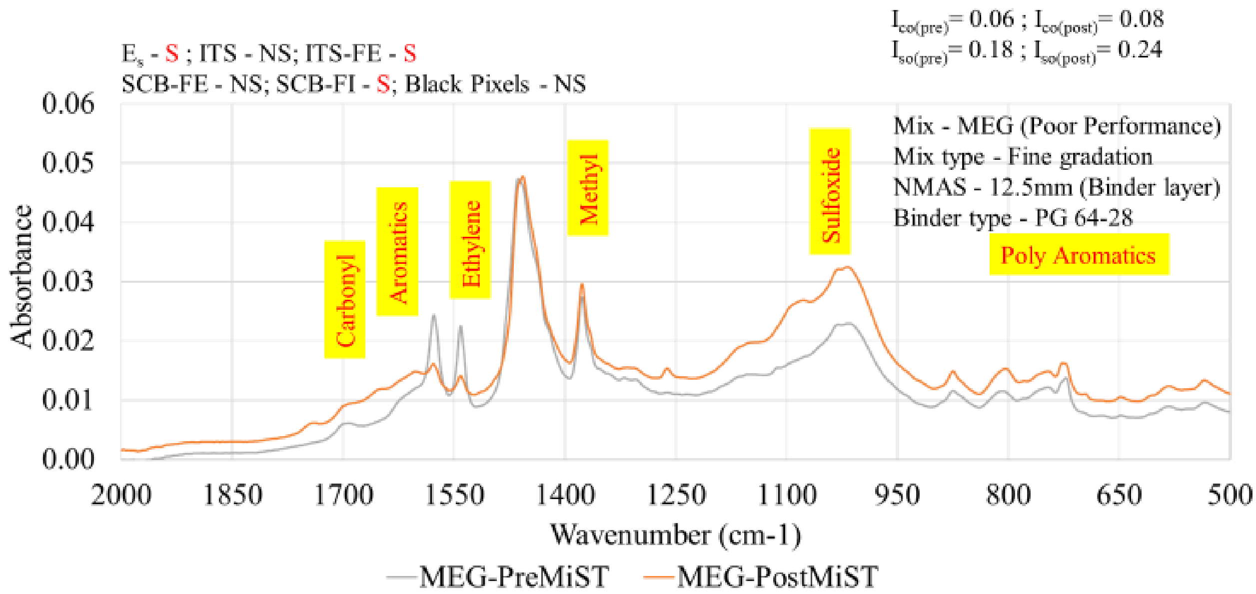
I_co(pre) = 0.06 ; I_co(post) = 0.08
I_so(pre) = 0.18 ; I_so(post) = 0.24
Es - S ; ITS - NS; ITS-FE - S
SCB-FE - NS; SCB-FI - S; Black Pixels - NS
Mix - MEG (Poor Performance)
Mix type - Fine gradation
NMAS - 12.5mm (Binder layer)
Binder type - PG 64-28
Poly Aromatics
Carbonyl
Aromatics
Ethylene
Methyl
Sulfoxide
Absorbance
Wavenumber (cm-1)
MEG-PreMiST
MEG-PostMiST

304

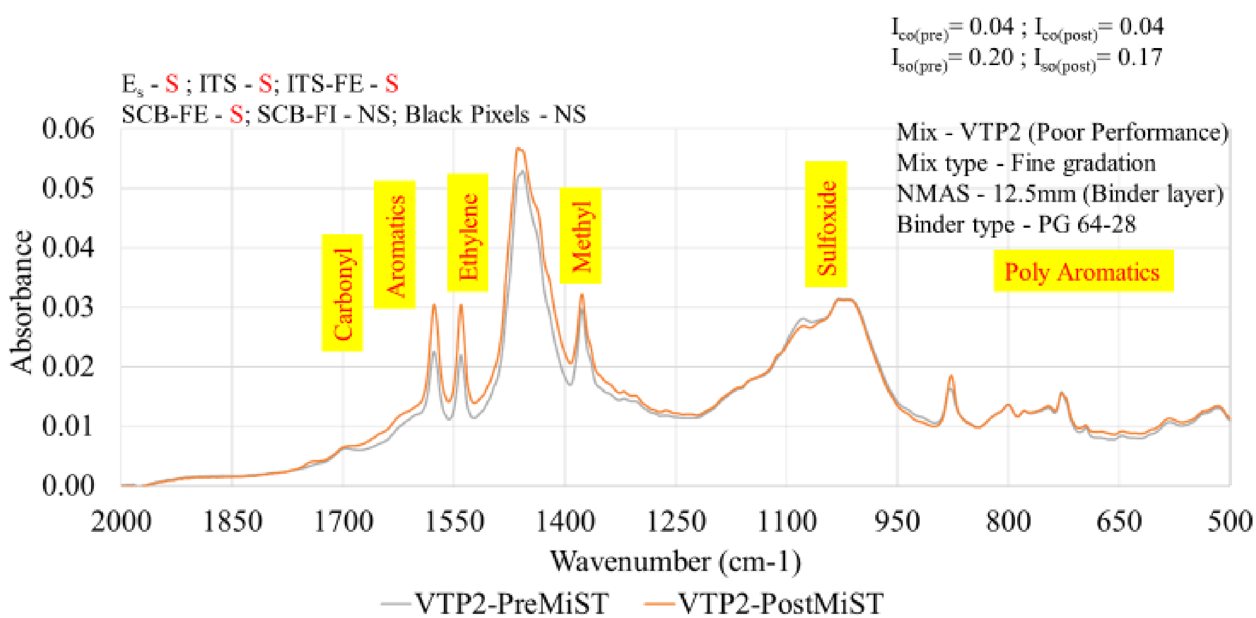
I_co(pre) = 0.04 ; I_co(post) = 0.04
I_so(pre) = 0.20 ; I_so(post) = 0.17
Es - S ; ITS - S; ITS-FE - S
SCB-FE - S; SCB-FI - NS; Black Pixels - NS
Mix - VTP2 (Poor Performance)
Mix type - Fine gradation
NMAS - 12.5mm (Binder layer)
Binder type - PG 64-28
Poly Aromatics
Carbonyl
Aromatics
Ethylene
Methyl
Sulfoxide
Absorbance
Wavenumber (cm-1)
VTP2-PreMiST
VTP2-PostMiST

305

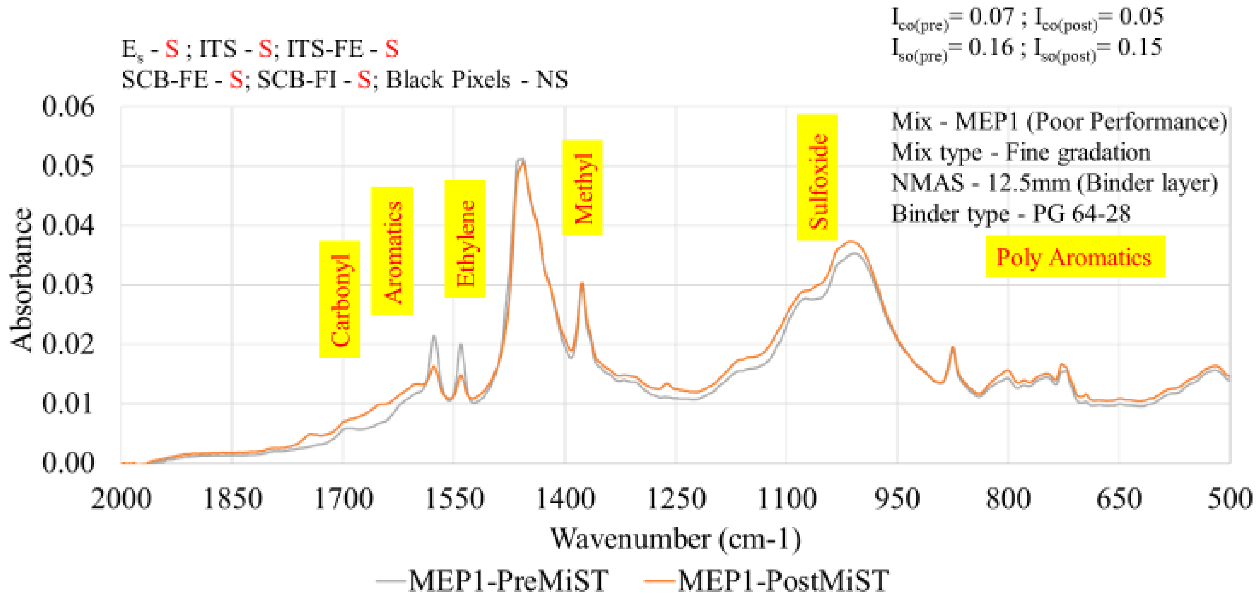
$I_{co(pre)}$= 0.07 ; $I_{co(post)}$= 0.05
$I_{so(pre)}$= 0.16 ; $I_{so(post)}$= 0.15
E_s - S ; ITS - S; ITS-FE - S
SCB-FE - S; SCB-FI - S; Black Pixels - NS
Mix - MEP1 (Poor Performance)
Mix type - Fine gradation
NMAS - 12.5mm (Binder layer)
Binder type - PG 64-28
Poly Aromatics
Carbonyl
Aromatics
Ethylene
Methyl
Sulfoxide
Absorbance
Wavenumber (cm-1)
MEP1-PreMiST
MEP1-PostMiST

306

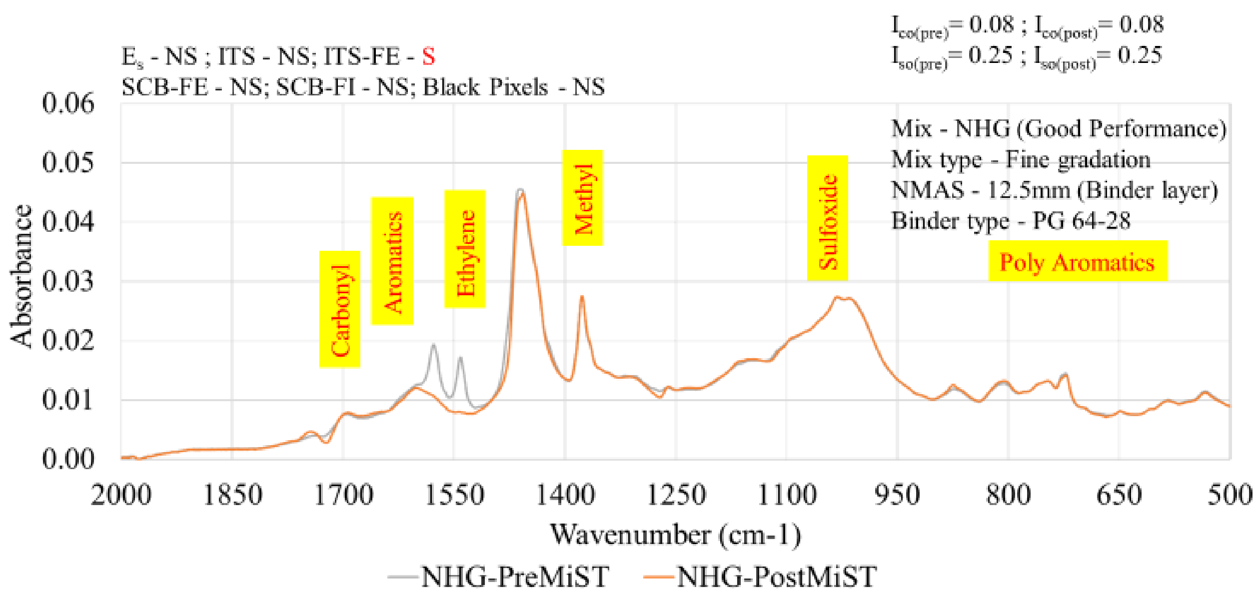
$I_{co(pre)}$= 0.08 ; $I_{co(post)}$= 0.08
$I_{so(pre)}$= 0.25 ; $I_{so(post)}$= 0.25
E_s - NS ; ITS - NS; ITS-FE - S
SCB-FE - NS; SCB-FI - NS; Black Pixels - NS
Mix - NHG (Good Performance)
Mix type - Fine gradation
NMAS - 12.5mm (Binder layer)
Binder type - PG 64-28
Poly Aromatics
Carbonyl
Aromatics
Ethylene
Methyl
Sulfoxide
Absorbance
Wavenumber (cm-1)
NHG-PreMiST
NHG-PostMiST

307

A 1.2: FTIR I_{CO} and I_{SO} indices Results:

Mix ID	Pre-MiST I_{CO}	Post-MiST I_{CO}	Pre-MiST I_{SO}	Post-MiST I_{SO}	Performance
1	0.07	0.03	0.18	0.12	Poor
	0.06	0.05	0.37	0.07	
	0.06	0.06	0.16	0.20	
2	0.06	0.04	0.17	0.15	Poor
	0.05	0.06	0.14	0.07	
	0.06	0.04	0.15	0.12	
3	0.07	0.05	0.09	0.09	Poor
	0.08	0.00	0.11	0.16	
	0.13	0.09	0.10	0.11	
4	0.08	0.10	0.21	0.33	Poor
	0.05	0.07	0.33	0.12	
	0.08	0.07	0.30	0.36	
5	0.06	0.07	0.08	0.17	Good
	0.03	0.06	0.08	0.16	
	0.06	0.07	0.07	0.14	
7	0.07	0.04	0.10	0.15	Poor
	0.08	0.05	0.06	0.15	
	0.07	0.05	0.15	0.14	
8	0.07	0.08	0.21	0.26	Poor
	0.08	0.08	0.20	0.26	
	0.07	0.09	0.21	0.27	
9	0.07	0.11	0.30	0.42	Good
	0.06	0.11	0.35	0.36	
	0.07	0.11	0.35	0.36	
11	0.06	0.03	0.16	0.15	Poor
	0.07	0.04	0.16	0.11	
	0.06	0.03	0.18	0.16	

A 1.2: FTIR I_{CO} and I_{SO} indices Results (Continued).

Mix ID	Pre-MiST I_{CO}	Post-MiST I_{CO}	Pre-MiST I_{SO}	Post-MiST I_{SO}	Performance
12	0.09	0.08	0.28	0.29	Poor
	0.09	0.07	0.28	0.28	
	0.11	0.12	0.28	0.27	
15	0.07	0.04	0.16	0.17	Poor
	0.07	0.04	0.16	0.17	
	0.07	0.04	0.16	0.17	
16	0.05	0.04	0.10	0.08	Good
	0.04	0.04	0.09	0.08	
	0.03	0.04	0.08	0.08	
17	0.04	0.04	0.20	0.17	Good
	0.04	0.04	0.20	0.17	
	0.04	0.04	0.19	0.17	
18	0.07	0.08	0.18	0.23	Poor
	0.06	0.09	0.18	0.24	
	0.06	0.08	0.18	0.25	
21	0.07	0.09	0.21	0.24	Good
	0.08	0.09	0.24	0.26	
	0.03	0.09	0.26	0.25	
23	0.06	0.04	0.16	0.12	Poor
	0.08	0.04	0.16	0.16	
	0.07	0.05	0.18	0.15	
24	0.08	0.07	0.27	0.21	Poor
	0.07	0.08	0.22	0.27	
	0.08	0.09	0.26	0.29	

APPENDIX B

Appendix B consists of raw obtained from various mixture testing. These test results include:

1. Seismic modulus (E_s), from Ultrasonic Pulse Velocity (UPV) test.
2. Indirect Tensile Strength (ITS) and Fracture Energy (FE-ITS) results obtained from tensile strength test.
3. Fracture Energy (FE-SCB) and Flexibility Index (FI-SCB) from semi-circular bending (SCB) test .
4. Black Pixels (BP) from image analysis.
5. Loss of Material (LOM), Dissolved Organic Carbon (DOC), Fineness Modulus (FM) from MiST effluent analysis

B 1.1: Ultrasonic Pulse Velocity (UPV) Test Results

Mix ID	Sample No.	Pre-MiST Es (MPa)	Post-MiST Es (MPa)	Performance
1	1	11,418	13,169	Poor
	2	14,196	13,741	
	3	13,721	12,473	
2	1	13,721	13,045	Poor
	2	12,542	12,507	
	3	13,238	13,128	
3	1	12,638	10,528	Poor
	2	12,555	11,376	
	3	11,735	10,687	
4	1	12,792	12,599	Poor
	2	12,282	11,403	
	3	12,757	11,331	
5	1	11,903	10,821	Good
	2	12,292	11,197	
	3	12,997	11,662	
6	1	14,389	13,650	Good
	2	14,761	13,248	
7	1	11,902	8,356	Poor
	2	11,009	8,384	
	3	11,240	7,928	
8	1	12,986	13,066	Poor
	2	13,262	13,435	
9	1	12,107	10,652	Good
	2	12,080	10,649	
10	1	12,631	11,703	Poor
	2	12,149	12,901	

B 1.1: Ultrasonic Pulse Velocity (UPV) Test Results (Continued)

Mix ID	Sample No.	Pre-MiST Es (MPa)	Post-MiST Es (MPa)	Performance
11	1	11,064	11,564	Poor
	2	12,218	11,784	
12	1	9,395	12,563	Poor
	2	9,552	11,721	
13	1	12,522	12,169	Poor
	2	14,420	13,631	
14	1	13,646	12,330	Poor
	2	12,779	12,793	
15	1	12,878	10,522	Poor
	2	12,943	10,022	
	3	13,344	10,492	
16	1	13,570	15,532	Good
	2	13,288	14,173	
	3	14,321	14,436	
17	1	12,295	10,825	Good
	2	11,781	11,411	
	3	12,093	11,625	
18	1	11,293	10,930	Poor
	2	11,442	10,792	
	3	12,346	11,707	
19	1	12,270	10,790	Poor
	2	11,247	9,691	
	3	11,573	9,681	
20	1	12,588	11,702	Poor
	2	11,957	10,875	
	3	12,324	11,247	

B 1.1: Ultrasonic Pulse Velocity (UPV) Test Results (Continued)

Mix ID	Sample No.	Pre-MiST Es (MPa)	Post-MiST Es (MPa)	Performance
21	1	12,790	11,065	Good
	2	12,472	11,305	
	3	12,175	11,533	
22	1	14,790	13,168	Poor
	2	13,601	12,991	
	3	13,294	12,041	
23	1	11,606	10,907	Poor
	2	11,872	11,710	
	3	12,088	11,611	
24	1	11,857	11,807	Poor
	2	12,739	11,898	
	3	12,139	10,867	
25	1	11,545	12,684	Good
	2	11,613	12,423	
	3	13,531	13,311	
26	1	12,428	12,647	Poor
	2	12,499	13,594	
	3	12,200	13,783	
27	1	11,097	11,388	Poor
	2	11,380	11,358	
	3	10,307	11,896	
28	1	12,346	12,087	Poor
	2	11,405	11,447	
	3	12,788	12,333	
29	1	11,115	10,234	Poor
	2	10,862	10,205	
	3	11,633	10,111	

B 1.1: Ultrasonic Pulse Velocity (UPV) Test Results (Continued)

Mix ID	Sample No.	Pre-MiST Es (MPa)	Post-MiST Es (MPa)	Performance
30	1	13,947	11,450	Poor
	2	11,124	10,397	
	3	11,024	11,848	
31	1	11,935	11,912	Poor
	2	11,925	11,157	
	3	10,617	11,164	
32	1	12,047	12,707	Poor
	2	11,342	12,747	
	3	11,343	12,702	
33	1	10,325	11,442	Poor
	2	10,387	12,110	
	3	10,883	11,410	
34	1	12,714	11,776	Poor
	2	11,990	11,893	
35	1	12,475	11,507	Poor
	2	11,888	11,285	
	3	12,133	12,320	
36	1	11,886	12,227	Good
	2	11,496	12,193	
37	1	11,476	12,320	Good
	2	11,385	12,944	
38	1	10,528	12,969	Poor
	2	10,666	12,555	
	3	11,549	12,583	

B 1.2: Indirect Tensile Strength (ITS) Test Results

Mix ID	Pre-MiST ITS (kPa)	Post-MiST ITS (kPa)	Pre-MiST FE-ITS (J/m^2)	Post-MiST FE-ITS (J/m^2)	Performance
1	803	855	1,975	3,335	Poor
	909	772	1,976	3,061	
	844	603	2,310	2,573	
2	1,041	1,019	3,133	3,866	Poor
	1,074	989	4,188	4,196	
	1,107	965	3,282	3,746	
3	677	546	2,410	3,113	Poor
	778	631	2,528	3,365	
	609	603	2,142	3,489	
4	667	900	1,965	3,287	Poor
	846	665	2,415	3,050	
	826	650	2,501	2,765	
5	638	567	1,993	2,439	Good
	736	581	2,392	2,524	
	636	626	2,008	2,738	
6	691	547	2,087	2,393	Good
	703	520	2,383	2,380	
7	732	375	2,447	2,068	Poor
	667	349	2,344	1,573	
	684	388	2,238	1,755	
8	836	831	2,503	3,882	Poor
	868	709	2,651	4,015	
9	641	602	2,547	3,600	Good
	725	567	2,310	3,283	
10	618	524	1,851	2,546	Poor
	601	554	1,789	2,740	

B 1.2: Indirect Tensile Strength (ITS) Test Results (Continued)

Mix ID	Pre-MiST ITS (kPa)	Post-MiST ITS (kPa)	Pre-MiST FE-ITS (J/m^2)	Post-MiST FE-ITS (J/m^2)	Performance
11	713	720	2,502	3,111	Poor
	795	724	2,372	3,092	
12	702	558	2,085	2,939	Poor
	681	569	1,944	2,803	
13	684	689	2,066	3,629	Poor
	748	678	2,111	3,196	
14	741	702	1,733	2,751	Poor
	699	665	1,666	2,757	
15	601	435	1,895	2,270	Poor
	572	431	1,892	2,275	
	592	432	1,867	2,496	
16	956	970	2,963	4,276	Good
	930	842	2,873	3,549	
	910	979	2,900	3,940	
17	544	415	1,822	2,352	Good
	545	387	1,954	2,571	
	550	415	2,020	2,588	
18	530	452	1,668	1,934	Poor
	547	506	1,530	2,245	
	546	494	1,668	2,023	
19	375	305	1,700	2,383	Poor
	416	309	1,709	2,082	
	410	309	1,656	2,311	
20	691	564	2,423	2,890	Poor
	632	561	2,127	2,657	
	617	525	2,244	2,101	

B 1.2: Indirect Tensile Strength (ITS) Test Results (Continued)

Mix ID	Pre-MiST ITS (kPa)	Post-MiST ITS (kPa)	Pre-MiST FE-ITS (J/m^2)	Post-MiST FE-ITS (J/m^2)	Performance
21	638	509	2,161	3,244	Good
	662	501	2,345	3,292	
	650	563	2,070	3,090	
22	646	577	2,417	2,741	Poor
	618	682	2,377	2,971	
	658	609	2,402	3,204	
23	495	381	1,954	3,139	Poor
	525	408	2,384	2,736	
	491	404	2,115	2,831	
24	742	745	2,322	3,305	Poor
	811	718	2,453	3,164	
	852	787	2,275	3,151	
25	573	533	1,779	2,837	Good
	629	482	2,087	3,169	
	607	495	2,240	3,250	
26	949	873	3,489	4,305	Poor
	969	850	3,714	4,557	
	932	926	4,383	4,434	
27	715	580	2,838	3,485	Poor
	655	555	2,816	3,793	
	695	609	3,053	3,662	
28	636	596	2,557	3,213	Poor
	599	565	2,008	3,106	
	606	594	1,164	3,276	
29	569	450	1,968	2,604	Poor
	667	502	2,222	2,666	
	588	512	2,144	2,739	

B 1.2: Indirect Tensile Strength (ITS) Test Results (Continued)

Mix ID	Pre-MiST ITS (kPa)	Post-MiST ITS (kPa)	Pre-MiST FE-ITS (J/m^2)	Post-MiST FE-ITS (J/m^2)	Performance
30	578	665	2,276	3,089	Poor
	641	760	2,391	3,007	
	761	678	2,807	3,406	
31	738	677	2,040	2,445	Poor
	716	698	2,154	2,715	
	731	671	2,259	2,563	
32	868	865	2,543	3,304	Poor
	952	869	2,932	3,217	
	953	801	2,861	3,282	
33	978	883	3,398	4,373	Poor
	968	1,037	3,434	4,824	
	1,010	1,026	3,702	4,761	
34	802	710	2,514	5,372	Poor
	890	748	2,382	2,216	
35	727	625	2,171	4,346	Poor
	761	568	2,625	3,766	
	777	654	2,767	3,784	
36	828	837	3,158	4,220	Good
	781	904	3,132	4,597	
37	1,064	865	3,018	2,904	Good
	917	875	3,542	4,151	
38	1,035	888	3,078	4,396	Poor
	963	860	3,309	4,566	
	1,013	941	3,358	4,880	

B 1.3: Semi-Circular Bend (SCB) Test Results

Mix ID	Pre-MIST FE-SCB (J/m^2)	Post-MIST FE-SCB (J/m^2)	Pre-MIST SCB-FI	Post-MIST SCB-FI	Performance
1	1,513	7,123	9.6	35.4	Poor
	2,247	4,897	7.7	49.5	
	2,224	2,706	14.5	17.8	
	4,363	3,998	26.6	33.9	
2	5,104	6,447	25.9	43.9	Poor
	2,281	4,946	9.2	37.5	
	7,415	9,932	17.1	62.5	
	4,603	7,634	13.3	39.2	
3	6,326	8,634	30.3	66.9	Poor
	4,709	7,307	21.7	89.0	
	3,758	6,426	16.7	136.7	
	3,141	6,635	14.0	90.9	
4	1,783	6,092	7.2	32.8	Poor
	2,968	4,672	11.0	20.5	
	5,512	4,230	27.8	31.6	
	2,571	6,218	15.9	56.5	
5	2,800	3,661	28.3	34.2	Good
	3,238	3,380	35.6	39.3	
	3,796	4,192	32.5	40.7	
	4,009	4,481	39.7	77.3	
6	6,783	5,894	30.2	90.7	Good
	5,686	3,275	69.3	17.2	
	6,190	3,269	95.2	24.0	
7	4,939	1,869	35.8	23.4	Poor
	3,806	2,276	21.1	39.3	
	4,394	2,490	18.6	30.0	
	4,490	1,777	16.4	30.6	

B 1.3: Semi-Circular Bend (SCB) Test Results (Continued)

Mix ID	Pre-MIST FE-SCB (J/m^2)	Post-MIST FE-SCB (J/m^2)	Pre-MIST SCB-FI	Post-MIST SCB-FI	Performance
8	4,100	9,642	11.8	83.0	Poor
	4,122	9,864	12.7	50.8	
	4,177	10,647	18.0	70.0	
	5,138	10,266	20.2	75.5	
9	3,982	8,209	39.8	161.0	Good
	4,644	8,636	36.3	134.0	
	4,206	9,273	37.2	79.9	
	4,686	8,731	47.8	140.3	
10	2,862	7,762	16.7	41.1	Poor
	2,030	5,596	8.8	53.8	
	4,021	4,622	15.5	39.2	
	2,388	4,336	10.1	36.4	
11	2,487	6,742	12.2	78.4	Poor
	2,903	4,673	13.1	22.4	
	2,971	3,933	19.7	19.7	
	2,440		15.2		
12	3,234	5,870	18.2	50.6	Poor
	3,457	7,913	17.0	68.8	
	3,578	5,831	21.2	28.7	
	6,314	5,997	30.1	30.0	
13	5,874	11,399	38.9	92.7	Poor
	1,705	8,969	8.4	85.4	
	4,128	10,783	31.3	52.1	
	3,540	8,406	30.5	129.3	
14	4,338	6,520	17.6	49.4	Poor
	2,631	7,400	7.4	33.0	
	3,174	6,624	11.3	36.4	
	3,043	6,052	8.7	31.7	

B 1.3: Semi-Circular Bend (SCB) Test Results (Continued)

Mix ID	Pre-MIST FE-SCB (J/m^2)	Post-MIST FE-SCB (J/m^2)	Pre-MIST SCB-FI	Post-MIST SCB-FI	Performance
15	8,289	9,256	47.9	106.4	Poor
	7,350	9,379	34.4	97.5	
	6,234	10,051	44.9	102.1	
	8,518	7,963	55.3	68.1	
16	3,764	6,520	20.5	49.4	Good
	4,747	7,400	22.5	33.0	
	4,096	6,624	23.5	36.4	
	3,868	6,052	31.7	31.7	
17	5,285	6,975	47.2	98.2	Poor
	4,361	6,278	40.0	51.9	
	4,701	6,030	56.0	54.4	
	4,664	5,623	46.6	156.0	
18	1,311	2,073	9.3	18.2	Poor
	2,224	2,095	13.7	24.4	
	1,409	1,988	11.6	32.1	
	1,249	2,319	10.7	27.9	
19	1,714	3,736	27.2	59.3	Poor
	1,703	4,828	22.4	73.2	
	1,889	3,371	20.5	153.2	
	1,865	4,244	25.2	47.7	
20	2,010	3,380	20.5	27.3	Poor
	2,228	8,126	16.3	40.0	
	2,290	3,053	15.7	29.1	
	1,936	3,098	11.3	19.4	
21	1,969	6,421	10.8	48.3	Good
	1,919	3,227	11.8	32.3	
	2,244	3,328	12.1	44.4	
	2,131	2,902	13.4	46.8	

B 1.3: Semi-Circular Bend (SCB) Test Results (Continued)

Mix ID	Pre-MIST FE-SCB (J/m^2)	Post-MIST FE-SCB (J/m^2)	Pre-MIST SCB-FI	Post-MIST SCB-FI	Performance
22	2,360	4,858	19.0	138.8	Poor
	2,351	4,414	17.0	52.6	
	2,812	4,178	18.4	78.8	
	2,089	3,625	14.2	100.7	
23	2,232	2,988	37.8	63.6	Poor
	1,634	2,657	22.4	44.3	
	2,105	3,036	21.3	108.4	
	2,052	3,628	21.4	60.5	
24	1,519	2,426	5.1	17.3	Poor
	1,631	2,241	7.8	15.7	
	1,745	2,130	10.0	18.2	
	1,265	2,206	5.5	20.2	
25	2025	2913	11.1	48.6	Good
	2278	3187	10.9	31.3	
26	2724	5076	11.5	38.9	Poor
	2927	5156	12.5	43.2	
27	2985	4983	18.2	29.6	Poor
	3155	5242	12.5	31.5	
28	3985	2101	32.7	15.9	Poor
	3381	2248	22.1	13.5	
29	2154	2511	14.2	29.1	Poor
	1830	1279	6.8	4.3	

B 1.3: Semi-Circular Bend (SCB) Test Results (Continued)

Mix ID	Pre-MIST FE-SCB (J/m^2)	Post-MIST FE-SCB (J/m^2)	Pre-MIST SCB-FI	Post-MIST SCB-FI	Performance
30	2116	1624	10.9	19.6	Poor
	1868	2167	10.0	13.9	
31	1656	1461	11.7	9.4	Poor
	1501	2098	8.3	10.0	
32	1618	2041	5.3	12.9	Poor
	1760	1981	6.5	9.3	
33	6373	7236	21.6	28.4	Poor
	7268	8250	15.6	27.3	
34	4647	6229	14	33.13	Poor
	3724	7071	9.24	42.09	
35	3472	3352	33	9	Poor
	3908	2018	28	14	
36	4464	7627	16.4	30.5	Good
	5224	6437	10.4	66.5	
37	4735	6603	19.2	65.4	Poor
	5469	7677	11.2	25.0	
38	4460	6475	10.8	35.5	Poor
	4126	5267	14.4	41.9	

B 1.4 Image Analysis Test Results

Mix ID	Pre-MiST BP	Post-MiST BP	Performance
1	1,010,291	978,408	Poor
	1,141,262	1,134,294	
	1,038,071	1,011,413	
2	1,007,005	925,790	Poor
	1,071,046	983,131	
	1,077,759	972,644	
3	1,033,228	972,356	Poor
	1,017,279	985,534	
	1,086,507	1,018,256	
4	814,911	706,196	Poor
	872,090	830,722	
	681,774	716,465	
5	693,578	629,041	Good
	888,052	762,772	
	749,112	686,108	
6	970,678	947,315	Good
	904,930	897,741	
7	1,137,475	1,038,928	Poor
	1,153,778	1,138,692	
	1,093,188	994,099	
8	956,945	788,959	Poor
	904,607	873,384	
9	1,154,746	1,063,228	Good
	1,008,781	999,374	
10	1,183,649	912,588	Poor
	1,127,065	959,536	

B 1.4 Image Analysis Test Results (Continued)

Mix ID	Pre-MiST BP	Post-MiST BP	Performance
11	1,391,946	1,063,004	Poor
	994,586	1,123,856	
12	1,727,461	1,537,324	Poor
	1,325,461	1,245,705	
13	975,145	1,118,488	Poor
	1,130,883	1,171,842	
14	1,131,818	1,258,295	Poor
	1,150,490	1,177,217	
15	1,137,475	1,038,928	Poor
	1,153,778	1,138,692	
	1,093,188	994,099	
16	1,174,631	1,145,773	Good
	1,095,687	1,046,168	
	1,069,659	1,068,777	
17	1,047,827	972,173	Good
	1,098,234	1,020,550	
	982,165	985,254	
18	1,150,506	938,538	Poor
	1,088,635	944,689	
	1,079,996	1,048,768	
19	1,277,342	1,248,508	Poor
	1,160,895	1,150,637	
	1,142,066	1,229,810	
20	1,060,752	839,974	Poor
	1,131,280	988,451	
	1,163,319	933,039	

B 1.4 Image Analysis Test Results (Continued)

Mix ID	Pre-MiST BP	Post-MiST BP	Performance
21	1,158,004	1,143,924	Good
	1,212,518	1,160,045	
	1,201,074	1,142,271	
22	1,051,077	1,047,136	Poor
	1,049,149	1,044,375	
	1,104,430	973,207	
23	1,191,804	1,128,308	Poor
	1,102,318	1,182,437	
	1,259,000	1,269,401	
24	1,137,475	1,038,928	Poor
	1,153,778	1,138,692	
	1,093,188	994,099	
25	1,216,311	1,173,882	Good
	1,268,376	1,335,062	
	1,231,424	1,267,254	
26	1,237,163	1,159,887	Poor
	1,221,850	1,139,165	
	1,276,713	1,197,743	
27	1,269,161	1,206,124	Poor
	1,279,569	1,239,816	
	1,279,079	1,218,941	
28	1,306,800	1,120,165	Poor
	1,126,651	1,043,230	
	1,139,342	1,044,185	
29	1,094,033	1,196,944	Poor
	1,083,729	1,278,013	
	1,187,779	750,163	

B 1.4 Image Analysis Test Results (Continued)

Mix ID	Pre-MiST BP	Post-MiST BP	Performance
30	1,020,421	1,063,842	Poor
	1,009,413	982,701	
	1,047,661	1,146,366	
31	1,126,095	1,038,668	Poor
	1,143,383	1,119,564	
	1,143,202	1,201,890	
32	1,176,559	1,139,186	Poor
	1,235,084	976,573	
	1,292,558	1,078,473	
33	1,157,109	984,341	Poor
	1,119,174	971,419	
	1,100,731	990,687	
34	969,999	985,392	Poor
	925,629	919,644	
35	1,172,117	978,559	Poor
	1,327,742	877,292	
	1,269,212	892,244	
36	1,266,053	1,229,098	Good
	1,171,153	1,288,366	
37	1,277,099	1,270,572	Good
	1,196,021	1,169,908	
38	1,210,191	1,171,279	Poor
	1,251,383	1,113,528	
	1,185,414	1,160,795	

B 1.5 MiST Effluent Analysis Results

Mix ID	DOC, mg	LOM, mg	FM	Performance
1	0.01	52	2.2	Poor
	4.3	62	1.9	
	1.1	135	3.2	
2	19.5	53	2.2	Poor
	2.8	139	2.7	
	4.8	107	2.2	
3	11.9	108	2.0	Poor
	0.4	144	2.0	
	7.7	88	2.3	
4	10.7	131	2.5	Poor
	13.1	106	2.4	
	11.0	155	4.1	
5	11.7	188	3.7	Good
	10.7	118	3.3	
	10.0	129	2.5	
6	11.8	159	3.1	Good
	8.7	117	3.9	
7	104.7	471	3.4	Poor
	131.0	877	2.2	
	163.0	245	1.3	
8	32.5	48	2.9	Poor
	13.3	129	2.7	
9	9.7	64	2.3	Good
	9.3	91	2.5	
10	12.6	256	3.8	Poor
	10.4	145	2.8	

B 1.5 MiST Effluent Analysis Results (Continued)

Mix ID	DOC, mg	LOM, mg	FM	Performance
11	9.4	187	1.8	Poor
	11.7	370	3.6	
12	16.0	142	3.2	Poor
	15.2	51	2.0	
13	15.2	308	1.7	Poor
	14.3	62	2.6	
14	10.2	107	3.6	Poor
	11.7	563	3.5	
15	13.7	208	3.0	Poor
	10.7	42	3.0	
	8.5	65	2.9	
16	13.8	208	2.1	Good
	11.7	150	4.3	
	10.9	214	2.8	
17	9.2	547	3.1	Good
	7.4	222	2.2	
	8.4	156	2.5	
18	10.1	153	2.6	Poor
	6.6	138	2.3	
	12.9	175	2.7	
19	6.4	173	3.3	Poor
	14.0	132	2.4	
	10.1	88	2.3	
20	10.4	51	2.8	Poor
	10.6	59	3.2	
	9.3	41	3.0	

B 1.5 MiST Effluent Analysis Results (Continued)

Mix ID	DOC, mg	LOM, mg	FM	Performance
21	11.7	87	2.2	Good
	10.4	54	2.8	
	9.3	55	2.7	
22	15.7	555	2.6	Poor
	17.8	429	2.3	
	19.1	441	1.9	
23	10.9	92	2.5	Poor
	11.7	121	2.4	
	10.7	95	2.8	
24	11.5	122	2.9	Poor
	10.7	68	3.1	
	10.2	98	2.5	
25	16.9	109.9	3.4	Good
	18.5	56.8	3.0	
	18.0	142.9	3.1	
26	19.9	146.5	2.3	Poor
	20.1	105.1	2.4	
	20.3	82.9	2.5	
27	8.0	110.1	2.9	Poor
	12.5	111.9	3.6	
	10.7	143.4	2.5	
28	7.8	43.8	2.6	Poor
	9.6	164.9	2.6	
	8.4	68.8	4.1	
29	13.2	98.5	2.4	Poor
	10.9	67.8	2.6	
	14.3	102.5	3.7	

B 1.5 MiST Effluent Analysis Results (Continued)

Mix ID	DOC, mg	LOM, mg	FM	Performance
30	19.0	128.7	2.4	Poor
	19.3	204.1	1.9	
	17.2	65.9	2.9	
31	14.4	176.1	3.2	Poor
	15.2	156.2	2.1	
	16.0	209.6	3.1	
32	12.8	100.8	2.2	Poor
	11.3	136.8	2.4	
	12.8	113.1	2.3	
33	8.1	148.5	3.1	Poor
	6.7	166.4	3.4	
	7.7	180.7	2.8	
34	12.8	171.0	2.4	Poor
	12.0	144.6	3.0	
35	10.9	116.7	3.2	Poor
	8.7	104.0	3.8	
	8.9	140.5	2.6	
36	12.0	131.4	2.2	Good
	10.8	41.1	2.0	
37	17.0	120.8	2.8	Good
	13.7	59.5	1.8	
38	11.6	136.6	2.3	Poor
	9.6	123.8	2.9	
	12.9	75.3	1.1	

APPENDIX C

Appendix C consist of the MATLAB script used in this study to perform Machine learning correlation analysis, PCA, K- Nearest Neighbor (K-NN) and Naïve Bayes (NB) model. Furthermore, MATLAB script to develop an app using exported NB model is presented below.

C 1.1: MATLAB Code for K-Nearest Neighbor Model

```
data.Esratio = (data.PostMistEs)./(data.PreMistEs);
data.ITSratio = (data.TSR)./100;
data.FEITSratio = data.PostMISTFEITS./data.PreMISTFEITS;
data.FESCBratio = data.PostMISTFESCB./data.PreMISTFESCB;
data.FIratio = data.PostMISTFI./data.PreMISTFI;
data.BPratio = data.PostMISTBP./data.PreMISTBP;
save('data');
%convert performance column to categorical data
Perf = categorical(data.Performance);
%-----------------------ACTUAL DATA for MODELING-----------------------------
-
% Create a numeric data with only ratios
numData = data{:,{'Esratio','ITSratio','FEITSratio',...
    'BPratio','DOC'}};
corrplot(numData)
numData = zscore(numData);
[coeff,scrs,~,~,pexp] = pca(numData);
fig1 = figure(1);
pareto(pexp)
set(gca,'fontsize',12,'box','off');
xlabel('PC','Fontname','TimesNewRoman','Fontsize',15);
ylabel('Percent variance','Fontname','TimesNewRoman','Fontsize',15);
saveas(gcf,'Barchartv18.jpg')
fig(2) = figure(2);
scatter3(scrs(:,1),scrs(:,2),scrs(:,3));
saveas(gcf,'3Dv18.jpg')
numData =
array2table(numData,'VariableNames',{'Esratio','ITSratio','FEITSratio',...
    'BPratio','DOC'});
%-------------------------MODELING-------------------------------------
% randomnly selecting train, test data
train = randsample(height(numData),24);
% Take data other than train data
test = setdiff(1:height(numData),train);
% Name them from the actual data
trainData = numData(train,:);
```

```
testData = numData(test,:);
trainPerf = Perf(train);
testPerf = Perf(test);

kLosses = -1*ones(1,10);
 % MODEL - here it is nearest neighbour
 knnFit = fitcknn(trainData,trainPerf,'NumNeighbors',k);
 % Carry out k-fold cross validation
    CVmdl = crossval(knnFit, 'KFold', 5);
    kLosses(k) = kfoldLoss(CVmdl);
fig(3) = figure(3);
bar(1:10,kLosses)
% plotting
set(gca,'fontsize',15,'box','off');
xlabel('No. of nearest neighbor','Fontname','TimesNewRoman','Fontsize',15);
ylabel('Validation Error','Fontname','TimesNewRoman','Fontsize',15);
saveas(gcf,'crossvalv18.jpg')

%-------------------PREDICTION, ERROR AND PLOTTING-------------------------
% predict the test data
predPerf = predict(knnFit,testData);
% testErr using loss function
testErr = loss(knnFit,testData,testPerf,'Lossfun','classiferror')
% Plotting confusion matrix
conf = confusionmat(testPerf,predPerf);
plotconfusion(dummyvar(testPerf)',dummyvar(predPerf)');
```

C 1.2: MATLAB Code for Naïve Bayes Model:

```
% finding the ratios
data.Esratio = (data.PostMistEs)./(data.PreMistEs);
data.ITSratio = (data.TSR)./100;
data.FEITSratio = data.PostMISTFEITS./data.PreMISTFEITS;
data.FESCBratio = data.PostMISTFESCB./data.PreMISTFESCB;
data.FIratio = data.PostMISTFI./data.PreMISTFI;
data.BPratio = data.PostMISTBP./data.PreMISTBP;
save('data');
%convert performance column to categorical data
Perf = categorical(data.Performance);
%-----------------------ACTUAL DATA for MODELING-----------------------------
-
% Create a numeric data with only ratios
numData = data{:,{'Esratio','ITSratio','FEITSratio',...
    'BPratio','DOC'}}
corrplot(numData)
numData = zscore(numData);
[coeff,scrs,~,~,pexp] = pca(numData);
fig1 = figure(1);
pareto(pexp)
set(gca,'fontsize',12,'box','off');
xlabel('PC','Fontname','TimesNewRoman','Fontsize',15);
ylabel('Percent variance','Fontname','TimesNewRoman','Fontsize',15);
saveas(gcf,'Barchartv18.jpg')
fig(2) = figure(2);
scatter3(scrs(:,1),scrs(:,2),scrs(:,3));
saveas(gcf,'3Dv18.jpg')
%-------------------------MODELING-------------------------------------
% randomnly selecting train, test data
train = randsample(height(numData),19);
% Take data other than train data
test = setdiff(1:height(numData),train);
% Name them from the actual data
trainData = numData(train,:);
testData = numData(test,:);
trainPerf = Perf(train);
testPerf = Perf(test);
kLosses = -1*ones(1,10);
```

```
knbFit = fitcnb(trainData,trainPerf);
% Carry out k-fold cross validation
CVmdl = crossval(knbFit, 'KFold', 4);
kLosses = kfoldLoss(CVmdl);
% plotting
set(gca,'fontsize',15,'box','off');
xlabel('No. of nearest neighbor','Fontname','TimesNewRoman','Fontsize',15);
ylabel('Validation Error','Fontname','TimesNewRoman','Fontsize',15);
saveas(gcf,'crossvalv18.jpg')
%--------------------PREDICTION, ERROR AND PLOTTING-------------------------
%predict the test data
predPerf = predict(knbFit,testData);
%testErr using loss function
testErr = loss(knbFit,testData,testPerf,'Lossfun','classiferror')
%Plotting confusion matrix
conf = confusionmat(testPerf,predPerf);
 plotconfusion(dummyvar(testPerf)',dummyvar(predPerf)');
```

C 1.3: MATLAB Code for The App Development:

```
classdef ramapp < matlab.apps.AppBase

    % Properties that correspond to app components
    properties (Access = public)
        UIFigure                      matlab.ui.Figure
        EsratioEditFieldLabel         matlab.ui.control.Label
        Esratio                       matlab.ui.control.NumericEditField
        ITSratioEditFieldLabel        matlab.ui.control.Label
        ITSratio                      matlab.ui.control.NumericEditField
        FEITSratioEditFieldLabel      matlab.ui.control.Label
        FEITSratio                    matlab.ui.control.NumericEditField
        BPratioEditFieldLabel         matlab.ui.control.Label
        BPratio                       matlab.ui.control.NumericEditField
        DOCEditFieldLabel             matlab.ui.control.Label
        DOC                           matlab.ui.control.NumericEditField
        ClassifyButton                matlab.ui.control.Button
        PerformanceEditFieldLabel     matlab.ui.control.Label
        Perf                          matlab.ui.control.EditField
    end

    methods (Access = private)

        % Callback function: ClassifyButton, Perf
        function ClassifyButtonPushed(app, event)
            load('knbFit.mat');
            X = [app.Esratio.Value app.ITSratio.Value app.FEITSratio.Value
app.BPratio.Value app.DOC.Value];
            z = predict(knbFit, X);
            app.Perf.Value = z{1};
           value = app.Perf.Value;
        end
    end

    % App initialization and construction
    methods (Access = private)
```

```
% Create UIFigure and components
function createComponents(app)

    % Create UIFigure
    app.UIFigure = uifigure;
    app.UIFigure.Position = [100 100 640 480];
    app.UIFigure.Name = 'UI Figure';

    % Create EsratioEditFieldLabel
    app.EsratioEditFieldLabel = uilabel(app.UIFigure);
    app.EsratioEditFieldLabel.HorizontalAlignment = 'right';
    app.EsratioEditFieldLabel.Position = [165 396 43 22];
    app.EsratioEditFieldLabel.Text = 'Esratio';

    % Create Esratio
    app.Esratio = uieditfield(app.UIFigure, 'numeric');
    app.Esratio.Position = [223 396 100 22];

    % Create ITSratioEditFieldLabel
    app.ITSratioEditFieldLabel = uilabel(app.UIFigure);
    app.ITSratioEditFieldLabel.HorizontalAlignment = 'right';
    app.ITSratioEditFieldLabel.Position = [160 351 47 22];
    app.ITSratioEditFieldLabel.Text = 'ITSratio';

    % Create ITSratio
    app.ITSratio = uieditfield(app.UIFigure, 'numeric');
    app.ITSratio.Position = [222 351 100 22];

    % Create FEITSratioEditFieldLabel
    app.FEITSratioEditFieldLabel = uilabel(app.UIFigure);
    app.FEITSratioEditFieldLabel.HorizontalAlignment = 'right';
    app.FEITSratioEditFieldLabel.Position = [142 299 63 22];
    app.FEITSratioEditFieldLabel.Text = 'FEITSratio';

    % Create FEITSratio
    app.FEITSratio = uieditfield(app.UIFigure, 'numeric');
    app.FEITSratio.Position = [220 299 100 22];
```

```
            % Create BPratioEditFieldLabel
            app.BPratioEditFieldLabel = uilabel(app.UIFigure);
            app.BPratioEditFieldLabel.HorizontalAlignment = 'right';
            app.BPratioEditFieldLabel.Position = [162 255 45 22];
            app.BPratioEditFieldLabel.Text = 'BPratio';

            % Create BPratio
            app.BPratio = uieditfield(app.UIFigure, 'numeric');
            app.BPratio.Position = [222 255 100 22];

            % Create DOCEditFieldLabel
            app.DOCEditFieldLabel = uilabel(app.UIFigure);
            app.DOCEditFieldLabel.HorizontalAlignment = 'right';
            app.DOCEditFieldLabel.Position = [176 209 32 22];
            app.DOCEditFieldLabel.Text = 'DOC';

            % Create DOC
            app.DOC = uieditfield(app.UIFigure, 'numeric');
            app.DOC.Position = [223 209 100 22];

            % Create ClassifyButton
            app.ClassifyButton = uibutton(app.UIFigure, 'push');
            app.ClassifyButton.ButtonPushedFcn = createCallbackFcn(app,
@ClassifyButtonPushed, true);
            app.ClassifyButton.Position = [223 131 100 22];
            app.ClassifyButton.Text = 'Classify';

            % Create PerformanceEditFieldLabel
            app.PerformanceEditFieldLabel = uilabel(app.UIFigure);
            app.PerformanceEditFieldLabel.HorizontalAlignment = 'right';
            app.PerformanceEditFieldLabel.Position = [185 78 74 22];
            app.PerformanceEditFieldLabel.Text = 'Performance';

            % Create Perf
            app.Perf = uieditfield(app.UIFigure, 'text');
            app.Perf.ValueChangingFcn = createCallbackFcn(app,
@ClassifyButtonPushed, true);
            app.Perf.Position = [274 78 100 22];
```

```
        end
    end

    methods (Access = public)

        % Construct app
        function app = ramapp

            % Create and configure components
            createComponents(app)

            % Register the app with App Designer
            registerApp(app, app.UIFigure)

            if nargout == 0
                clear app
            end
        end

        % Code that executes before app deletion
        function delete(app)

            % Delete UIFigure when app is deleted
            delete(app.UIFigure)
        end
    end
end
```